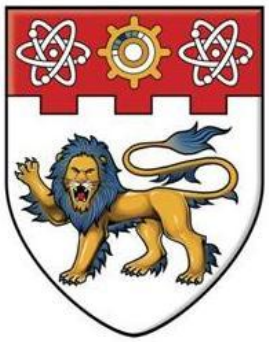

NANYANG TECHNOLOGICAL UNIVERSITY

PREPARATION AND LUMINESCENT PROPERTIES OF ZNO QUANTUM DOTS NANOCOMPOSITES

WANG LIBO

School of Materials Science and Engineering

2014

PREPARATION AND LUMINESCENT PROPERTIES OF ZNO QUANTUM DOTS NANOCOMPOSITES

WANG LIBO

School of Materials Science and Engineering

A thesis submitted to the Nanyang Technological University
in partial fulfillment of the requirement for the degree of Doctor of Philosophy

2014

This thesis is dedicated to my parents:

Wang Yafang & Wang Zhuidi

Acknowledgements

I would like to take this opportunity to express my gratitude to all the people who have provided help and support to my PhD study.

Firstly, I would like to express my deep sense of gratitude to my supervisor, Prof. Hu Xiao who has given me invaluable advices and encouragement. In addition, many thanks go to my co-supervisor, Prof. Mei Ting for his insightful comments and fruitful discussion in my research journey. They always play influential role in my knowledge pursuing and character building processes throughout my PhD study.

On the other hand, I have been blessed with a group of cheerful and supporting teammates: Liu Ming, Yin Ming, Jinhua, and so on. With their assistance in daily laboratory work and knowledge sharing, the clarity of my research work was improved. Their help and friendship are appreciated. I should not forget to send my special thank to Mr. Liang Yen Nan in giving me lots of help on my research and useful suggestion in improving my thesis.

Many thanks also go to the lab technicians from Organic Service Lab and FACTS in MSE as well as Photonics Lab 1, 2, Nano-Photonics Lab and N^2FC in EEE for their useful assistance in countless ways.

Finally, I am gratitude to my beloved family members who always stand by my side through all the ups and downs. All the tolerance and encouragement support me to complete my PhD study.

Table of Contents

List of Figures

List of Tables

List of Equations

Abbreviations

AFM	Atomic force microscopy
Alq_3	Tris(8-hydroxyquinoline) aluminum
ATRP	Atom transfer radical polymerization
CB	Conduction band
CIE	Commission Internationale de l'Eclairage
DMF	N,N-Dimethylformamide
E_g	Energy band gap
EL	Electroluminescence
EQE	External quantum efficiencies
ETL	Electron transport layer
FN	Fowler-Nordheim
FRET	Förster resonance energy transfer
FTIR	Fourier transform infrared
FWHM	Full width at half maximum
HBL	Hole block layer
HIL	Hole injection layer

HOMO	Highest occupied molecular orbital
HR-TEM	High resolution transmission electron microscopy
HTL	Hole transport layer
ITO	Indium tin oxide
LEDs	Light-emitting diodes (devices)
LUMO	Lowest unoccupied molecular orbital
MAA	Methacrylate anion
MEH-PPV	Poly[2-methoxy-5-(2-ethylhexyloxy)-1,4-phenylenevinylene]
MMA	Methyl methacrylate
NIR	Near infrared
NUV	Near ultraviolet
OLEDs	Organic light-emitting diodes
P4VP	Poly(4-vinylpyridine)
PEDOT:PSS	Poly(3,4-ethylene dioxythiophene):poly(styrene sulphonate)
PEG	Poly(ethylene glycol)
PEGME	Poly(ethylene glycol methyl ether)
PFH-MEH	Poly[(9,9-dihexyloxyfluoren-2,7-diyl)-*alt*-*co*-(2-methoxy-5-(2-ethylhexyloxy) phenylen-1,4-diyl)]
PHEMA	Poly(hydroxyethyl methacrylate)

PMMA	Poly(methyl methacrylate)
PL	Photoluminescence
PPEGMA	Poly[poly(ethylene glycol) methyl ether monomethacrylate]
PPV	*p*-paraphenylene vinylene
PS	Polystyrene
PVDF	Poly(vinylidene fluoride)
PVK	Poly(9-vinylcarbazole)
PVP	Poly(vinyl pyrrolidone)
QDs	Quantum dots
QD-LEDs	Quantum dot light-emitting diodes (devices)
SAED	Selected area electron diffraction
SCLC	Space-charge-limited-current
TAZ	3-(4-biphenyl)-4-phenyl-5-*tert*-butylphenyl-1,2,4-triazole
TCO	Transparent conductive oxide
TE	Thermionic emission
TEM	Transmission electron microscopy
TPD	*N*,*N'*-bis(4-butylphenyl)-*N*,*N'*-bis(phenyl)benzidine
TPM	3-trimethoxysilylpropyl methacrylate
UV	Ultraviolet

UV-VIS	Ultraviolet-visible
VB	Valence band
V_O	Oxygen vacancies
V_O^+	Single charged oxygen vacancies
V_O^{++}	Double charged oxygen vacancies
V_{Zn}	Zinc vacancies
XPS	X-ray photoelectron spectroscopy
XRD	X-ray diffraction
Zn_i	Zinc interstitial
ZnO	Zinc oxide

Abstract

Nanocomposites consisting of quantum dots (QDs) incorporated within polymer matrices have attracted great research interests due to their unique functional properties combining the advantages of both inorganic semiconductors and organic polymers. Among various inorganic-organic nanocomposites being studied, ZnO QDs incorporated within different polymer matrices have been widely studied and the nanocomposites exhibit good luminescent properties with high photostability. Nevertheless, there is still lack of study concerning the electroluminescent properties of ZnO QDs nanocomposites.

The objectives of this work are to explore a facile method to synthesize polymer/ZnO QDs nanocomposites thin films and to further investigate their luminescent properties. Nanocomposites synthesized *via* in-situ thermal decomposition of zinc precursor at relatively low temperature, termed as 'polymerothermal method', are free of impurity and therefore very suitable for fundamental studies on luminescent properties. Furthermore, the large interface area between polymers and ZnO QDs is very important to study the defect related emission from ZnO QDs and the possible interaction between them.

In this work, poly(methyl methacrylate) (PMMA)with good optical transparency was firstly employed for preparation of nanocomposite with uniformly embedded ZnO QDs. The as-prepared PMMA/ZnO QDs nanocomposite exhibits photoluminescence (PL) with strong UV emission but weak visible emission, which is similar to those nanocomposites that synthesized *via* physical blending method. However, it is

interesting to find that the electroluminescence (EL) of PMMA/ZnO QDs nanocomposite based light-emitting devices (LEDs) shows broad emission covering the entire visible range. Based on a detailed analysis carried out by comparing both the PL and EL emission spectra; different carrier recombination pathways corresponding to band edge and defect energy levels are proposed. This finding indicates that the luminescent properties of the nanocomposite are largely depended on the carrier injection method as well as the intrinsic properties of embedded ZnO QDs.

The synthetic method was further extended to other polymers. The luminescent properties of nanocomposites can obviously be affected by the polymer matrices; as the polymers can passivate the surface of embedded ZnO QDs to different extents. EL of as-fabricated ZnO QDs based LEDs can be potentially tuned by selection of polymer matrices. The results indicate that the interaction involved between polymers and ZnO QDs could be the key factor of changing the properties of hybrid nanocomposites system.

1. Introduction

Zero-dimensional semiconductor nanoparticles (so-called quantum dots, QDs) have been studied for decades owing to their wide range of promising applications in the field of electronics and optoelectronics. On the other hand, organic molecules, *e.g.*, surfactants, polymers, and polyelectrolytes are often used to assist the synthesis of inorganic nanoparticles. The morphological and functional properties of QDs can be tailored by the surface functional groups of the organic molecules in the synthesis. Inorganic-organic nanocomposites, *e.g.*, PPV/CdSe QDs, PMMA/ZnO QDs, have attracted much attention due to their unique and synergistic properties contributed by combination of the advantages of both nanostructured semiconductors and organic polymers.[1-5] Among various applications of these nanocomposites, light-emitting device (LED) is a highly pursued direction. The LEDs based on QDs cooperated with organic materials, terms as 'quantum dot LEDs' (QD-LEDs), are expected to combine the long-term stability and efficiency of inorganic semiconductors (widely used for traditional LED products[6-10]), with flexible, low-cost, solution processable, and large area deposition techniques of organic LEDs (OLEDs)[11-15].

Since the first QD-LEDs was demonstrated by Colvin and co-workers in 1994[1], tremendous effort has been put in to improve the device performances, including: brightness, external quantum efficiency (EQE), life time, and color tunability.[16-21] However, most of the efficient and highly luminescent QD-LEDs involve using of cadmium (Cd), *e.g.*, CdS, CdSe, and CdTe. The usage of such type of toxic heavy

metals retards QD-LEDs from widespread commercialization. Therefore, there is a need to explore the usage of other non-toxic QDs for LED application.

Zinc oxide (ZnO) with its favorable physical and chemical properties, including large exciton binding energy, direct band gap, and chemical stabilities, offers high potential to be used as the luminescent active layer. It is also worth noting that ZnO is non-toxic, cheap and naturally abundant. Moreover, quantum-sized ZnO coated with polymers can exhibit unique optical properties due to different interaction between polymers and ZnO. Comparing to uncapped ZnO QDs, the photoluminescence (PL) of nanocomposites is somehow better controlled and of higher quantum yield.

Conventionally, there are two strategies of preparing ZnO-based polymer nanocomposites which can be classified as (i) physical blending and (ii) chemical reactions. Physical blending method could lead to serious aggregation, while chemical reaction method usually requires multiple steps. Both of these two methods introduce impurities in the synthesis, such as Li^+, Na^+, or other side-products; making the PL mechanism of nanocomposites more complicated for analysis. Furthermore, more fundamental studies concerning the electroluminescence (EL) properties of polymer/ZnO QDs nanocomposite and the influence of polymer matrices are need.

The objective of this work is to explore a facile and effective method to synthesize polymer/ZnO QDs nanocomposites that are free of impurity. Furthermore, these nanocomposites are used in the fabrication of ZnO QDs based LEDs and investigate the device performance. The chemically clean nanocomposites are very suitable to be used for study on their fundamental optical properties; as the complexity due to extra species could be minimized.

The organization of the rest of this thesis is as following: The potential of controlling and manipulating the light emission properties were also explored in the study of different polymer matrices.

In Chapter 2, literature review focuses on mainly two parts is done. The first part introduces QDs and the development of QDs-LEDs. The second part focuses on the preparation method of ZnO QDs-based polymer nanocomposites and their optical properties.

Chapter 3 proposes a new facile method to prepare PMMA/ZnO QDs nanocomposite. The PL of this nanocomposite are carried out to study the optical properties; with detailed discussion on the possible emission mechanism.

In Chapter 4, as-prepared device-ready PMMA/ZnO QDs nanocomposite is utilized for fabrication of ZnO QDs-based QD-LEDs. The EL mechanisms light emitting from the devices are discussed with comparison to the PL properties. The possible recombination centers of ZnO QDs is also proposed.

Chapter 5 includes work on extending the facile method to prepare nanocomposites containing other polymer; together with the investigation of their optical properties. Some of the polymer/ZnO QDs nanocomposites that are applicable for QD-LEDs are used for the study of the mechanisms of light emission. Discussion about the influence of polymer on ZnO QDs has been given by comparing the PL and EL properties of different polymer-based nanocomposites.

Finally in Chapter 6, the summary and conclusion of this work on ZnO QDs-based polymer nanocomposites; together with recommended future work are given.

2. Literature Review

In this chapter, a literature review is presented with the focuses on the following two topics:

1. QD-LEDs: concepts, mechanisms, and development
2. Polymer/ZnO QDs nanocomposites: preparation, photoluminescence (PL) properties and applications

2.1 QD-LEDs: Concepts, Mechanisms, and Development

Light-emitting diodes (LEDs) are one specific type of semiconductor devices that emit noncoherent, narrow-spectrum light when a forward voltage is applied.[22] Nowadays, LED-based solid-state lighting is used in a wide range of applications, including visual indicator, communications, display backlighting, and general illumination.[8, 10, 23-26] Switching from traditional light sources, *e.g.*, incandescent light bulb and compact fluorescent lamp, to LED-based solid-state lighting is very important, especially for lowering the consumption of energy by 3 to 6 times.[27] At the same time, the market of LEDs is growing rapidly with annual growth rate of 11.8 % and expected to reach $18.9 billion in 2015.[28]

In the past two decades, the increasing demand of low-cost, solution processable techniques for fabricating large-area light-emitting panels has spurred further development of organic LEDs (OLEDs).[11-15] To date, OLEDs have started to earn

credibility in displays and lighting markets. However, the color emission quality of OLEDs is still far from satisfactory and, it is difficult to tune the emission color. Thanks to the rapid development of quantum dots synthesis technology, such problems can be overcome by integrating semiconductor nanocrystals into LEDs because QDs are known to have high quantum yield, very narrow band emission as well as color tunability by varying the size of QDs.[29-34] QD-LEDs are expected to combine the advantages of both traditional inorganic semiconductor materials and flexible low-cost large-area deposition techniques from organic devices. Therefore, QD-LEDs are considered to be a promising light source in the future.

2.1.1 Brief Introduction of Colloidal Quantum Dots and the Advantages for Light-Emitting Applications

Semiconductors possess electronic band structures that consist of valence band and conduction band. A specific empty energy interval which is also known as band gap separates those two bands at different energy levels. The electrical conductivity of semiconductors is originated from the net movements of charges (either electrons or holes) that occupy those two bands; which results in many novel electronic and opto-electronic properties, such as field effective conductivity and electron-hole recombination. Generally, both organic and inorganic materials can be semiconductors intrinsically or through extrinsic doping. In terms of quantum dots (QDs) that will be discussed in this thesis, it is mainly focusing on the inorganic semiconductors.

Generally speaking, colloidal quantum dots (QDs), also called semiconductor nanocrystals, are composed of (i) an inorganic core, which has comparable size with its Bohr exciton diameter of the bulk material, surrounded by (ii) inorganic shells and/or organic ligands.[33] In comparison with bulk semiconductors, QDs with

excitons confined in all three spatial dimensions significantly affect the momentum of electrons and distort the electronic band structures, which results in size-dependent separation of originally overlapped energy states into discrete energy levels.(Fig. 2-1(a)) Meanwhile, the band gap of QDs can be enlarged with its particle size is reduced. This phenomenon is generally termed as quantum confinement effect.[29] Therefore, the QDs exhibit novel alterations in their material properties, especially the optical properties (*e.g.* absorbance and luminescence).

Quantum dots, also semiconductors, can absorb photons (electromagnetic radiation) with higher energy (shorter wavelength) than band gap energy to excite electrons in valance band into conduction band. The transition of electrons will form a positive charged place, so called holes, in the valence band. The excitations then undergo energy and momentum relaxation process that electrons recombine with holes. The recombination process is accompanied with emission of phonons (non-radiative recombination) and, sometimes, photons (radiative recombination). For optical properties of QDs, radiative recombination is desirable and it requires the semiconductors with direct band gap. The above mentioned process with radiative recombination is also known as photoluminescence (PL).(Fig. 2-1(b)) Due to quantum confinement effect, QDs with larger band gap than its bulk material have blue-shifted spectrum on its PL property, which is from longer wavelength to shorter wavelength. For instance, CdSe QDs provide emission from red through blue by reducing the size from about 6 nm to 2 nm (Fig. 2-1(c)).[35] In addition, all the QDs solutions show very good color purity indicating narrow size distribution achieved during synthesis. Besides the charges transition between band edges, the electrons and holes could also be seized by defect energy levels which corresponding to defect emissions shown in Fig. 2-1(b). The defect states of semiconductors can be formed natively or through

impurities. The whole PL spectrum is corresponding to recombination of electrons and holes form different energy levels including band edges and defects. However, the formation of electron-hole pairs can be realized not only by optical excitation but also *via* electrical pump. The details will be introduced in the next section.

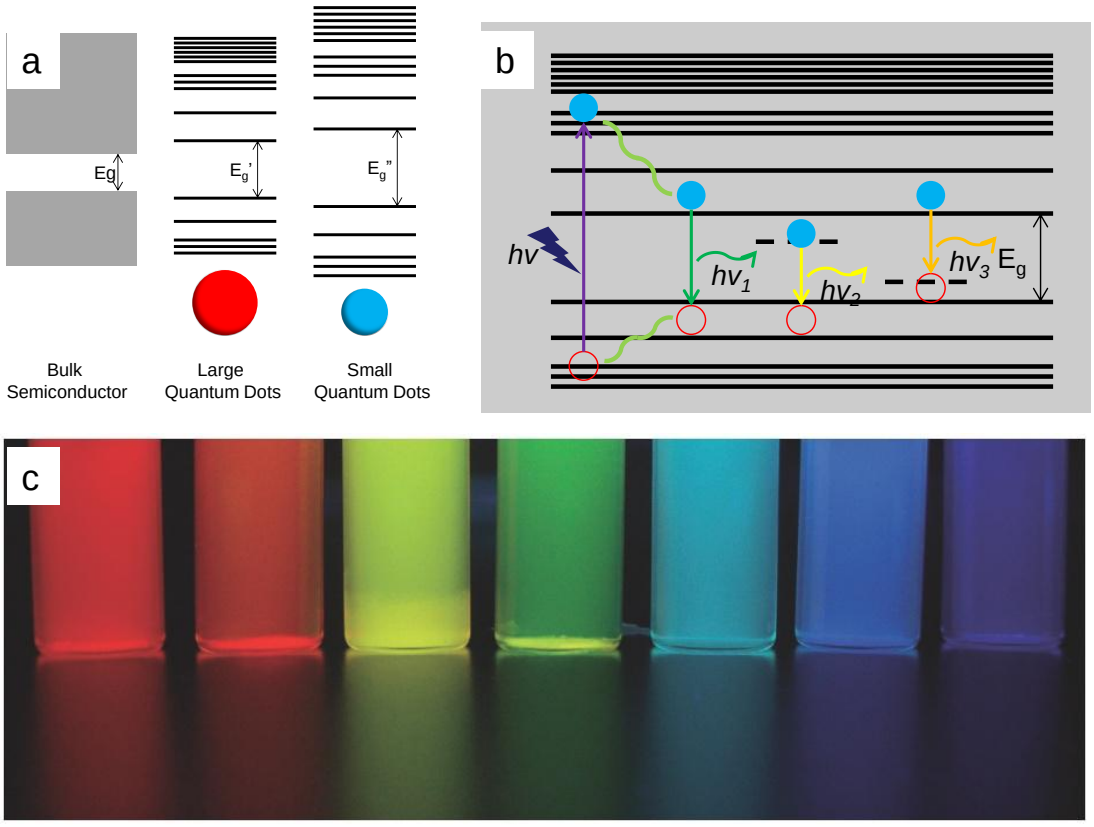

Fig. 2-1 Properties of quantum dots (QDs). **a**. Illustration of quantum confinement effect that the energy levels are quantized and shifted. The band gap between valence band and conduction band increases with the size of nanoparticles reduces (E_g" > E_g' > E_g). **b**. Schematic process of absorption and photoluminescence of QDs. Electrons are excited by absorbing photons and electron-hole pairs are formed. The subsequent relaxation process makes the excitations between different energy levels (either band edge or defect energy levels) recombine again with emission of photons. **c**. Colloidal CdSe QDs with variations in particle size exhibit a range of fluorescent colors under an ultraviolet lamp. The QD size for the red emission is about 6 nm in diameter and decreases to 2 nm for blue emission QDs. Reprinted from [35]. Copyright (2011) with permission from Elsevier.

Since the synthesis of colloidal QDs are usually done by solution-based approaches, it thereby makes QDs solution processable for further applications.[33] Therefore, a

variety of low-cost and large-area deposition techniques, *e.g.*, spin coating, phase separation, inkjet printing and contact printing, can be applied for device fabrication.[16, 36-39] Furthermore, compare to organic dyes, QDs show better resistance to degradation caused by photobleaching.[40, 41] The photostability of QDs can be further improved by coating with wider bang gap shells, such as ZnS.[33, 42]

After decades of development, high-quality QDs (mainly Cd-based) with good optical properties and photostability are ready for light emitting application *via* low-cost solution process.

2.1.2 Concepts and Mechanisms of QD-LEDs

Distinguished from optical excitation that requires electromagnetic radiation with short wavelength (high energy) to excite electrons and form electron-hole pairs, it is also possible to be realized *via* electrical pump for QDs. With the subsequent recombination of electron-hole pairs, the whole process is known as electroluminescence (EL), which is the basic concept of QD-based light-emitting devices (QD-LEDs). Similar to photoluminescence, the electroluminescence also gives spectrum with different EL bands that corresponds to recombination of electron-hole pairs with different energy intervals.

The schematic structure of QD-LEDs is adopted from OLEDs and shown in Fig. 2-2. The transparent conductive oxide (TCO) coated glass is normally used as the substrate as well as the anode. On top of anode, an active light emitting layer containing QDs, either blended with organic host materials (Fig. 2-2a) or sandwiched between two functional layers (Fig. 2-2b), is deposited *via* a variety of techniques. Metals with low work function are subsequently deposited and worked as top electrode (cathode).

Indium tin oxide (ITO) and aluminum (Al) are most frequently used as anode and cathode, respectively.

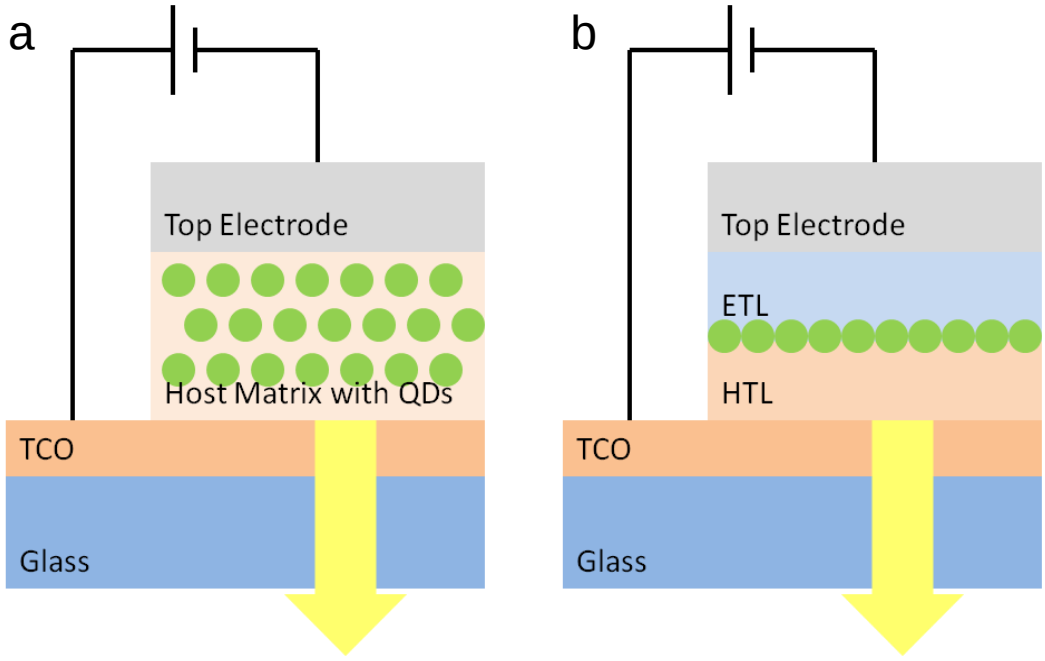

Fig. 2-2 Different device design of QD-LEDs. **a**. QDs are incorporated within an organic host matrix. **b**. QDs are assembled as a tight layer sandwiched between hole transport layer (HTL) and electron transport layer (ETL). TCO and top electrode are used as anode and cathode, respectively. The light comes out through the TCO coated glass substrate under operation.

When a forward bias is applied on a QD-LED, excitons on QDs can be generated by electrons injected from the top electrode and holes injected from TCO. The recombination of electron-hole pairs gives a light emission with wavelength corresponding to the band gap of QDs. This mechanism, termed as direct charge injection, is widely proposed for most QD-LEDs.[18, 43, 44] The process is schematically illustrated in Fig. 2-3(a). In case of QDs cooperated with organic semiconductors as matrices or functional layers in the LEDs, exciton generation on QDs can be realized *via* direct charge injection accompanied with exciton energy transfer which is also known as Förster resonance energy transfer (FRET).[17, 45, 46] In FRET process, excitons are firstly formed in the organic layers and transferred to

the QDs layer non-radiatively in the case when the formed excitons are very near to QDs. The schematic illustration of FRET process is shown in Fig. 2-3(b).

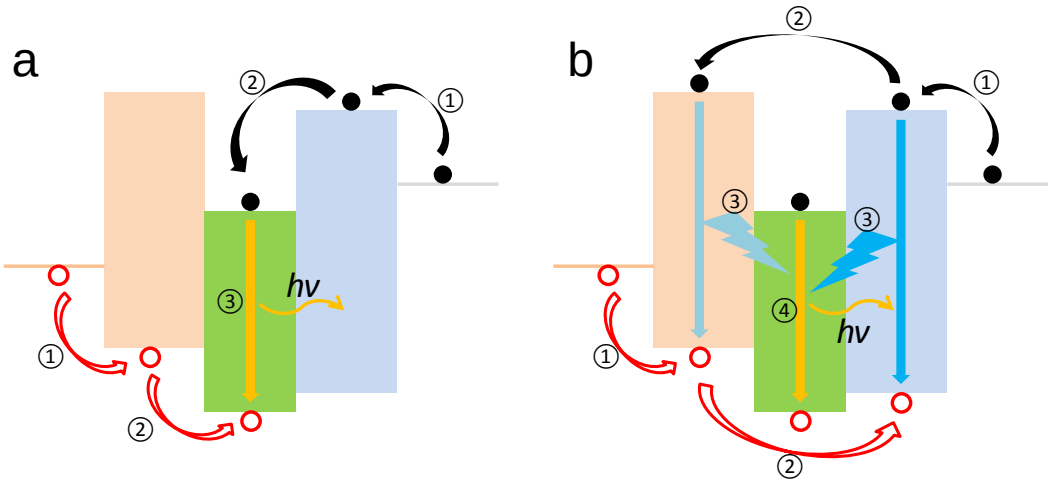

Fig. 2-3 Mechanisms of light emission in QD-LEDs. a. Direct charge injection: ①charge injection into carrier transport layer (HTL and ETL); ②charge injection into QDs and forming excitons; ③radiative recombination of excitons in QDs. b. Exciton energy transfer (Förster resonance energy transfer, FRET): ①charge injection into carrier transport layer; ②formation of excitons in carrier transport layer; ③nonradiative energy transfer from organic layers to QDs and form excitons in QDs; ④radiative recombination of excitons in QDs.

2.1.3 Development of QD-LEDs

In the first reported QD-LED, a layer of organic semiconducting polymer, *p*-paraphenylene vinylene (PPV) that was covered with a multilayer structure of CdSe QDs was used as the light emission layer, sandwiched between ITO and Mg electrodes.[1] Electroluminescence of this ITO/PPV/CdSe/Mg device showed voltage-dependent spectra, besides the fact that its EL from PPV increased significantly and became dominant under higher voltages. It also suggested, by changing the size of QDs, the emission color could be tuned from red to yellow. Soon after that, Dabbousi *et al.* demonstrated a single-layer QD-LEDs with CdSe QDs incorporated into a blended thin film of poly(9-vinylcarbazole) (PVK) and an oxadiazole derivative (*t*-Bu-

PBD).[2] Although the external quantum efficiencies (EQE) of the early devices were quite low, 0.001-0.01 %[1] and 0.0005 %[2] respectively, these studies demonstrated the possibility of utilizing quantum confined semiconductor nanocrystals in hybrid light-emitting devices.

The first breakthrough in performance of QD-LEDs was achieved by replacing bare QDs (capped with organic ligands, most probably trioctylphosphine oxide, TOPO) with core/shell structures of semiconductor nanocrystals (also termed as QDs).[47, 48] In comparison with the bare CdSe-based QD LEDs, the devices consisting of CdSe/CdS (core/shell) QDs with similar device structure as the first QD-LED showed a significant improvements in EQE and lifetime.[47] The devices could emit from red to green color with EQE up to 0.22 % at brightness of 600 $cd \cdot m^{-2}$ and current density of 1 $A \cdot cm^{-2}$. The QD-LEDs could last hundreds of hours under operating voltages as low as 4 V. The great improvement in device performance should be attributed to the material system of QDs. Fig. 2-4 showed a schematic structure of core/shell QD with its energy band diagram. The wider band gap of shell material caused tighter confinement and localization of the exciton in the core and therefore, core/shell QDs exhibited higher photoluminescence (PL) quantum yield and photostability.[30] However, the charge injection from electrodes to QDs layer was imbalance due to poor electron transport through the QD multilayers. As a result, the luminescence efficiency of the QD-LEDs was still low.

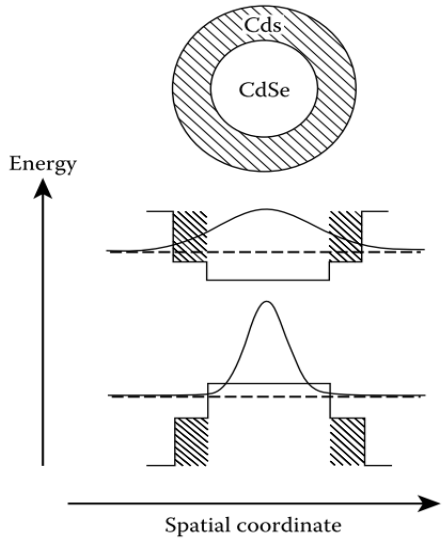

Fig. 2-4 Energy band diagram of core/shell structured CdSe/CdS QD. The solid lines indicate the position of energy potentials of bulk materials (CdS and CdSe), while the dashed lines represent the HOMO and LUMO of CdSe core with larger band gap. Energy interval between the core and shell are 0.5 eV for valence band and 0.3 eV for conduction band. Reprinted with permission from [47]. Copyright (1997) American Institute of Physics.

The device performance of QD-LEDs was largely improved by introducing a sandwich structure of hole transport layer (HTL)/QDs layer/electron transport layer (ETL) as the emission layer.[16] Phase separation technique was used and optimized to fabricate a tight QDs monolayer on top of continuous HTL (*N*,*N'*-bis(4-butylphenyl)-*N*,*N'*-bis(phenyl)benzidine (TPD)). Subsequently, a layer of tris(8-hydroxyquinoline) aluminum (Alq_3) was thermally deposited on top of QDs layer and worked as ETL. ITO and Mg/Ag (similar work function as Al) were used as the anode and cathode, respectively. The device structure is shown in the inset of Fig. 2-5(a) and the EL showed a dominant emission from CdSe/ZnS QDs with a small contribution from Alq_3, which caused color impurity. The emission from Alq_3 was suppressed by inserting a 10 nm thick 3-(4-biphenyl)-4-phenyl-5-*tert*-butylphenyl-1,2,4-triazole (TAZ) hole and exciton blocking layer between ETL and QDs layer (Fig. 2-5(b)). It is worth noting that a dramatic improvement in luminance efficiency was achieved with

the peak EQE of 0.52 % and brightness of 2000 $cd \cdot m^{-2}$. The significant improvement of device performance should be attributed to device structure that balanced the carrier injection and helped in preventing QD charging. As described in previous section, the exciton on QDs was generated *via* two parallel processes: direct charge injection and exciton energy transfer also known as FRET. Additional studies on the devices utilizing CdSe core material capped with various thicknesses of ZnS shell showed that FRET of excitons from organic materials to the emissive QDs layer dominated the electroluminescence process of the QD-LEDs, rather than direct charge injection.[17] EQE of 1.1 % was achieved in the CdSe/ZnS-based QD-LEDs with thicker ZnS shells.

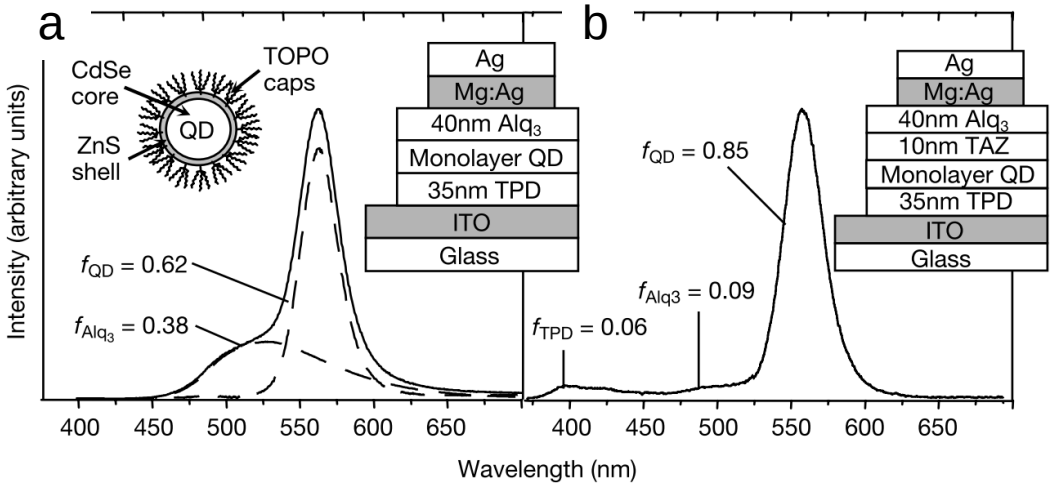

Fig. 2-5 EL spectra and schematic device structures of two types of QD-LEDs. **a**. QD-LEDs without TAZ layer. EL emission from Alq_3 and QD components are shown as dashed lines which are deconvoluted from the whole spectrum. The inset illustrates the structure of QDs with CdSe core and 1.5 monolayers of ZnS. **b**. QD-LEDs with TAZ as a hole block layer. Only QDs emission is observed, while the emission from Alq_3 is minimized. Reprinted by permission from Macmillan Publishers Ltd: Nature [16], copyright (2002).

Sun and co-workers, in 2007, reported high-performance QD-LEDs with saturated red, orange, yellow and green emissions.[21] QDs based on core material of CdSe with ZnS shell or CdS/ZnS multishell were utilized in their devices. As compared to the previous QD-LEDs, they firstly introduced a layer of PEDOT:PSS, poly(3,4-ethylene

dioxythiophene):poly(styrene sulphonate), between ITO and HTL to improve the hole injection, so-called hole injection layer (HIL). This resulted in reducing turn-on voltage of the devices to 3-4 V with improved injection efficiency of 1.1-2.8 $cd \cdot A^{-1}$. More important, they found the thickness of QDs layer had significant influence on the efficiency and luminance of QD-LEDs and optimized the thicknesses of QDs layers were 21.0 nm, 22.0 nm, 18.75 nm, and 17.0 nm for green, yellow, orange, and red light emission QD-LEDs, respectively. The maximum luminance of 3700, 4470, 3200, and 9064 $cd \cdot m^{-2}$ were achieved for green, yellow, orange, and red, respectively.

Despite significant improvements on device performances, the lifetime of QD-LEDs was always limited by the degradation of organic charge transport layers under high electric field and moisture in ambient atmosphere. One possible way to overcome this problem is replacing the organic layers with inorganic materials.[19, 39, 49-60] Caurge and co-workers reported QD-LEDs with p-type inorganic NiO film as hole transport layer.[19] A maximum EQE of 0.18% and brightness of 3000 $cd \cdot m^{-2}$ were achieved by optimizing resistivity of NiO layer. In their further studies, the organic ETL (TAZ and Alq_3 layers) was replaced by sputtered amorphous ZnO:SnO_2 semiconductor.[49] The all-inorganic QD-LEDs (HTL: NiO) shown in Fig. 2-6 presented pure QD emission with maximum EQE of 0.1 %, brightness of 1950 $cd \cdot m^{-2}$ and high injection currents of 3.5 $A \cdot cm^{-2}$.The poor performance of all-inorganic QD-LEDs was ascribed to quenching of excitons when the QDs contact with the carrier transport layer and nonradiative recombination of excitons due to QD charging.[52]

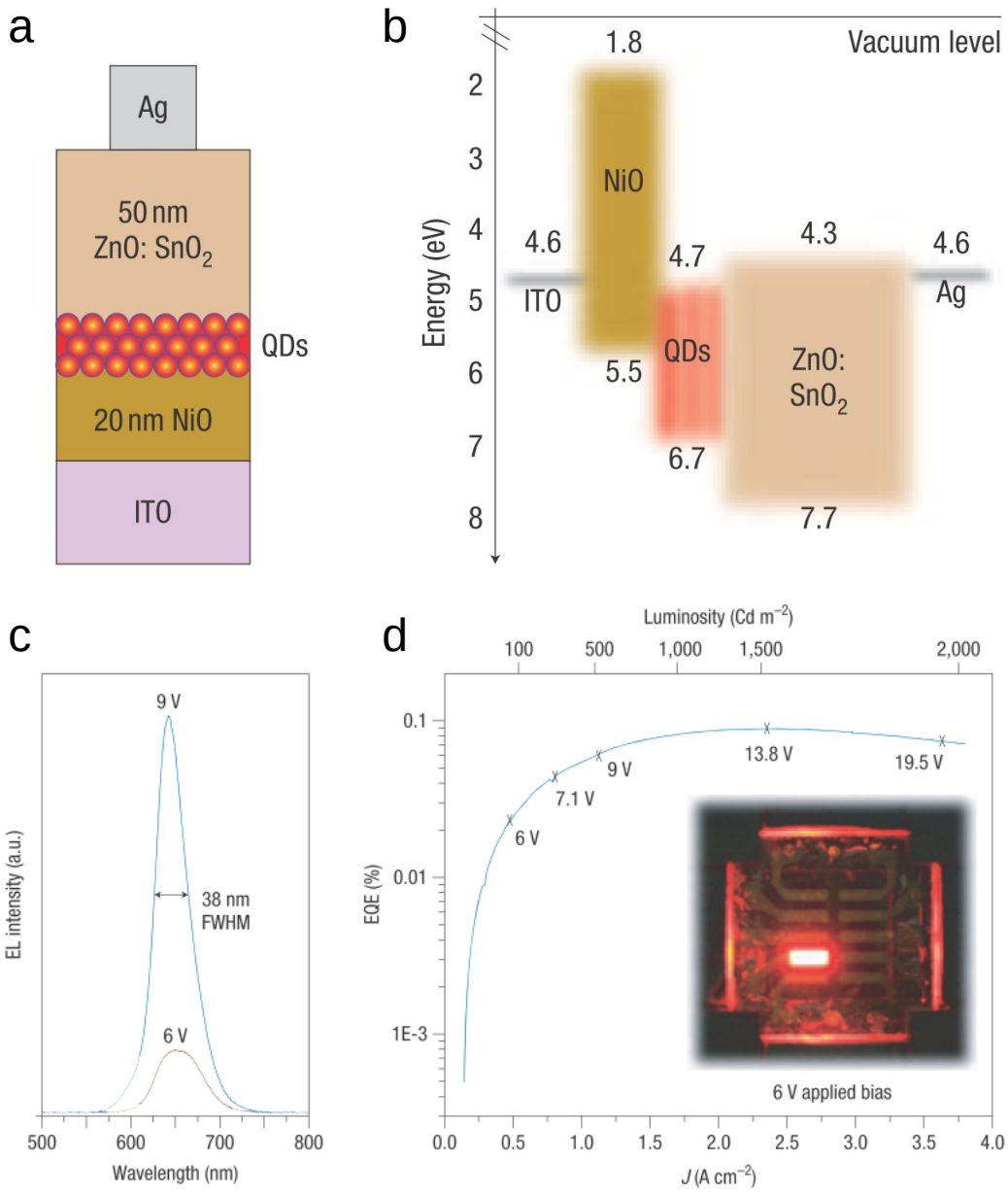

Fig. 2-6 All-inorganic QD-LED. **a**. Schematic structure of all-inorganic QD-LEDs showing silver cathode, ZnO;SnO_2 ETL, $Cd_{1-x}Zn_xSe$ QDs as the active luminescent layer, NiO HTL, and ITO anode. **b**. Energy band diagram presents the work functions and energy levels of all the QD-LED layers. **c**. EL spectra of the QD-LED operated at the bias of 6 V and 9 V. **d**. EQE of the device as a function of current density, J. The inset shows a photograph of the QD-LED under 6 V applied bias. Reprinted by permission from Macmillan Publishers Ltd: Nature Photonics [49], copyright (2008).

Instead of replacing organic HTL with inorganic materials in QD-LEDs, several research groups from South Korea, USA and France preferred to replace the organic

ETL (Alq_3) which normally needed expensive thermal deposition technique by inorganic materials *via* solution process [39, 50, 56, 58, 60], whereas Cho *et al.* fabricated QD-LEDs using so-gel synthesized TiO_2 thin film as ETL (Fig. 2-7).[50] Owing to the high electron mobility and low band offset to Al electrode, electron injection in the TiO_2-based QD-LEDs was significantly enhanced. Therefore, the turn-on voltage of the devices was low. Furthermore, TiO_2 also worked as a hole blocking layer due to its HOMO was much lower than that of QDs. Finally, the TiO_2-based QD-LEDs exhibited low turn-on voltage (~2.0 V), high luminance (12380 $cd \cdot m^{-2}$), and high power efficiency (2.41 $lm \cdot W^{-1}$). Further progress was achieved by Qian and co-workers using ZnO nanoparticles thin film instead of TiO_2. As compared to TiO_2, ZnO has even higher electron mobility and lower band offset to Al electrode. The device performance was further improved in term of maximum luminance for blue, green and orange-red QD-LEDs as high as 4200 $cd \cdot m^{-2}$, 68000 $cd \cdot m^{-2}$, and 31000 $cd \cdot m^{-2}$, respectively.

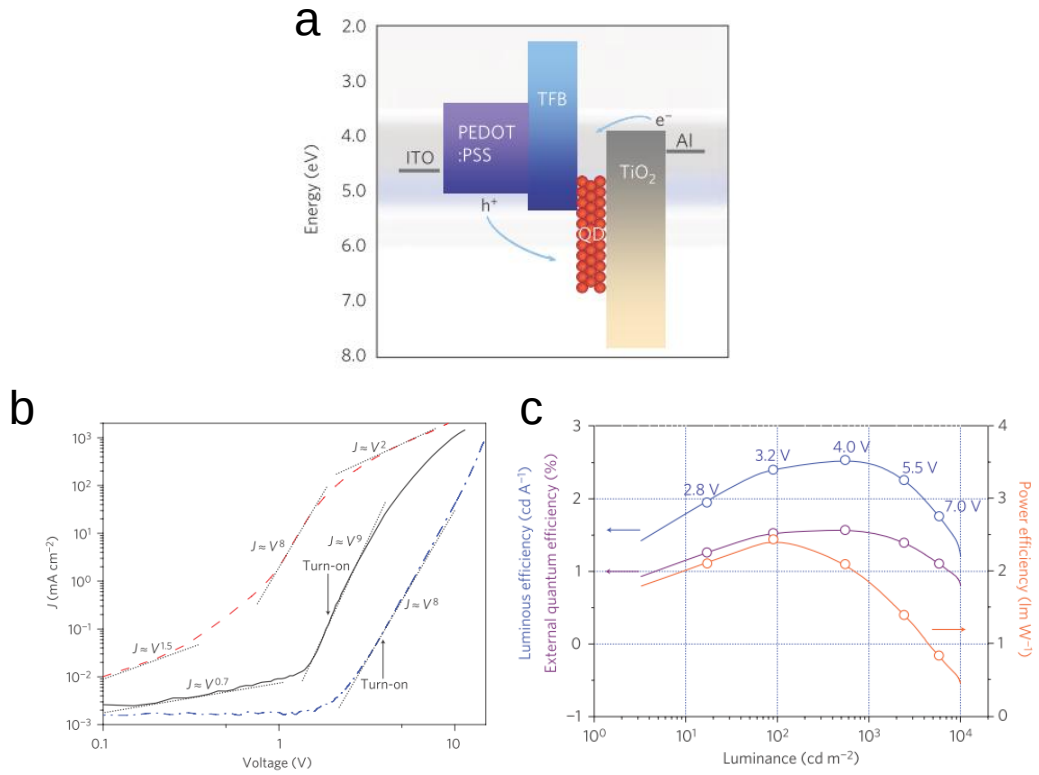

Fig. 2-7 QD-LEDs with TiO_2 as the electron transport layer. **a**. Energy band diagram of QD-LEDs with sol-gel synthesized TiO_2 ETL. **b**. Current density (J) *vs.* voltage (V) characteristics of the QD-LED with TiO_2 ETL (black solid line), the QD-LED with Alq_3 ETL (blue dash dot line), and the control device of TiO_2-based QD-LED without QDs layer (red dash line). **c** Luminous efficiency, external quantum efficiency, and power efficiency as a function of luminance. Reprinted by permission from Macmillan Publishers Ltd: Nature Photonics [50], copyright (2009).

In addition to QD-LEDs with monochromatic emission, QD-based white color light-emitting devices were also attracted much attention due to their potential applications, *e.g.*, display backlighting.[61, 62] Since QDs exhibit tunable emission colors covered almost full visible range by tailoring their size, white color can be obtained by simply mixing red, green, and blue QDs with balanced ratio. Anikeeva *et al.* from MIT reported white EL from a mixed monolayer of Cd-based blue-, green-, and red-emitting QDs in a hybrid QD-LEDs (Fig. 2-8).[61] The emission color of the devices could be precisely tuned by alternating the mixed ratio of different color-emitting QDs.

The optimized white QD-LEDs exhibited uniform white light emission with the Commission Internationale de l'Eclairage (CIE) chromaticity coordinates of (0.35, 0.41) at an applied forward bias of 9 V. The highest EQE of the QD-LED was obtained as 0.36 % with bias of 5 V.

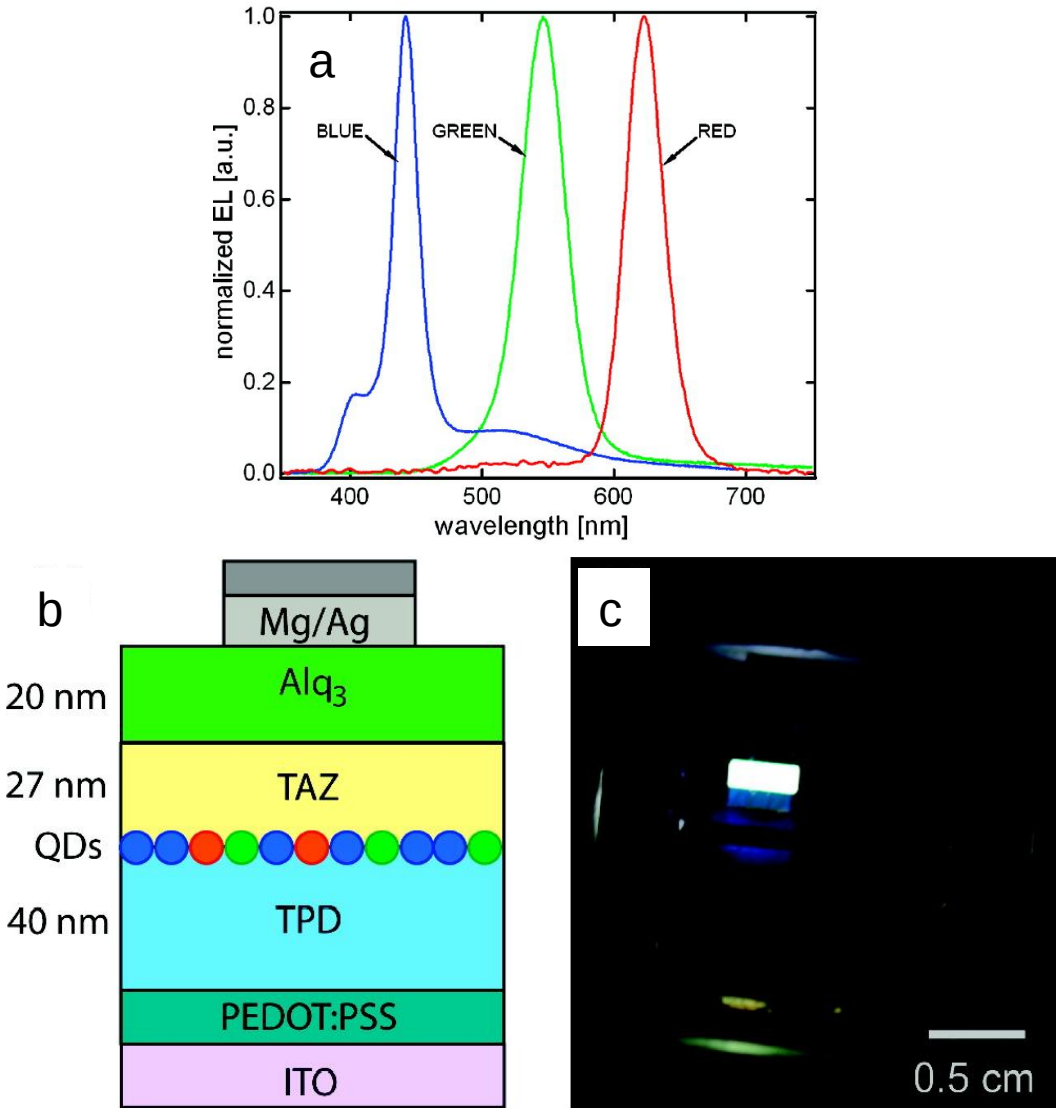

Fig. 2-8 White QD-LED utilizing a mixed monolayer of red-, green-, and blue-emitting QDs. **a**. Normalized EL spectra of devices with only blue-, green-, and red-emitting QDs. **b**. Schematic structure of the QD-LEDs with TPD as HTL and TAZ:Alq_3 as ETL. **c**. A photograph of device under operation of 10 V. Reprinted with permission from [61]. Copyright (2007) American Chemical Society.

Instead of color mixing from different QDs, white light emission from hybrid organic materials and inorganic QDs were frequently studied.[62-74] Li *et al.* reported white hybrid organic-inorganic LEDs combining emission from host matrix (blue-emitting polymer, poly[(9,9-dihexyloxyfluoren-2,7-diyl)-*alt-co*-(2-methoxy-5-(2-ethylhexyloxy) phenylen-1,4-diyl)], PFH-MEH), ETL (green-emitting organic material, Alq_3) and red-emitting QDs.[62] The device showed fairly pure white color with CIE coordinates of (0.30, 0.33) and maximum EQE of 0.24 %. Recently, similar work based on poly-TPD incorporated with InP/ZnS core/shell QDs showed uniform white emission with CIE coordinates of (0.332, 0.338) and luminance of 270 $cd \cdot m^{-2}$.[74]

As mentioned above, the development of QD-LEDs largely relied on Cd-based QDs. The toxicity of Cd is the main obstacle for QD-LEDs to be commercialized. To address this issue, one of the possible attempts is to develop highly luminescent QDs based on non-toxic or less toxic elements, *e.g.*, InP, ZnS, $CuInSe_2$, Si NCs, and ZnO.[75-87] However, the efficiencies of QD-LEDs based on these materials are still much lower than Cd-based QD-LEDs.

2.2 Polymer/ZnO QDs Nanocomposites: Preparation, Photoluminescence (PL) Properties and Applications

Zinc oxide (ZnO), a II-VI semiconductor, has a direct wide band gap of 3.2-3.3 eV and a relatively large exciton binding energy of 60 meV at room temperature.[88-90] It has attracted lots of interest and also been widely studied in the past decades, especially the formation of nanostructures. Among various ZnO nanomaterial morphologies,

such as nanowires[91-94], nanorods[95-98], tetrapods[99-101], nanobelts[102-104] and nanoparticles[88, 105-108], ZnO nanoparticles (also termed as nanocrystals, NCs; quantum dots, QDs) are considered as a promising multifunctional material in the future due to its unique properties and potential applications in electronic and optoelectronic devices.[87, 109-120]

The most widely used synthetic method for ZnO QDs is sol-gel synthesis, in which zinc precursor is hydrolyzed in a base alcoholic solution to form ZnO QDs.[121-123] The obtained ZnO QDs usually exhibit a typical visible emission at 500-570 nm shown as green-yellow. The origin of this visible emission is widely known as defect-related electron-hole recombination. However, the actual mechanism is still controversial even after decades of study. Oxygen vacancies (V_O) are considered to be the main reason of defect emission, this issue is especially important in the QDs system due to its large surface-to-volume ratio. However, colloidal ZnO QDs prepared by sol-gel method are not stable in the mother-liquor because of Ostwald ripening and agglomeration effect. Therefore, the optical properties, such as UV-VIS absorption and photoluminescence spectra, are redshifted as the quantum confinement effect is suppressed on the larger particles. Meanwhile, the emission intensity of ZnO QDs is also quenched significantly.

By applying surface modification on ZnO QDs, the small nano-scale particles are effectively prevented from spontaneous growth and aggregation. Up to now, research attempts have been made to modify the surface of ZnO QDs, *e.g.*, inorganic shells (such as SiO_2), organic ligands, and polymers.[124-133] It has been proved that coating ZnO QDs with polymers is a simple and effective way to realize surface modification. The as-prepared polymer/ZnO QDs nanocomposites are more stable in

photoluminescence properties. Furthermore, the QDs exhibit less aggregation in solution when comparing to the sol-gel synthesized QDs. The functional groups of polymer matrices can have great impact on tuning the properties of the nanocomposite due to the presence of synergistic interaction.

2.2.1 Preparation of Polymer/ZnO QDs Nanocomposites

The preparation methods for polymer/ZnO QDs nanocomposites can be classified into two categories: (1) physical blending method; (2) chemical reaction method.

2.2.1.1 Physical Blending Method

Physical blending, as the most commonly used method, is also known as one of the simple way to prepare nanocomposites with inorganic nanomaterials embedded in polymers. In order to synthesize polymer/ZnO QDs nanocomposites, two synthetic routes are generally used: (1) synthesize ZnO QDs in the present of polymer; (2) mix sol-gel synthesized ZnO QDs with polymers in solution.

For the former method, zinc precursor is firstly mixed with polymer solution which requires polymer and zinc precursor to be dissolved in a common solvent. Zinc acetate, the most widely used zinc precursor for ZnO QDs synthesis, is normally dissolved in alcoholic solvent, *e.g.*, methanol, ethanol, and isopropyl alcohol. Therefore, alcohol-soluble polymers are required for synthesizing the nanocomposites. Zinc precursor is hydrolyzed by alkali solution in the presence of polymer and followed by solvent evaporation. Guo et al synthesized ZnO QDs in poly(vinyl pyrrolidone) (PVP) ethanol solution.[129, 134] Abdullah et al. synthesized PEG/ZnO QDs nanocomposite by mixing alkaline polymer solution with zinc precursor solution for ZnO to form inside polymer matrix.[135]

In the latter method, a two step synthetic approach is adopted. Firstly, the ZnO QDs were pre-synthesized and subsequently, mixed with polymer in solution. In this case, ZnO QDs are just redispersed in polymer solution. Therefore, it does not require a common solvent for both QDs and polymer. Neves *et al.* reported synthesis of nanocomposite with ZnO QDs embedded poly[2-methoxy-5-(2-ethylhexyloxy)-1,4-phenylenevinylene] (MEH-PPV) for light-emitting application.[136] Some other ZnO QDs nanocomposites based on different polymers were also synthesized by this method.[137-147]

By using this physical blending method to synthesize polymer/ZnO QDs nanocomposites, the polymers and ZnO QDs are connected *via* Lewis acid-base interactions, static interactions or van der Waals forces. Owing to the surface free energy of the nanoparticles, ZnO QDs tend to aggregate, which makes them difficult to reach a homogeneous dispersion by using physical blending method. The best way to reduce aggregation of ZnO nanoparticles in polymer matrices is to carry out surface modification of ZnO nanoparticles before mixing with polymer solution. Immobilizing organic ligands on the ZnO QDs surface could decrease the interparticle attraction and therefore, it is an effective way in tackling the agglomeration issue. For example, Khrenov *et al.* synthesized hydrophobic ZnO nanoparticles stabilized by amphiphilic copolymers, and embedded them into PMMA matrix for UV-absorptive coating.[148]

2.2.1.2 Chemical Reaction Method

Chemical reaction method can be used to synthesize nanocomposites with stronger interactions between polymers and ZnO QDs because of creation of chemical bond, making the synthesized nanocomposites more stable.

In the typical reaction procedures, monomers are used to react with surface modified ZnO QDs *via* ligand exchange process. After that, polymer/ZnO QDs nanocomposites can be obtained as monomer is polymerized and simultaneously coated on the outer surface of ZnO QDs. Alternatively, the formation of ZnO QDs *via* the sol-gel method and the polymerization processes can occur concurrently to yield high quality polymer/ZnO QDs nanocomposites. This method is usually applicable to those polymers that can readily undergo polymerization, such as polystyrene (PS), poly(methyl methacrylate) (PMMA), poly(hydroxyethyl methacrylate) (PHEMA), and so on.[131, 132, 149-156]

Taking PMMA as an example, Xiong *et al.*[132] firstly used methacrylate anion (MAA) to modify the surface of ZnO QDs and dispersed the modified QDs in methyl methacrylate (MMA) monomers solution. Polymerization occurred when the temperature was increased to 60^{o}C. For further polymerization, $K_2S_2O_4$ (initiator) together with the mixture of MMA and ZnO QDs were added into boiling water. After refluxing, PMMA/ZnO QDs nanocomposite was obtained and the final products exhibited strong blue fluorescence under UV illumination. Using the same procedures, PS/ZnO QDs nanocomposite was obtained by replacing MMA with styrene monomer. In the work, ZnO QDs were reportedly to be homogenously dispersed in both PMMA and PS matrices.

In another work by Zhang *et al*. and Huang *et al*. on the synthesis of PS and PHEMA based nanocomposites reported, 3-trimethoxysilylpropyl methacrylate (TPM) was coated onto surface of ZnO QDs.[155, 156] Both of the obtained nanocomposites showed strong luminescence because of the homogeneous dispersion of ZnO QDs in polymer matrices.

2.2.2 Photoluminescence (PL) Property of Polymer/ZnO QDs Nanocomposites

As mentioned above, ZnO is a good light-emitting material with emission at UV and visible range. The visible emission is known to be originated from defect related to oxygen vacancies. For ZnO QDs which have large surface-to-volume ratio, the surface defect has significant influence on the photoluminescence properties. The polymers can influence the luminescence of ZnO QDs in two aspects: (1) polymers passivate the surface of ZnO QDs and thus, the nanocomposites exhibit enhanced UV emission and their visible emission is quenched; (2) polymers protect the ZnO QDs surface defect and enhance the visible emission from the nanocomposites. In addition, when embedding ZnO QDs in light-emitting polymer matrix, the emission from both QDs and polymers will interfere with each other.

2.2.2.1 Polymer/ZnO QDs Nanocomposite with Enhanced UV Emission

In the early attempts to synthesize polymer/ZnO QDs nanocomposites, Guo *et al.* used poly(vinyl pyrrolidone) (PVP) as the capping polymer to modify the surface of ZnO QDs *via* physical blending method.[129, 134] The as-prepared nanocomposite exhibited strong UV emission and its visible emission was significantly quenched in comparison with the uncapped ZnO QDs. The PL spectra of non-modified and PVP-modified ZnO QDs as well as the UV-VIS absorption were shown in Fig. 2-9. In the presence of PVP, ZnO QDs with smaller size were synthesized, which could be seen from the onset of UV-VIS absorption spectra. Moreover, monodispersed ZnO QDs corresponding to narrow full width at half maximum (FWHM ~27 nm) were achieved by surface modification. It was confirmed that the visible emission was originated from the surface defect of ZnO QDs which was also known as oxygen vacancies.

However, the surface passivation effect was not completely effective as the defect emission could be seen from the PL spectrum of PVP-modified ZnO QDs. It should be mentioned that PVP itself had a strong blue emission which could overlap with the emission from ZnO QDs when the content of PVP was high enough in the nanocomposite.[157] Similar conclusions were also obtained in the works involving polyaniline and poly(vinyl alcohol) based nanocomposites with embedded ZnO QDs.[158-160]

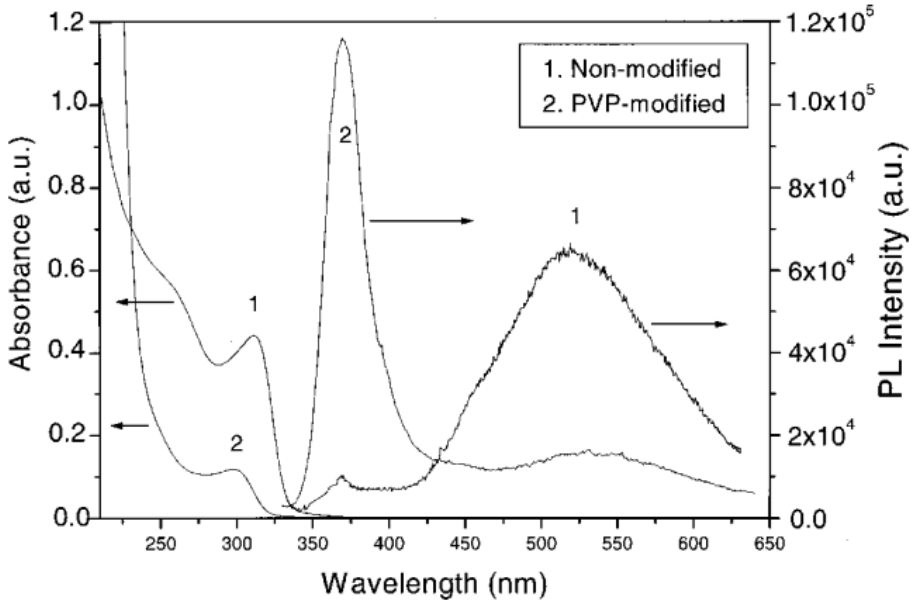

Fig. 2-9 Optical absorption and photoluminescence spectra of non-modified and PVP-modified ZnO QDs. Reprinted with permission from [129]. Copyright (2000) American Institute of Physics.

Sun and co-workers mixed ZnO QDs, α-zirconium phosphate nanoplatelets and poly(methyl methacrylate) (PMMA) in acetone, and then evaporated the solvent to obtain nanocomposite.[147] The nanocomposite was further dried in ambient atmosphere at 120^{o}C overnight to remove the residual solvent. The as-prepared PMMA/ZnO QDs nanocomposite showed only singly strong UV emission and the surface defects were fully passivated by PMMA during heat treatment. It was also

found that increasing the concentration of ZnO QDs would lead to redshift in PL emission peak position. Such phenomenon was explained to be due to the coupling effect between QDs, *i.e.*, when two QDs were close enough with each other, dipole-dipole interactions between closely contacted QDs led to quantum tunneling.[161] Zhang *et al.* reported the time effect of heat treatment on the PL emission of nanocomposite and found that UV emission was increased while visible emission decreased.[152]

Peng *et al.* reported ZnO nanoparticles with their surface modified by poly[poly(ethylene glycol) methyl ether monomethacrylate] (PPEGMA) *via* surface-initiated atom transfer radical polymerization (ATRP).[153] The nanocomposite showed only UV emission. They proposed that the surface of ZnO nanoparticles were grafted by polymer that helped to reduce the defect concentration.

In summary, when the interactions between ZnO QDs and polymers were weak, the surface defects could be passivated by polymers and lead to quenching of the visible emission. On the contrary, the UV emission of ZnO QDs was enhanced. Normally, polymer/ZnO QDs nanocomposites prepared *via* physical blending method showed only strong UV emission. Also, it was found annealing effect would lead to better coverage of polymers on the surface of ZnO QDs which also improves UV emission and reduces visible emission.

2.2.2.2 Polymer/ZnO QDs Nanocomposite with Strong Visible Emission

ZnO is a defect-rich semiconductor that always show strong defect related emission at visible region.[88, 89, 162] Although defect-related emission in the visible range has been studied for decades, the mechanism is still controversial. Generally, defect related to oxygen vacancies (V_O) is believed to be one of the possible origins of defect

emission. Recently, Xu *et al.* reported tunable color emission from sol-gel synthesized ZnO QDs with different size.[163] The size-dependent PL and PLE spectra exhibiting the visible emission was attributed to the recombination of electrons from the conduction band to certain deep trapped holes. Therefore, besides UV emission from polymer/ZnO QDs nanocomposites discussed above, visible emission originated from defect is also widely reported.[132, 134, 135, 140, 155, 164-166] In some cases, the nanocomposites even only show visible emission with different color from blue to orange. For this type of nanocomposites, surface defect of ZnO QDs is protected by the polymer and thus, the visible emission is enhanced and much more stable in comparison with non-modified ZnO QDs.

Xiong and co-workers synthesized ZnO QDs in a double-layer of polymer which had a hydrophobic PMMA layer inside and hydrophilic poly(ethylene glycol methyl ether) (PEGME) layer outside.[154] Additionally, a layer of methacrylic acid (MAA) was applied to modify the surface of ZnO QDs and protect the surface defect. As-prepared nanocomposites showed green and yellow color with different size and were used for cell labeling (Fig. 2-10). They also synthesized PMMA and PS based nanocomposites *via* chemical reaction method.[132, 166] Similar work was also reported by Li *et al.* for bulk PMMA/ZnO QDs nanocomposite structure.[131] All these samples showed blue emission with high quantum yield of more than 50 %. Moreover, TPM-modified ZnO QDs were used for synthesizing PHEMA-based nanocomposite and the bulk material exhibited strong blue luminescence because of better confinement on the nanoparticle size.

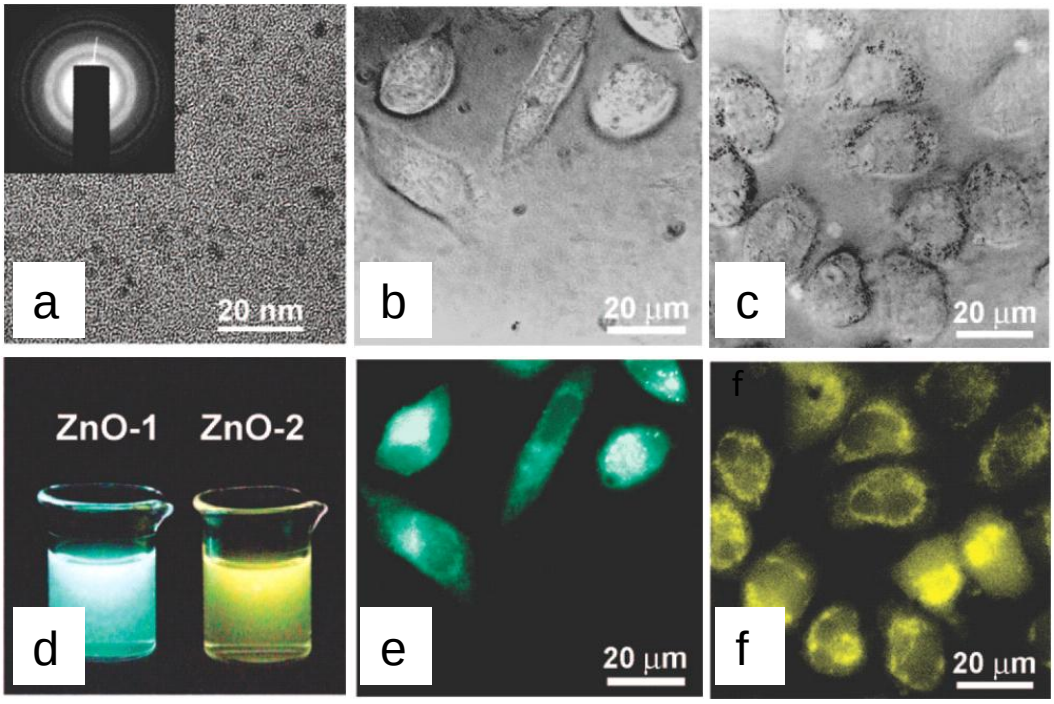

Fig. 2-10 PEGMEMA modified ZnO QDs and the application for cells labeling. **a**. TEM image of ZnO QDs in polymer matrix with ED pattern (inset). **b**, **c**. two differential interface contrast pictures of living cancer cells labeled by ZnO-1 and ZnO-2 respectively. **d**. photo of ZnO@polymer aqueous solutions under a UV lamp. **e**, **f**. two confocal microscope images of cells labeled by ZnO-1 and ZnO-2, respectively. Reprinted with permission from [154]. Copyright (2008) American Chemical Society.

2.2.2.3 Polymer/ZnO QDs Nanocomposite with Luminescent Polymers

In the case that light-emitting polymers with ZnO QDs incorporated, the PL intensity of polymers normally decreased due to excitons transportation from polymers to ZnO QDs. Wang et al. reported mixing ZnO nanoparticles in PPV/PVA composite film to form nanocomposite; the luminescence of PPV was quenched significantly.[167] Increasing the content of ZnO in the nanocomposite further reduced the intensity of PPV photoluminescence. It was ascribed to the excitons separation at the interface between PPV chain and ZnO. Similar conclusion was also drawn by Ton-That and co-workers by incorporating ZnO QDs with MEH-PPV for solar cell application.[168] In

comparison with polymers luminescence, ZnO emission was still relatively weak in the nanocomposites.

2.2.2.4 Summary

In general, surface state is considered to be the main factor that determines visible emission of ZnO QDs, because emission originates from recombination related to defects which are mainly located on the surface of nanoparticles. On one hand, by simply capping the polymers onto the surface of QDs without chemical bond, the surface passivation effect reduces the defect concentration; thus, the defect related visible emission from ZnO QDs is quenched. Correspondingly, the UV emission originated from free exciton recombination is improved. On the other hand, coordination between ZnO QDs and functional groups can protect the surface defect by forming strong chemical bond. Further protection of defect states can be achieved by surface modification by polymers, resulting in strong visible emission from. as-prepared polymer/ZnO QDs nanocomposites. The emission color can be tuned by varying the size of QDs. Moreover, incorporation of ZnO QDs inside light-emitting polymers to form nanocomposites normally usually reduces the luminescence intensity of polymers, due to exciton separation at the interface. These above phenomena can be utilized to realize the potential applications of nanocomposites in solar cells and photodetectors.

It should be emphasized that the interactions between polymers and ZnO QDs are sensitive by the nature of two components and the preparation process. Therefore, nanocomposites with same compositions may exhibit quite different photoluminescence properties.

2.2.3 Applications of Polymer/ZnO QDs Nanocomposites

After surface modification of polymers, ZnO QDs will show higher quantum yield and better stability in ambient atmosphere; in comparison with bare ZnO QDs. Moreover, the emission color can also be tuned by changing its size. Therefore, polymer/ZnO QDs nanocomposites can be used for optoelectronic applications. White light-emitting devices based on PVK/PMMA/ZnO QDs nanocomposite was reported recently.[86] With an applied bias on the ITO/PEDOT:PSS/PVK/ZnO QDs/Al devices, white color emission, that mixed red, green, and blue lights, was observed from the glass window. The emission was ascribed to carrier recombination at the interface of PVK and ZnO QDs.

Besides being utilized to prepare nanocomposites with excellent photoluminescence properties, polymers also modify the surface functional states of QDs and improve the compatibility of ZnO QDs in solvents. It allows the QDs to be redispersed in different solvents to form a homogeneous solution. Fig. 2-10(d) showed the ZnO QDs with surface modification using PEGMEMA are well dispersed in water.[154] Therefore, it is possible to use this type of nanocomposite in cell labeling application; more examples are included in Fig. 2-10(b, c, e, and f).

Due to homogeneous dispersion of ZnO QDs in polymer matrices, the nanocomposites show optical transparency under normal illumination but emit different colors under UV illumination. Strong absorption at UV region makes bulk nanocomposites very good UV-shielding materials.[131, 151] The UV light absorbance in the range from 290 nm to 370 nm can reach 98 % with only 0.1 wt % ZnO nanoparticles in nanocomposite.[169]

Further study is still needed to investigate the mechanism of photoluminescence from polymer/ZnO QDs nanocomposites and to have better control on their luminescent properties. Nevertheless, there is no doubt that such polymer/ZnO QDs nanocomposites have promising potential and many more novel applications.

2.3 Summary

In this chapter, a literature review has been presented from mainly two aspects. First of all, the concept and mechanisms of QD-based light-emitting devices have been introduced. The key breakthrough in the development of QD-LEDs has also been reviewed and discussed. In addition, the main challenges for commercializing QD-LEDs have been given. In the second part, nanocomposites of surface modified ZnO QDs by polymers have been reviewed. The optical properties, especially photoluminescence properties, have been discussed in details based on the possible mechanisms of light emission process. The potential applications that can utilize polymer/ZnO QDs nanocomposites have also been summarized.

3. Preparation of PMMA/ZnO QDs Nanocomposite and Its Optical Properties

3.1 Introduction

Nanocomposites utilizing ZnO QDs dispersed in polymer matrices have been studied for decades.[134, 154, 164, 170, 171] This trend is mainly caused by the favorable ZnO properties and potential applications for electronic and optoelectronic devices, including field effect transistors (FETs), photodetectors, solar cell, and light-emitting devices (LEDs).[119, 172-180] Examples of the polymers commonly utilized as matrices are PMMA, PS, PEG, PVP, etc.[133, 135, 142, 147, 181-183] Specifically for poly(methyl methacrylate) (PMMA), it is a good dielectric medium that has high optical transparency over the whole visible range. Therefore, it has been widely studied as the host matrix for the nanocomposite.[131-133, 139, 151, 164-166, 181]

However, synthesis of nanocomposite with homogeneous dispersion of uniform size ZnO QDs in PMMA matrix is still a challenge. Physical blending method, *i.e.*, mixing pre-prepared ZnO QDs with PMMA in a common solvent, usually cause aggregation of QDs in the polymer matrix.[184-186] In order to avoid agglomeration of ZnO QDs in the nanocomposite, chemical reaction method, *e.g.*, *in situ* sol-gel synthesis of QDs and polymerization of methyl methacrylate monomer (MMA), has also been widely studied.[131, 151, 166, 187] However, the chemical reaction method is somewhat

complicated and involves many chemicals and synthesis steps. In addition, chemical reaction method usually gave large-scale material after polymerization, which restricts potential applications for optoelectronic devices (*e.g.*, LEDs) that require nanocomposite thin film.

In this chapter, a new and facile method, which is described as 'polymerothermal' method, was proposed to synthesize PMMA/ZnO QDs nanocomposite. During the precursor decomposition stage; conversion to QDs took place in purely polymer medium that is literally without any solvent. The objective of this project is to fabricate light-emitting devices based on the nanocomposite. Therefore, high concentration of ZnO QDs in polymer matrix thin film is desirable for higher intensity. As suggested by Sun *et al.*, a typical thin film thickness should be about 20 nm for QDs emission layer in QD-LEDs.[21] Therefore, in this work, the as-prepared nanocomposite thin film was firstly characterized by atomic force microscopy (AFM) for studying the thickness and surface morphology. Other techniques which are UV-VIS absorption spectroscopy and photoluminescence (PL) were also used to characterize the optical properties of nanocomposite. With a detailed analysis on the experimental results of optical properties, relationship between the combined band structures and PL emission was discussed; the possible PL mechanism was also proposed.

3.2 Experimental Details

3.2.1 Materials

Zinc acetate dehydrate ($Zn(Ac)_2 \cdot 2H_2O$, ≥ 99.0 %), poly(methyl methacrylate) (PMMA, M_w = 120,000 $g \cdot mol^{-1}$, ≤ 2.0 % toluene), anisole ($CH_3OC_6H_5$, anhydrous, ≥ 99.7 %)

were purchased from Sigma Aldrich and used without purification. Methanol (CH_3OH, HPLC grade, ≥ 99.9 %)) was purchased from Fisher Scientific.

3.2.2 Preparation of PMMA/ZnO QDs Nanocomposite

The preparation procedures of 'polymerothermal' method could also be found in our previous report.[188] Typically, a solid sample of $Zn(Ac)_2{\cdot}2H_2O$ was dissolved in methanol with assistance of ultra-sonication. The concentration of $Zn(Ac)_2{\cdot}2H_2O$ were controlled at 1 $mg{\cdot}ml^{-1}$, 2 $mg{\cdot}ml^{-1}$, 5 mg and 10 $mg{\cdot}ml^{-1}$. The solvent for dissolving PMMA was anisole and the concentrations were controlled at 2 $mg{\cdot}ml^{-1}$, 5 $mg{\cdot}ml^{-1}$ and 10 $mg{\cdot}ml^{-1}$. Compared to $Zn(Ac)_2{\cdot}2H_2O$, the dissolution process for PMMA took much longer time. In order to accelerate dissolving of PMMA in anisole, the mixture was firstly ultra-sonicated for 30 mins; followed by stirring at 50 ^oC for 10 mins. After cooling, the transparent PMMA solution was obtained. All the solutions were stored at room temperature after preparation.

The mixing process of above two solutions was carried out by adding $Zn(Ac)_2{\cdot}2H_2O$ solution into PMMA solution dropwise under vigorous stirring. The volume ratio was controlled as 1:10 ($Zn(Ac)_2{\cdot}2H_2O$ solution : PMMA solution). It was found that the thin films were not uniform *via* spin-coating when the volume ratio was increased to 2:10. This issue might be due to the poor solubility of PMMA in methanol. The mixtures were stirred overnight for homogenous mixing and stored as the stock precursor solutions. For the one with higher concentration of zinc precursor, such as 20 $mg{\cdot}ml^{-1}$ of zinc acetate, transparent precipitation that separated out from the stock precursor solutions was observed because of poor miscibility. The solutions containing PMMA and zinc precursor were spin-coated or drop-casted on different substrates for characterizations. The thin film samples were transferred to a conventional oven for

heat treatment under 160 ^{o}C, 180 ^{o}C and 200 ^{o}C. In fact, the thermal decomposition process of zinc precursor was relatively slow or even not occurred when the temperature lower than 200 ^{o}C was applied (to be discussed later). Therefore, the nanocomposite with ZnO QDs embedded in PMMA matrix was prepared with heat treatment at 200 ^{o}C for different time.

3.2.3 Characterization of PMMA/ZnO QDs Nanocomposite

Atomic force microscopy (AFM) images of the nanocomposite thin films were collected from Veeco Dimension 3100. Fourier transform infrared (FTIR) transmission spectra of the nanocomposite were measured *via* Frontier FT-NIR/MIR Spectrometers. X-ray diffraction (XRD) measurements were performed using Shimadzu X-ray diffractometer with a CuK_{α} radiation source with λ = 1.54 Å. The XRD samples were prepared on glass slides and scanning was carried out in the 2θ range of 20^{o} – 70^{o} at scan speed of 2 $^{o}\cdot min^{-1}$. The ultraviolet-visible (UV-VIS) absorption spectra were measured with a Shimadzu UV-2501PC spectrophotometer and the films were prepared on quartz substrates. The photoluminescence (PL) spectra were measured with a Nanometrics RPM2000 Rapid Photoluminescence Mapper and all the samples were prepared on Si wafer. The excitation wavelength for PL measurements is 325 nm from He-Cd laser. Transmission electron microscopy (TEM) images and the SAED pattern were collected from JEOL JEM-2010 or JEOL JEM-2100F under operation voltage of 200 kV.

3.3 Results and Discussion

3.3.1 Thickness and Surface Morphology of Nanocomposite Thin Film

The thickness and surface morphologies of spin-coated nanocomposites thin films were measured using AFM. Fig. 3-1(a) shows the thickness of PMMA and the nanocomposites thin films prepared by spin-coating solutions with different concentrations at 3000 rpm for 60 s. The thickness increases from 4 nm to 19 nm when the concentration of PMMA increased from 2 $mg{\cdot}ml^{-1}$ to 10 $mg{\cdot}ml^{-1}$. The thickness of the nanocomposite thin films is thinner than that of pure polymer thin films at the same spin speed, because thickness is mainly affected by the concentration of polymer which became diluted when zinc precursor solution was added. Fig. 3-1(b) shows the thicknesses of PMMA/ZnO QDs nanocomposite thin film prepared at different spin speed varying from 1000 rpm to 3000 rpm with the same PMMA concentration of 10 $mg{\cdot}ml^{-1}$. The thin film thickness increases from 19 nm to 28 nm when the spin speed decreases. As mentioned previously, the optimum thickness of thin film for light-emitting application is about 20 nm. Therefore, the thickness of the sample with the highest concentration (*i.e.*, 10 $mg{\cdot}ml^{-1}$) studied here is closer to the desired value. Furthermore, the surface morphologies of the as-prepared PMMA/ZnO QDs nanocomposites thin films *via* thermal decomposition were measured by AFM; the images are shown in Fig. 3-2. The AFM images clearly indicate that, at the same concentration of PMMA, increasing concentration of $Zn(Ac)_2{\cdot}2H_2O$ in the precursor solution causes a rougher surface and larger nanoparticles found on the thin film surface. This phenomenon was observed because the heat treatment temperature used for decomposition of zinc acetate into ZnO (200 ^{o}C; TGA analysis is shown in

Appendix - I.) was higher than the glass transition temperature of PMMA (T_g: 85 ^oC ~ 165 ^oC). In this case, solid polymeric chain movement took place. Therefore, ZnO seeds could not be well confined by the polymer chain. It is worthwhile to mention that zinc acetate was selected as the precursor as it has a relatively lower decomposition temperature as compared to other conventional zinc complexes. Furthermore, ideally the precursor decomposition temperature cannot be not too much higher than the polymeric T_g, as excessive chain movement may result in QDs aggregation. After the nucleation process, the seeds could grow as the nearby zinc precursor diffused towards and attach to them. However, too high the concentration of zinc precursor caused undesirable large nano-particles which could even be phased out from the PMMA thin film. On the other hand, at fixed concentration of zinc acetate, increasing the PMMA concentration gave smoother surface because of better confinement of ZnO QDs in thicker PMMA films.

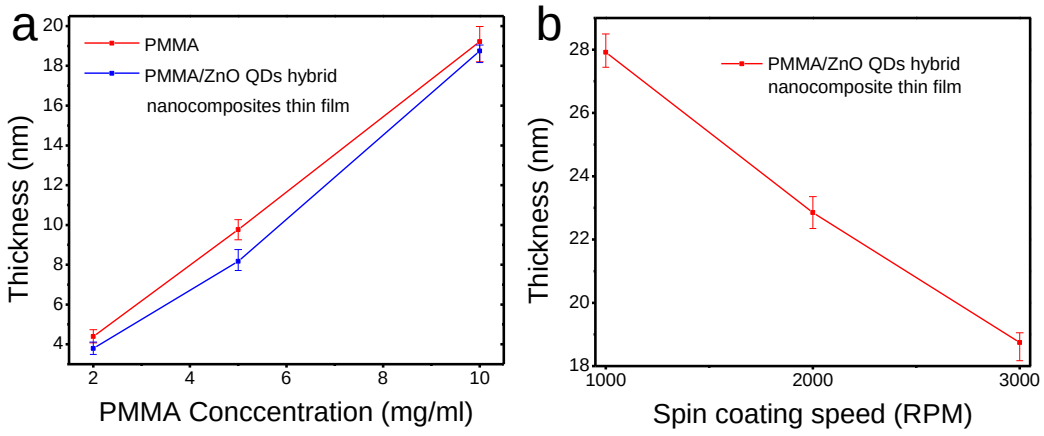

Fig. 3-1 Relationship between thin film thickness and polymer concentration as well as spin speed. **a**. Thickness of pure PMMA thin films and PMMA/ZnO QDs nanocomposite thin films with different concentrations of polymer. The spin speed was 3000 rpm for all samples. **b**. Thickness of nanocomposite thin film obtained *via* spin coating technique with different spin speed. Both polymer and zinc precursor concentration were 10 $mg \cdot ml^{-1}$ and volume ratio was controlled as 10 to 1.

For light-emitting application, both surface roughness of thin film and QDs concentration in the matrix are critical parameters that determine the device performance. From AFM studies (Fig. 3-2), it shows that the surface morphologies of thin films are seriously influenced by the concentrations of both PMMA and zinc precursor solutions. With higher concentration of zinc precursor solution, large particles are separated out from the thin film. The bright dots indicate the ZnO particles on the surface of thin film, while the shadows next to them were obtained when the AFM tip scanned over the large particles and it resulted in the flat area that appeared to be lower than the normal area. After comparison, it leads us to select the thin film prepared using mixture 10 $mg \cdot ml^{-1}$ PMMA solution with 10 $mg \cdot ml^{-1}$ $Zn(Ac)_2 \cdot 2H_2O$ solution at volume ratio of 10 : 1. The selected thin film is fulfilled the above two parameters the best; and will be used in the subsequent studies.

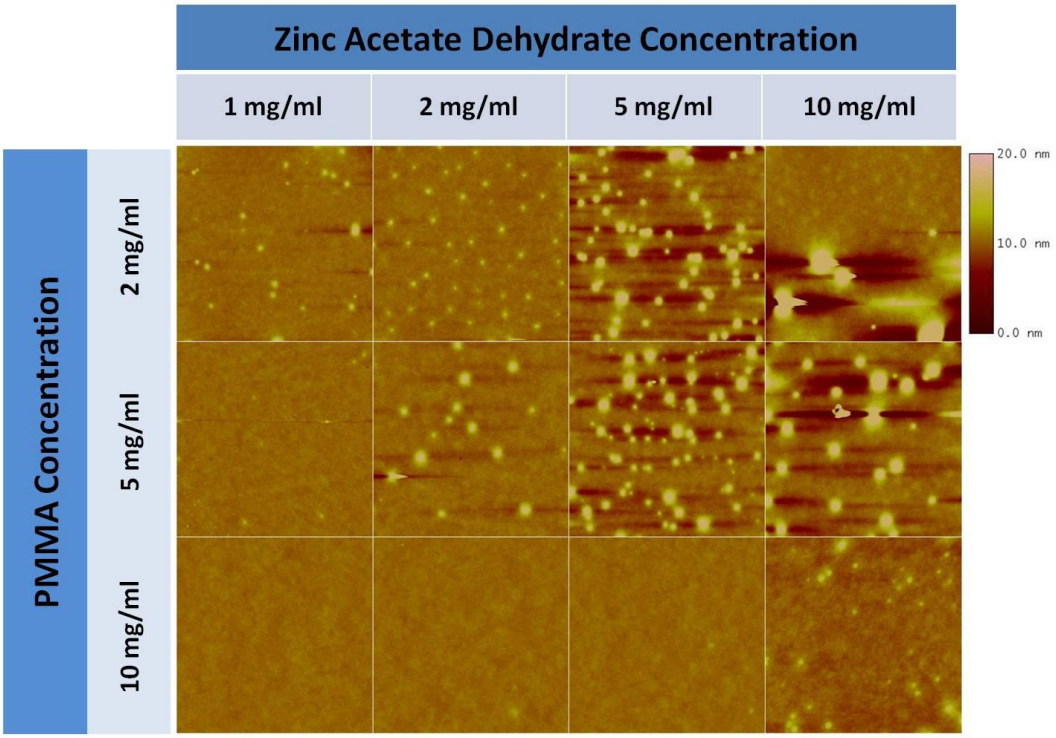

Fig. 3-2 AFM images of PMMA/ZnO QDs nanocomposite thin films with different concentrations of polymer and zinc precursor. The concentrations of PMMA in anisole were controlled as 2, 5, and 10 $mg \cdot ml^{-1}$, while that of zinc acetate in methanol were 1, 2, 5, and 10

$mg \cdot ml^{-1}$. Volume ration between polymer solution and zinc precursor was fixed as 10 to 1. The spin speed for all samples was 3000 rpm for 60 s. The size of each image is 5 μm by 5 μm.

3.3.2 Characterization of ZnO QDs in Nanocomposite

Transmission electron microscopy was conducted to investigate the morphology of ZnO QDs in as-prepared nanocomposites. The lower magnification TEM image shows high-density and well-dispersed ZnO QDs in PMMA matrix, presented in Fig. 3-3(a-b). The bottom-right inset of Fig. 3-3(b) shows the high-resolution TEM (HR-TEM) image of one individual ZnO QD where the lattice spacing is clearly seen; the size of the QD is approximately 4 nm. In addition, the size distribution histogram of ZnO QDs embedded in PMMA matrix is shown in the inset of Fig. 3-3(a). The size distribution of ZnO QDs matches well with the Gaussian distribution and the size is restrictedly less than 7 nm. According to the SAED pattern that is shown in Fig. 3-3(c), the ZnO QDs are polycrystalline in nature and the diffraction rings are well-matched with the referential X-ray diffraction (XRD) pattern of sol-gel synthesized ZnO QDs shown in the inset of Fig. 3-3(c). The formation mechanism of nano-sized ZnO can be explained as follows: in the precursor solution, the much low amount of zinc acetate molecules (compared to PMMA) are surrounded and capped by the long PMMA chain. During the heat treatment process, zinc acetate decomposed and converted into ZnO. The ZnO QDs were inhibited from growing into larger particles because the surface were capped and passivated by PMMA. For comparison, TEM image showing morphology of ZnO QDs synthesized using sol-gel method is included in Fig. 3-3(d); evidencing that the size of ZnO QDs in the nanocomposite is comparable.

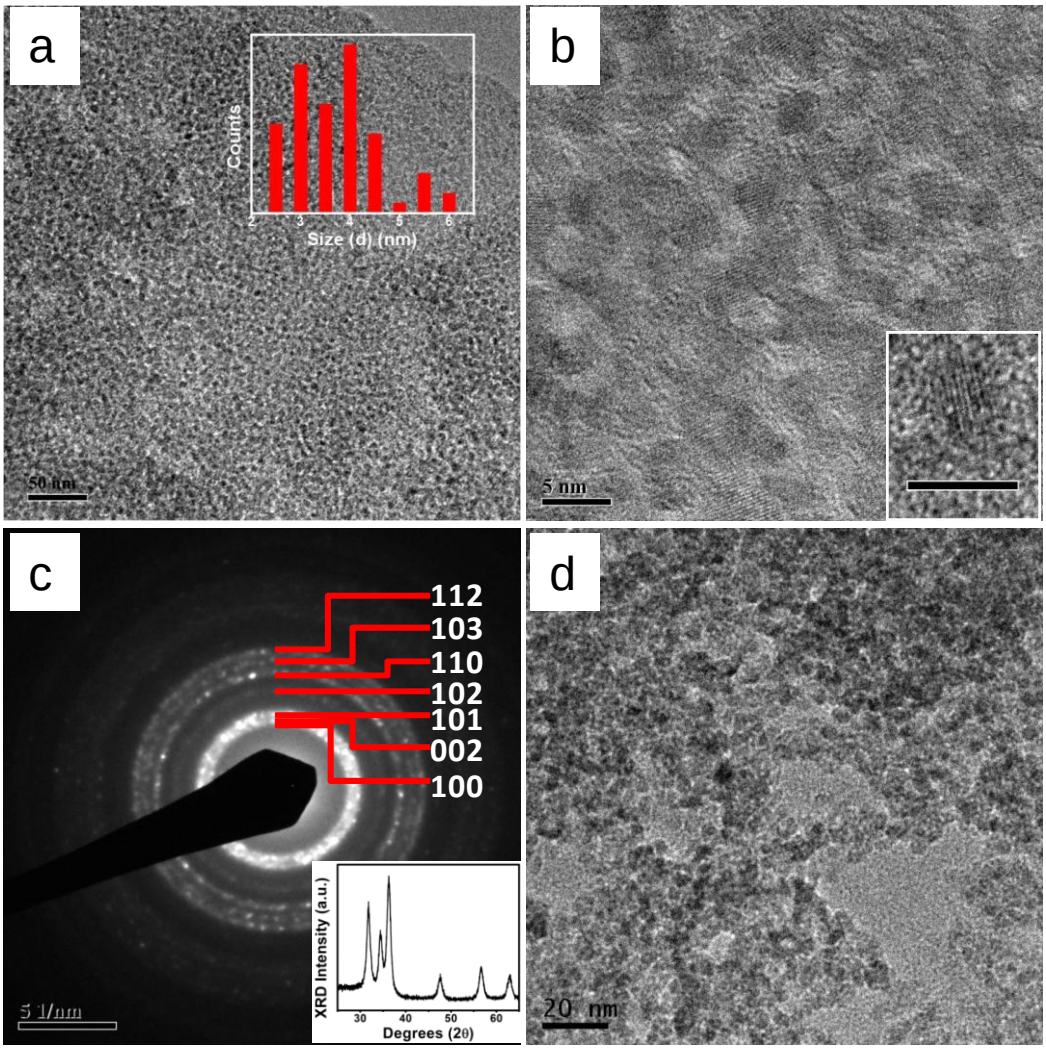

Fig. 3-3 TEM images of ZnO QDs in PMMA host matrix. **a**. ZnO QDs under low magnification. The inset shows the size distribution histogram of ZnO QDs in nanocomposite. **b**. Enlarged TEM image shows lattice spacing of ZnO. The inset presents a HR-TEM image of an individual ZnO QD. The scale bar is 5 nm. **c**. SAED pattern depicts ZnO QDs with polycrystallized structure. The inset is the XRD result of sol-gel synthesized ZnO QDs. **d**. TEM image of sol-gel synthesized ZnO QDs with average size of 5-6 nm.

3.3.3 Optical Absorption Property of PMMA/ZnO QDs Nanocomposite

To further investigate the optical properties of PMMA/ZnO nanocomposites, UV-VIS absorption and PL measurements were performed. The UV-VIS results are shown in Fig. 3-4. For comparison, two types of samples were prepared: i. Pure PMMA (black

curve); ii. PMMA/ZnO QDs nanocomposite (red curve). The UV-VIS absorption spectra of the two samples before (dash dot curve) and after (solid curve) heat treatment at 200 ^{o}C for different time are also shown in the Fig. 3-4(a). For the spectra of pure PMMA without zinc precursor before and after heat treatment, no absorption peaks at the region between 350 nm and 380 nm was observed. It indicates that PMMA has good optical transparency from UV region to the end of visible region and good thermal stability up to 200 ^{o}C without degradation. For the sample of polymer matrix with zinc precursor before heat treatment, its absorption spectrum is almost the same as that of pure PMMA. With increasing time of heat treatment, ZnO related UV absorption emerged; shown as red solid curves in Fig. 3-4(a), indicating the formation of ZnO QDs. Fig. 3-4(b) presents the UV-VIS absorption spectrum of nanocomposite with heat treated for 1 hr. In comparison with ZnO single crystals reported by Pesika *et al.*[189], the absorption onset observed in our nanocomposite has a significant blueshift from 395 nm (3.14 eV) to 378 nm (3.28 eV, the location of pink dash line). Further increasing the annealing time, *i.e.*, 2 hr, redshift of absorption spectrum was observed, indicating the undesirable formation of larger particles or agglomeration of ZnO QDs in nanocomposite.

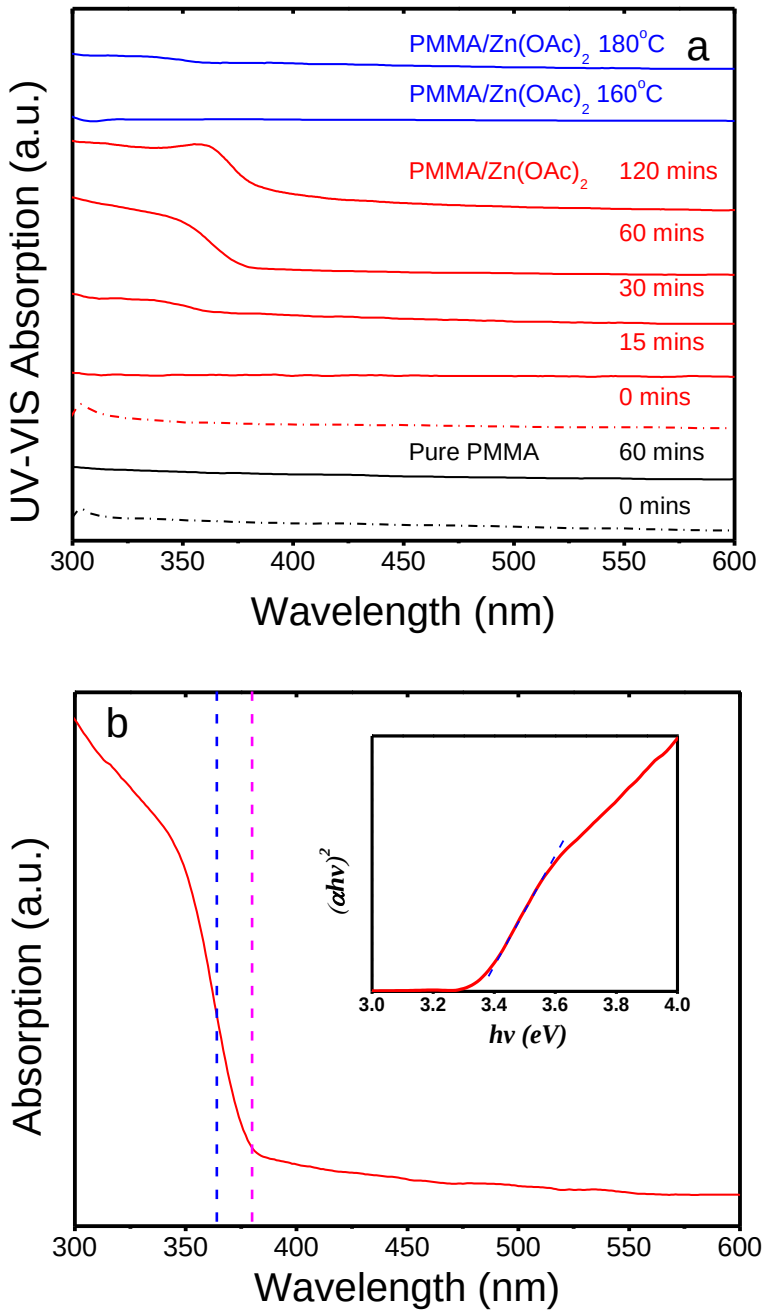

Fig. 3-4 UV-VIS absorption spectra of pure PMMA and nanocomposite. **a**. Time-dependent UV-VIS absorption spectra of pure PMMA (0, 60 mins; 200 °C) and nanocomposite (0, 15, 30, 60, and 120 mins; 200 °C). Before heat treatment, both pure PMMA (black dash dot curve) and PMMA with zinc precursor (red dash dot curve) show similar spectra with no absorption at NUV region. The nanocomposite exhibits stronger absorption at range of 350 nm to 380 nm (red solid curve) with increasing the annealing time, while the absorption spectrum of pure PMMA remains the same (black solid curve) as that of before heat treatment. The absorption curves shown as blue solid lines represent the nanocomposite with heat treatment for 1 hour under 160 °C and 180 °C, respectively. It indicates that the decomposition process of zinc

precursor is very slow or even not occurred. **b**. Absorption spectrum of nanocomposite with 1 hr of heat treatment. The pink and blue dash lines show the location of absorption onset and $\lambda_{1/2}$. The inset shows the absorption spectrum replotted as $(\alpha hv)^2$ *vs. hv*; from it, the band gap can be deduced.

The large blueshift of UV-VIS absorption spectra indicates the band gap of QDs is larger than bulk material due to quantum confinement effect. The evitable relationship between band gap and size of QDs lead us to investigate the size of ZnO QDs from UV-VIS spectra. Among a number of models, the effective mass model for spherical shapes with a coulomb interaction term has been proved to be an effective way. According to Brus' findings, the relationship between band gap and particles size can be described in the Eq. 3-1.[190, 191]

Eq. 3-1 $$E^* \cong E_g^{bulk} + \frac{\hbar^2\pi^2}{2er^2}\left(\frac{1}{m_e m_0} + \frac{1}{m_h m_0}\right) - \frac{1.8e}{4\pi\varepsilon\varepsilon_o r}$$

where E^* is the band gap of nanoparticles, E_g^{bulk} is the band gap of bulk material, $\hbar$ is the Planck's constant divided by 2π, r is the particle radius, m_e is the effective mass of electrons, m_h is the effective mass of the holes, m_0 is the free electron mass, e is the charge on an electron, ε_o is the permittivity of free space and ε is the relative permittivity. For ZnO nanoparticles with size less than 8 nm (mean in the quantum regime), the effective masses of electrons and holes for ZnO are m_e = 0.26 and m_h = 0.59, respectively.[189, 192] The relative permittivity for ZnO is ε = 8.5 and the band gap of the bulk ZnO is E_g^{bulk} = 3.2 eV.[123, 189] In order to get the band gap of ZnO QDs, the UV-VIS spectrum of PMMA/ZnO QDs nanocomposite is replotted as $(\alpha hv)^2$ *vs. hv* shown in the inset of Fig. 3-4(b). The principle of analysis is as following. For direct band gap semiconductors, a sharp edge in the UV-VIS absorption spectra is observed because light with energy lower than the band gap does not have sufficient energy to excite the electrons. However, in case the energy of incident light is high

enough, the absorption spectrum increases rapidly. According to REF. [192], the absorbance near the onset region can be described as:

$$\text{Eq. 3-2} \qquad \alpha = \frac{C(h\nu - E_g^{bulk})^{1/2}}{h\nu}$$

where α is the absorption coefficient, *C* is a constant, *hν* is the photon energy and E_g^{bulk} is the bulk band gap. The linear region indicates a direct gap transition and the value of interception corresponds to the band gap. Therefore, the band gap of ZnO QDs in the nanocomposite obtained is about 3.35 eV. The average radius of ZnO QDs is about 5.70 nm as deduced from the Eq. 3-1. Another method proposed by Meulenkamp[122] is also widely used to determine the particle size based on the experimental results of the relationship between the absorption shoulder ($\lambda_{1/2}$) and the diameter (D) of ZnO QDs. In Eq. 3-3,

$$\text{Eq. 3-3} \qquad \frac{1240}{\lambda_{\frac{1}{2}}} = 3.301 + \frac{294.07}{D^2} + \frac{1.09}{D}$$

$\lambda_{1/2}$ (nm) is wavelength at which the absorption intensity is half of the excitonic peak or shoulder and D (Å) is the particle diameter. The blue straight dash line in Fig. 3-4 represents the position of $\lambda_{1/2}$ and the diameter of ZnO QDs is calculated as 5.74 nm. The result matches well with that obtained from the effective mass model. Nevertheless, there are limitations with both methods and are not adequate to give the accurate estimate of average diameter. The particle size obtained from both of the two methods is larger than that observed in TEM images, because ZnO QDs in nanocomposites are capped by PMMA and the absorption spectra can be affected by the interaction between polymer and QDs.[131] Additionally, it was found that when the heat treatment temperature was lower than 200 ^{o}C, *i.e.*, 160 ^{o}C, 180 ^{o}C, the thermal decomposition process was very slow or even not occurred, in those cases, no ZnO

related absorption was observed from the UV-VIS spectra (shown as blue solid curves in Fig. 3-4(a)).[188]

3.3.4 Luminescent Property of PMMA/ZnO QDs Nanocomposite

PL spectra of pure PMMA and the PMMA/ZnO QDs nanocomposite before and after heat treatment at 200^{o}C for 1 hr are shown in Fig. 3-5. As could be seen in Fig. 3-5(a), no emission is observed from the PL spectra for both pure PMMA (black dash dot curve) and PMMA with zinc precursor (red dash dot curve). A very weak emission is detected from pure PMMA after heat treatment (black solid curve). As for the nanocomposite, a strong UV emission with a peak at ~ 376 nm and a long tail of visible emission covered from 400 nm to 600 nm are observed in the PL spectrum (red solid curve). PL emission of referential sol-gel synthesized ZnO QDs is included as the top right inset of Fig. 3-5(a). (Appendix - II) PL spectrum of the bare ZnO QDs exhibits a small peak at UV region (free exciton emission) and a very strong defect emission with peak at ~ 580 nm (related to the surface defect, mainly known as oxygen vacancies, V_O). It needs to be highlighted here that the mechanisms of defect emission in ZnO is still controversial in literatures.[193] Borseth *et al.*[194] attributed a PL emission near 580 nm to the transition of Li^+ from a shallow donor to the deep acceptor as the LiOH is commonly used in the sol-gel synthesis. However, in our present work, the impurities, such as Li^+, Na^+ and K^+, are minimized and their concentrations are less than 0.005 % according to the purity of precursor.

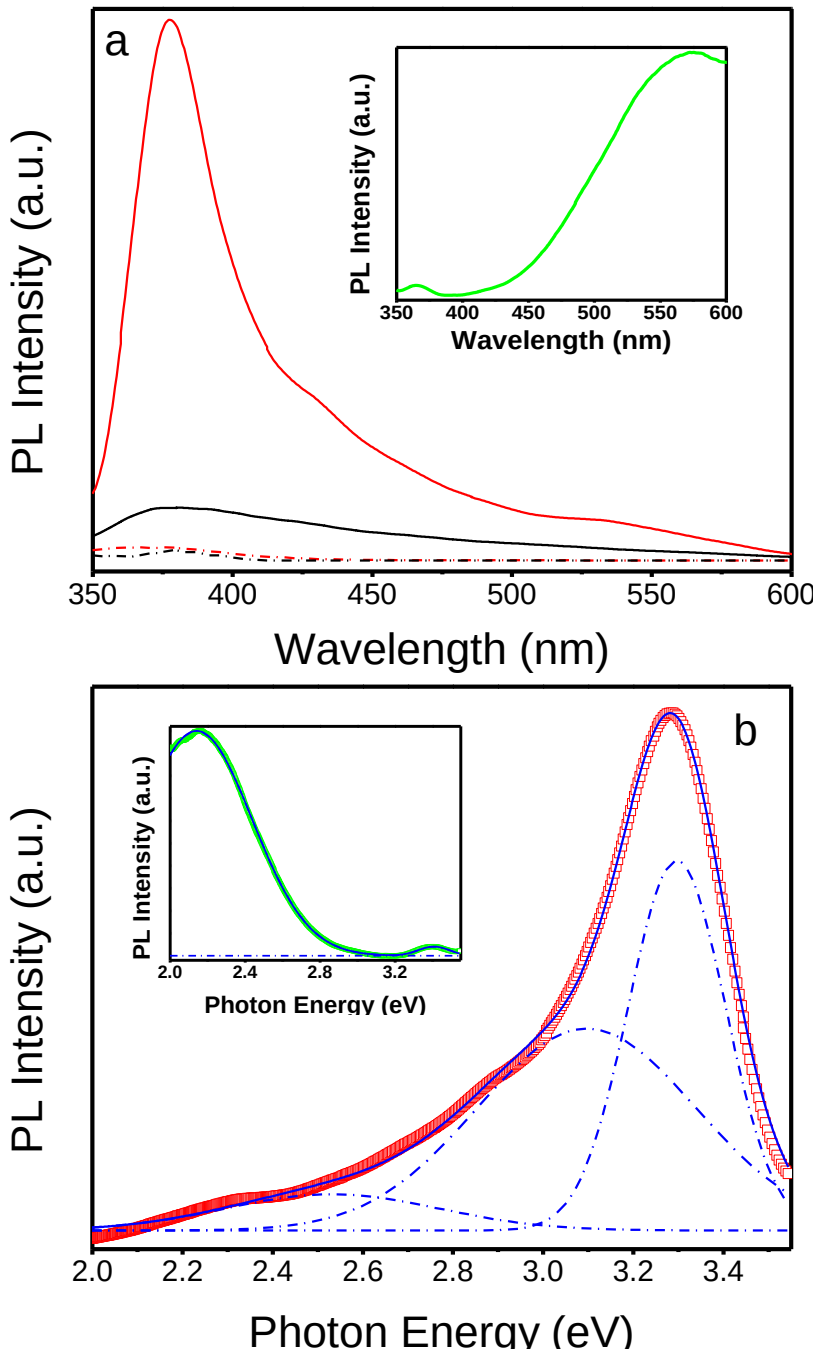

Fig. 3-5 PL spectra of pure PMMA and PMMA/ZnO QDs nanocomposite. **a**. Pure PMMA before (black dash dot curve) and after (black solid curve) heat treatment; nanocomposite before (red dash dot curve) and after (red solid curve) heat treatment. The nanocomposite exhibits strong NUV emission but very weak visible emission. The top right inset shows PL spectrum of sol-gel synthesized ZnO QDs. **b**. Deconvoluted Gaussian bands from PL spectrum of PMMA/ZnO QDs nanocomposite. The top left inset corresponds to the deconvolution of PL spectrum of bare ZnO QDs.

One significant observation is the fact that: in comparison with PL spectrum of bare sol-gel synthesized ZnO QDs, the PL emission of PMMA/ZnO nanocomposite exhibits significant UV emission but very weak visible emission. The near UV PL emission of PMMA/ZnO QDs nanocomposite observed in this study was also reported previously.[130, 147, 152, 187, 195] Furthermore, according to literature, the PL emission at the visible range was also widely studied.[131, 132, 151, 152, 166, 195-198] Up to the present, the PL mechanism of PMMA/ZnO QDs nanocomposite is still unclear and controversial. Sun *et al.*[147] reported that the complete UV emission could be achieved contributed by the well dispersion of ZnO QDs in PMMA matrix with the assistance of exfoliated ZrP nanoplatelets; as the defect emission can be fully quenched by the surface passivation effect. However, in the presented study, the surface passivation effect is not complete as the surface defect related visible emission could still be seen.

In order to find the hidden PL emission bands and investigate their origination, the spectrum was replotted as intensity *vs.* photon energy and the result is shown in the Fig. 3-5(b). The whole PL spectrum can be well fitted with multiple Gaussians line shape functions that show the accurate peak positions and the relative intensities. The blue dashed curves depict the deconvoluted Gaussian bands and the sum of the three Gaussian bands is shown as solid blue curve which fits well with the original experimental data (open square). The coefficient of determination R^2 (best = 1, worst = 0) equals to 0.999. The peak positions of the three Gaussian bands are ~ 3.30 eV (376 nm, near ultraviolet or NUV band), ~ 3.08 eV (403 nm, violet band) and ~ 2.58 eV (481 nm, blue band) from UV region to visible region, respectively. Since pure PMMA only shows very weak PL emission, the PL emission of nanocomposite is mainly contributed from ZnO QDs or complex of PMMA and ZnO. The peak position

and intensity contribution of the three bands are summarized in Tab. 3-1. The blue emission band contributed less than 10 % of the total PL emission, while the contribution of violet band (403 nm or 3.08 eV) and NUV band (376 nm or 3.30 eV) were 50.3 % and 40.9 %, respectively. The peak located at photon energy of 3.30 eV should correspond to the band edge recombination of ZnO QDs which matches well with the UV-VIS absorption. For the violet band, Lin *et al.*[199] reported the calculation results and suggested the shallow accepter level of zinc vacancies (V_{Zn}) above the valence band (VB) of ZnO. The energy interval from the bottom of the conduction band (CB) to V_{Zn} is about 3.06 eV (405 nm) which is close to the value obtained in our study. However, according to recent studies, Zeng and co-workers suggested violet emission from ZnO QDs should correspond to recombination of electrons trapped at shallow donor level near CB (zinc interstitial, Zn_i) and photogenerated holes from VB.[108] Similar conclusion was also drawn by many other researchers.[163, 200-202] Moreover, the blue band observed in the present study was also reported by Zhang *et al.*[151] in a similar PMMA/ZnO QDs nanocomposite system. The mechanism of blue emission was the recombination of photogenerated electrons, followed by surface defect (mainly doubly charged oxygen vacancies, V_o^{++}) trapping to form single charged oxygen vacancies (V_o^{+}) [203]. Based on the above discussion, mechanism of the whole PL emission can be described and shown in Fig. 3-6 with all the energy levels and the possible pathways depicted. Firstly, the photogenerated electrons and holes occupy the CB and VB of ZnO QDs, respectively. The electrons can be further trapped at the shallow energy level below CB known as Zn_i, while the holes are trapped at the oxygen related defect levels near VB, *i.e.*, V_O^{+}, V_O^{++}. Based on our experimental results, the oxygen vacancies are mostly double charged formed by trapping holes from VB. According to the PL results,

it can be deduced that the oxygen vacancies located on the surface of ZnO QDs is significantly quenched by the PMMA surface passivation. The recombinations between each band constitute the whole PL spectrum of PMMA/ZnO QDs nanocomposite. Correspondingly, only two PL bands, located at 2.14 eV (579 nm, yellow-orange band) and 3.41 eV (364 nm, NUV band), are deconvoluted from PL spectrum of sol-gel synthesized ZnO QDs and shown in the inset of Fig. 3-5(b). The visible band contributes significantly 98.4 % of the whole PL intensity, indicating the PL emission from bare ZnO QDs mainly originates from the defect on the surface of nanoparticles.[163] The peak position and intensity contribution are also summarized in Tab. 3-1.

Tab. 3-1 Summary of Gaussian bands deconvoluted from PL spectrum of PMMA/ZnO QDs nanocomposite and bare sol-gel synthesized ZnO QDs.

	PMMA/ZnO QDs nanocomposite		Sol-gel synthesized ZnO QDs	
	Peak position	Intensity[a]	Peak position	Intensity[a]
NUV band	3.30 eV (376 nm)	40.9 %	3.41 eV (364 nm)	1.6 %
Violet band	3.08 eV (403 nm)	50.3 %	-[b]	-[b]
Blue band	2.58 eV (481 nm)	8.8 %	-[b]	-[b]
Yellow-orange band	-[b]	-[b]	2.14 eV (579 nm)	98.4 %

[a]: percentage of integrated intensity for each PL band.

[b]: Peaks cannot be deconvoluted from the PL spectra.

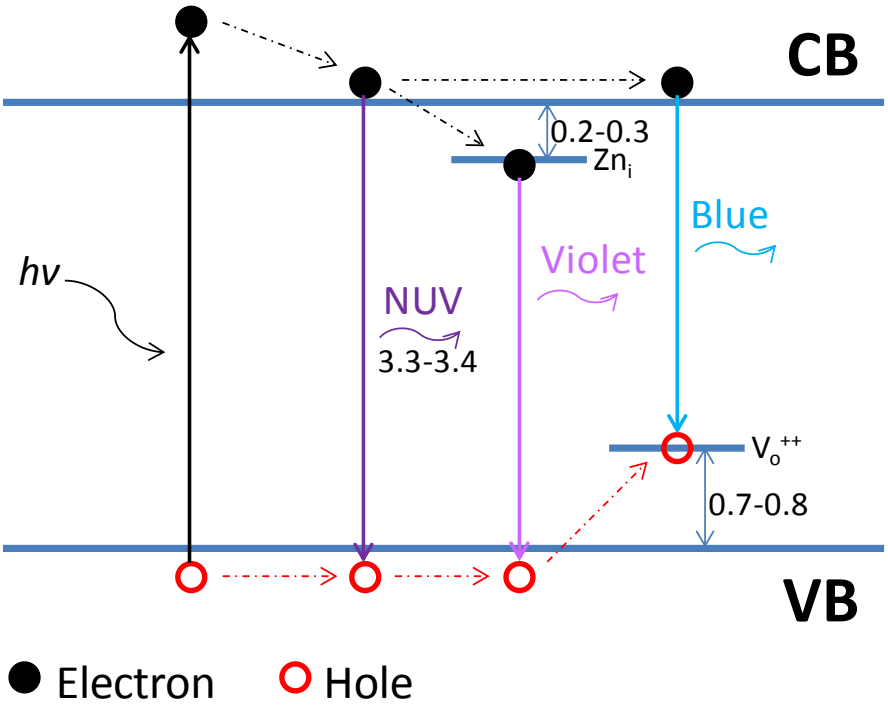

Fig. 3-6 Proposed energy diagram of ZnO QDs in the nanocomposite and the possible recombination pathway for different emission bands.

It is also worth noting that, compared to the conventional sol-gel followed by polymerization method to prepare PMMA/ZnO nanocomposite, the whole preparation process in this work is free of impurity. That might be another reason why the defect emission of ZnO QDs was quenched significantly in the nanocomposite. Moreover, the defect emission can still be observed the PL spectrum (although not the dominant portion), indicating that the surface oxygen vacancies were not well protected by the polymer. It suggests that there were no strong interaction between PMMA and ZnO QDs; which is similar to the case of synthesizing nanocomposite *via* physical blending method.

3.3.5 Interaction between PMMA and ZnO QDs

To further confirm the possible interaction between PMMA and ZnO QDs, ATR-FTIR measurements were performed; and the spectra are shown in Fig. 3-7. Fig. 3-7(b) only

shows the wavenumber from 650 cm^{-1} to 2000 cm^{-1} of the spectra presented in Fig. 3-7(a). The black solid curve represents the FTIR spectrum of pure PMMA. The absorption peaks in the region of 2800-3000 cm^{-1} correspond to the CH_2 and CH_3 group. Two characteristic strong absorption peaks located at 1723 cm^{-1} and 1143 cm^{-1} are originated from the C=O and C-O-C stretching vibration of PMMA. The absorption peak near 1437 cm^{-1} is attributed to the bending and stretching of CH_2 and CH_3 groups. All peaks shown in pure PMMA are all observed in the FTIR spectrum of PMMA/ZnO QDs nanocomposite (red solid curve). Neither clear shift of peak positions nor change of absorption intensities is observed in the spectrum. Similar results were also obtained by Ge *et al.*.[204] However, some research groups [130, 198] reported that the C=O stretching vibration near 1730 cm^{-1} shifted to lower wavenumber and the absorption intensity of C-O-C stretching vibration near 1147cm^{-1} changed due to the coordination between –COOR group of PMMA and Zn^{2+} on the surface of ZnO particles. FTIR spectrum of sol-gel synthesized ZnO QDs is shown as green solid curve in Fig. 3-7. The broad peak at near 3390 cm^{-1} should be assigned to -OH group on the surface of ZnO QDs, while peaks at 1566 cm^{-1} and 1406 cm^{-1} originated from the C=O and C-O stretching vibrations of acetate groups. No peaks of ZnO could be observed in the nanocomposite. It might be due to the low concentration of ZnO QDs or weakening of the interface affinity between PMMA and ZnO QDs caused by the facile polymerothermal method.

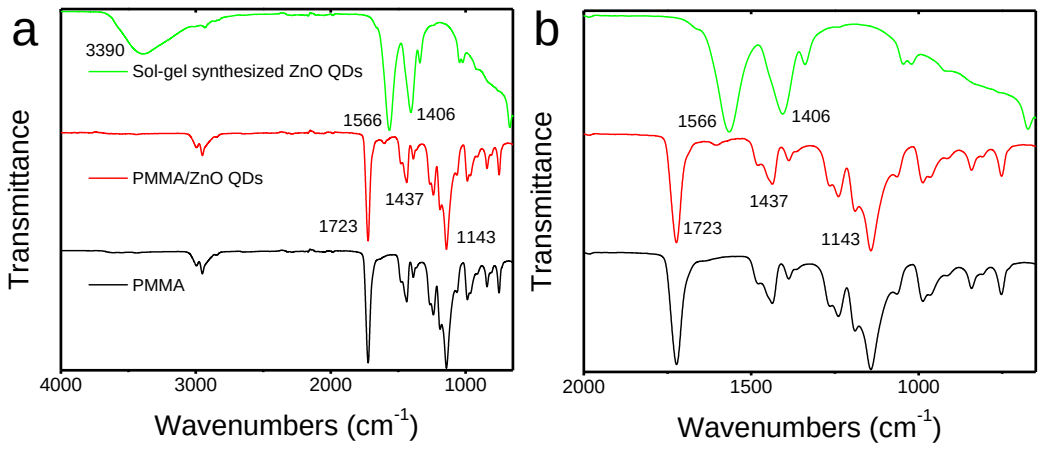

Fig. 3-7 FTIR spectra of ZnO QDs, PMMA/ZnO QDs nanocomposite and pure PMMA. **a**. Spectra with whole range of 4000 cm^{-1} ~ 650 cm^{-1}. **b**. Enlarged spectra that presented in figure a.

3.4 Conclusion

PMMA/ZnO QDs nanocomposite was synthesized by thermal decomposing zinc acetate in PMMA host matrix, which is described as a 'polymerothermal' synthesis. The as-prepared ZnO QDs with average size of 4 nm were embedded in the polymer with good dispersion. The UV-VIS absorption and photoluminescence study show that the nanocomposite was a good UV absorber and emitter. Compared to sol-gel synthesized ZnO QDs, those in nanocomposite exhibited excellent UV emission but relatively weak visible emission. It was known as surface passivation effect that reduces the concentration of defect states located on the surface of ZnO QDs. On one hand, oxygen vacancies (V_O), which corresponding to the defect emission, are filled up by the carbonyl group from polymer chain that cause the significant quenching in the PL visible emission. Furthermore, in comparison with bare sol-gel synthesized ZnO QDs, emission from free exciton and shallow donor (Zn_i) related defect are enhanced relative to emissions of other bands. Particularly, about the methodology used in this work, PMMA/ZnO QDs nanocomposite thin film with desired thickness

and surface morphology can be easily fabricated by spin coating technique; making it suitable for further fabrication of electronics and optoelectronics devices, such as light-emitting devices.

4. Fabrication and Characterization of Light-emitting Devices based on PMMA/ZnO QDs Nanocomposite

4.1 Introduction

Light-emitting devices utilizing QDs as the emission media have been studied extensively since it was first fabricated in the year of 1994.[1, 17, 21, 39, 47, 205-208] To date, QD-LEDs have been significantly improved in terms of their performance, *i.e.*, external quantum efficiency, luminance, and lifetime; which are now comparable with those of OLEDs.[39, 50, 56, 58] However, the usage of toxic heavy elements (*e.g.*, cadmium or lead) retards commercialization of QD-LEDs.

ZnO, as a II-VI semiconductor, has a direct wide band gap with a relatively large exciton binding energy at room temperature.[88-90] Moreover, this material is non-toxic, chemical stable and cheap. All these merits make ZnO a good candidate for light-emitting application. Up to now, LEDs utilizing different nanostructured ZnO including nanowires, nanorods, and thin film have been realized.[178, 180, 209-211] For most of the devices, their luminescent properties mainly rely on the defect related emission instead of the band edge emission. Compared with bulk ZnO, the advantage of using QDs is the small nanoparticles have much larger surface area and fortunately, the defects of ZnO are mostly located on the surface of QDs. However, ZnO nanoparticles or QDs are seldom used as the sole emission layer in the light-emitting

application because the bare QDs easily agglomerate in solution or atmosphere. For instances, ZnO nanoparticles have been used in CdSe-based QD-LEDs as the electron transport layer (ETL) and the hole block layer (HBL).[56, 58] Furthermore, some studies concerning white light emission that combines emission from light sources with PL from ZnO nanoparticles were reported by several research groups.[212, 213] In general, by applying the strategy of surface modification by polymers, ZnO QDs can exhibit higher quantum yield and better stability in ambient atmosphere; in comparison with bare ZnO QDs.[132, 133] As shown in certain previous works, the emission color can also be tuned by changing the size of ZnO QDs.[154, 165] In particular, Son *et al.* demonstrated white electroluminescence from heterojunction structure of ZnO QDs and poly(9-vinylcarbazole) (PVK); PVK itself is a good organic semiconductor.[86] Therefore, polymer/ZnO QDs nanocomposites have great potential in the optoelectronic applications, such as light-emitting devices (LEDs).

In this chapter, PMMA/ZnO QDs nanocomposite prepared *via* polymerothermal method is utilized for light-emitting application. Devices based on this nanocomposite thin film are fabricated using usual spin coating technique that does not require complicated fabrication steps. The LED device exhibited white color emission. Characterizations, such as current-voltage measurement, electroluminescence (EL), are performed. To the best of our knowledge, this is the first time that a detailed EL study has been carried out on the LEDs with PMMA/ZnO QDs nanocomposite as the emission layer.

4.2 Experimental details

4.2.1 Fabrication of LEDs based on PMMA/ZnO QDs nanocomposite

The two types of LED structures studied in this work are schematically depicted in Fig. 4-1. In the typical procedure of device fabrication, patterned indium-tin-oxide (ITO) glass substrates were used. The ITO substrates were standard cleaned by acetone and isopropyl alcohol (IPA) *via* ultra-sonication for 8 mins sequentially and rinsed by distilled water for three times. Pre-heat treatment of the substrates were carried out at 110 ^{o}C for 5 mins to remove the residual water; followed by oxygen plasma treatment for 3 ~ 4 mins. For device A (Fig. 4-1(a)), the as-prepared solutions (details of formula were described in previous chapter) containing zinc precursor were spin-coated directly on top of the ITO substrates at different spin speed to form thin films with different thicknesses. For device B (Fig. 4-1(b)), prior to spin-coating PMMA/zinc solutions, a layer of conducting polymer, poly(3,4-ethylene dioxythiophene): poly(styrene sulfonate) (PEDOT:PSS, Sigma Aldrich), was firstly spin-coated on top of ITO substrates and followed by heat treatment at 120 ^{o}C for 30 mins on hotplate in ambient atmosphere. The PEDOT:PSS thin film was not visibly damaged by the deposition of PMMA and zinc precursor film because the polarities of the solvents (*i.e.*, water and anisole) used for each layer are different. Subsequently, all the samples were transferred to a conventional oven for heat treatment at 200 ^{o}C for 1 hr. Finally, aluminum (Al) electrodes with thickness about 150 nm was deposited using Edwards E-beam Evaporator Auto 306 under pressure below 5e-6 mbar with deposition rate of 0.07 nm·s^{-1}. The emission area of the devices was 4 mm × 4 mm.

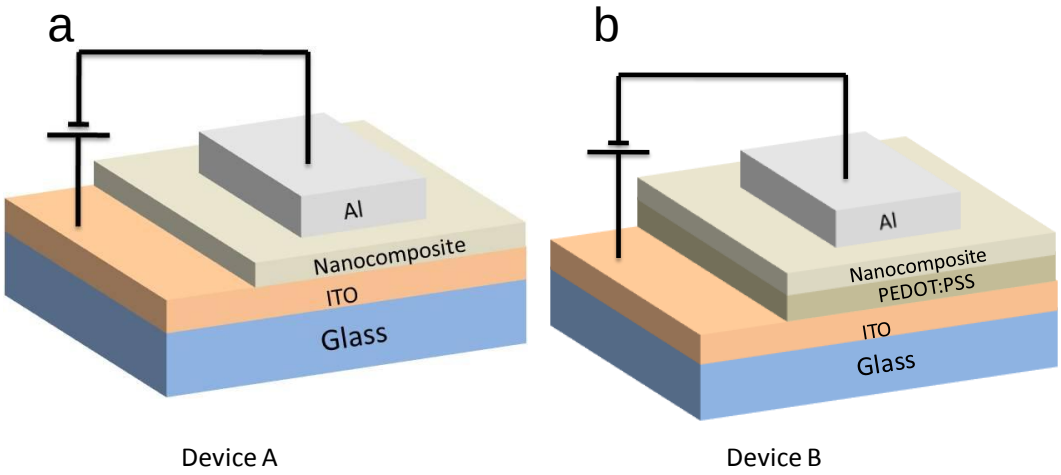

Fig. 4-1 Schematic diagrams of two types of light-emitting devices. **a**. LEDs based on single layer of PMMA/ZnO QDs nanocomposite thin film. **b**. LEDs based on double layers with additional PEDOT:PSS layer between nanocomposite thin film and ITO.

4.2.2 Characterization of LEDs based on PMMA/ZnO QDs nanocomposite

All the characterizations of LEDs were performed in ambient atmosphere. The current-voltage (I-V) characteristics of the devices were measured using HP 4155B semiconductor analyzer. The current of devices was obtained by sweeping the voltage from negative to positive bias with step of 0.1 V. The electroluminescence (EL) measurements were conducted using a PDS-1 photomultiplier tube detector assembly coupled with a monochromator. Keithley digital source meter with model number of 2400 was using to provide constant voltages for devices in the EL measurement. Using a multi-fiber, the light emission was collected and transferred to the monochromator for analysis.

4.3 Results and discussion

The characterization results of LEDs based on PMMA/ZnO QDs nanocomposite were discussed from three aspects:

1. Electrical properties of PMMA/ZnO QDs nanocomposite LEDs

2. Electroluminescence properties of PMMA/ZnO QDs nanocomposite LEDs

3. Mechanisms of electroluminescence from LEDs based on PMMA/ZnO QDs nanocomposite

4.3.1 Current-voltage characteristic of PMMA/ZnO QDs nanocomposite LEDs

Fig. 4-2 presents typical current-voltage characteristics of device A with the applied bias sweeping between -12 V to 12 V. The I-V curve shows diode characteristic when either forward bias or reverse bias is applied. This inversion symmetric behavior is mainly due to the similarity of work function for both ITO and Al. The energy band diagram of device A is shown in the inset of Fig. 4-2. The work function of ITO is 4.7 eV, which is 0.4 eV lower than that of Al. Therefore, when a bias voltage is applied on the device, carriers can flow through the dielectric polymer layer under the strong electric field, regardless of the bias direction. Similar phenomenon was also reported by Que *et al.*[214] in the device of Cu-doped ZnS nanocrystal/PMMA nanocomposite as well as by Son *et al.*[86] in the ZnO QDs based hybrid LEDs. To investigate the effect of thickness on the electrical properties of LEDs, PMMA/ZnO QDs nanocomposite thin films with same concentration of ZnO QDs but different thicknesses were prepared. The thickness of thin film changed from 18 nm to 28 nm

when the spin coating speed of PMMA/zinc precursor solutions was varied from 3000 rpm to 1000 rpm. For thicker thin film, the electric field through the film decreased under the same applied voltage, giving lower device current; this is shown in Fig. 4-2. Furthermore, the turn on voltages of devices increased with larger thickness. Under forward bias, the turn on voltages for the three devices can be deduced from the I-V curves, and are approximately 7.44 eV, 8.48 eV, and 8.98 eV, respectively. Similar conclusion could also be drawn from the I-V curves when reverse bias was applied onto the device.

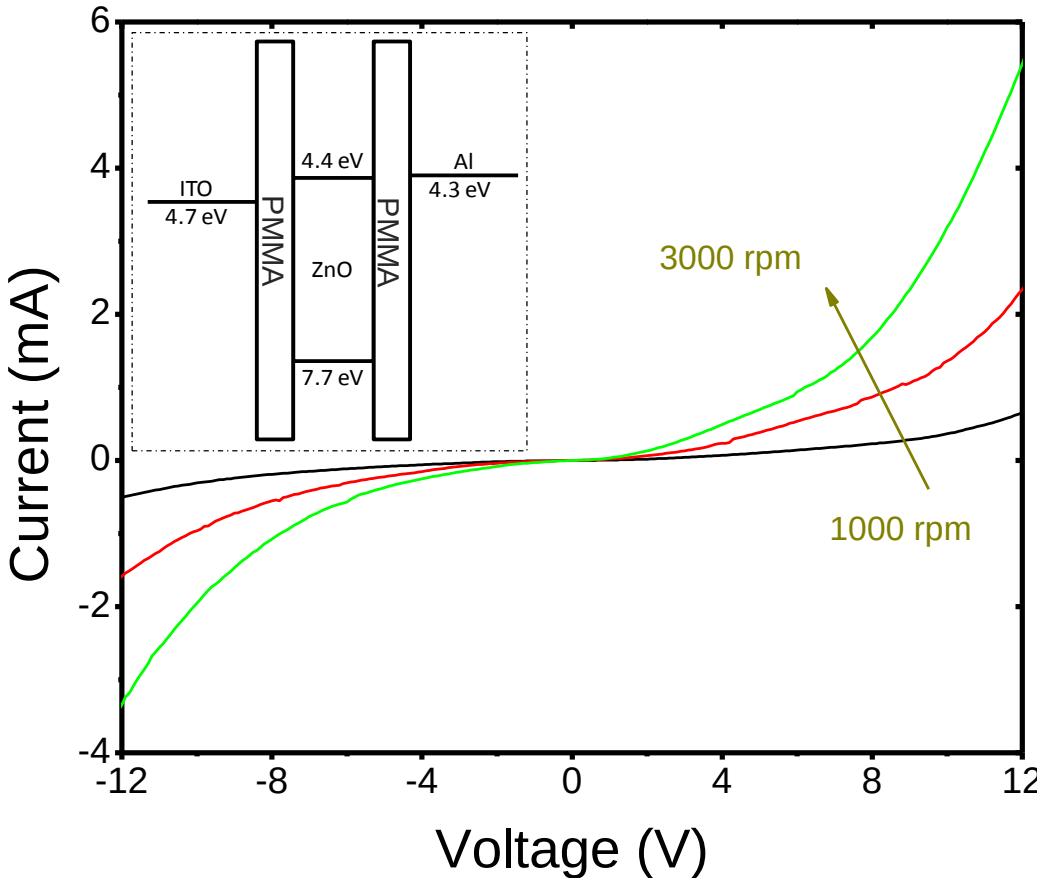

Fig. 4-2 Current-voltage characteristics of single layer LEDs (device A) with different thicknesses of emission layer show inversion symmetric behavior. Reducing the spin speed of preparing the nanocomposite thin film, thicker emission layer was fabricated and the current of the corresponding device was lower under the same applied voltage. The inset shows the energy band diagram of device A.

The device B was fabricated by adding a layer of conducting polymer, PEDOT:PSS, between ITO and PMMA/ZnO QDs nanocomposite. The I-V characteristics of as-fabricated LEDs with nanocomposite thin films of different thicknesses are shown in Fig. 4-3. The thickness of the thin film was controlled by varying the spin speed; similar to the procedures described previously for device A. Compared to the I-V curve of device A, inversion symmetric behavior is not observed on device B when the applied bias sweeping between -12 V to 12 V. When sweeping from reverse bias of -12 V, the current remains constant at near zero value before the bias voltage reaches the threshold of the device. After the forward sweeping bias crosses over the turn on voltage, a dramatic increase in current is observed with increasing applied voltage; showing a typical diode characteristic. The inset of Fig. 4-3 shows the energy band diagram of device B. The band gap of PEDOT:PSS is 1.9 eV with the energy levels of lowest unoccupied molecular orbital (LUMO) and highest occupied molecular orbital (HOMO) at -3.3 eV and -5.2 eV, respectively. The HOMO of PEDOT:PSS is 0.5 eV lower than the work function of ITO. As a result, the potential barrier for hole injection from ITO to ZnO QDs is reduced; thus, lowering the turn on voltages. The turn on voltages of the devices are estimated to be 6.73 eV, 8.40 eV, and 8.89 eV from thinner nanocomposite film to thicker film, respectively. It is also worthy to note that the current of the device is also increased significantly when a high forward bias is applied, *e.g.*, 12 V. The LUMO of PEDOT:PSS is 1.4 eV higher than the work function of ITO. Therefore, under reverse bias, the electrons generated from ITO have to firstly overcome the potential barrier of 1.4 eV between ITO and PEDOT:PSS and then, follow by tunneling through the PMMA thin layer. Therefore, compared to device A without PEDOT:PSS layer, the electron injection is reduced significantly in device B when reverse bias is applied. Moreover, the layer of PEDOT:PSS also works

as an electron block layer (EBL) that blocked the electrons transporting from PMMA/ZnO QDs nanocomposite to ITO and improved the device performance.

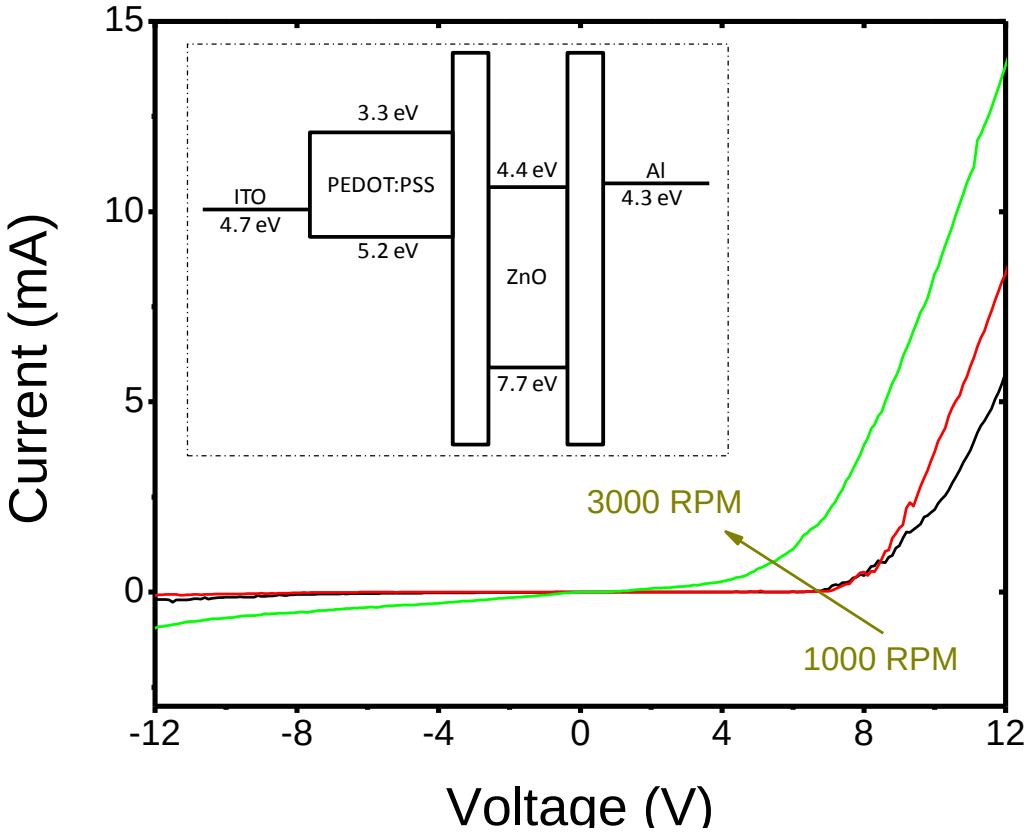

Fig. 4-3 Current-voltage characteristics of double layer LEDs (device B) with different thickness of emission layers obtained by varying spin speed. All the I-V curves show typical diode behavior only under forward bias. The current remains as constant at small value when reverse bias is applied. Turn-on voltage for the LED with thinner emission is lower. The inset shows the energy band diagram of device B.

The charge transport properties of PMMA/ZnO QDs nanocomposite LEDs are very complex. It involves transportation of both electrons and holes. Furthermore, it is also affected by the properties of materials as well as their interfaces. As mentioned previously, the structure of QD-LEDs is adopted from OLEDs because of the similarity of these two kinds of devices. Therefore, the charge transport models used for OLEDs are also widely applied to explain the I-V behavior of QD-LEDs. Generally, the current through the device can be fitted in different ranges of applied

voltage using different models, which are thermionic emission (TE) conduction model,[215] space-charge-limited-current (SCLC) conduction model,[216] and Fowler-Nordheim (FN) tunneling model.[217] The thermionic emission (also Richardson-Schottky emission) is temperature dependent charge transportation that the thermally activated charges hop over the energy barrier. The TE current is very low and, in fact, it only can be identified at low applied voltage as other current is not significant. Increasing the applied voltage, more carriers are generated and injected into materials from electrodes. The carriers may accumulate in the materials in case of energy barriers or trapping states, inhibiting the further injection. The current at the equilibrium status is called space charge limited current. The SCLC is mainly depended on the applied electric field (or voltage in case the thickness of material is constant). When the applied voltage is high enough, the carriers may tunnel through the potential barrier following Fowler-Nordheim (FN) relation. Similar to SCLC, FN tunneling current is also electric field dependent. The three fundamental carrier injection processes can be described as following:

i. Thermionic emission (TE) conduction model

$$I \propto A^{*}T^{2}\exp\left[-\frac{q\phi_0}{kT}+q\left(\frac{q^3V}{4\pi\varepsilon}\right)^{1/2}\right] \qquad \text{Eq. 4–1}$$

ii. Space-charge-limited-current (SCLC) conduction model

$$I \propto V^{\alpha} \qquad \text{Eq. 4–2}$$

iii. Fowler-Nordheim (FN) tunneling model

$$I \propto V^{2}\exp\left(\frac{-k}{V}\right) \qquad \text{Eq. 4–3}$$

where k is Boltzmann's constant, A^* is Richardson's constant, T is absolute temperature, ε is dielectric permittivity, ϕ_o is energy barrier and q is electronic charge.

Fig. 4-4(a) presents a ln-ln plot of current (I) as a function of the voltage (V) (green curve in Fig. 4-3). It shows four distinct regions with different slopes in the ln(I) *vs.* ln(V) curve. However, at low voltage, the I-V curve can be well fitted with the TE conduction model, where ln(I) is linearly increasing with $V^{1/2}$, this is shown in the inset of Fig. 4-4(a). Due to the small thickness of film, the carrier injection *via* TE mechanism is also accompanied by SCLC model; shown in the first region ($\alpha = 1.68$). With increasing applied voltage, the slope of the curve increased to 2.90, suggesting the carriers injection process is mainly following the SCLC mechanism in this region. However, when the voltage further increased, the slope of ln(I) ~ ln(V) curve decreased to 1.24, indicating the current is nearly proportional to the applied voltage. It is probably because of the fact that the ZnO QDs are completely trapped by the injected carriers; which lowers the increment of current. A significant increase of the slope value ($\alpha = 4.10$) is observed when the voltage increases more than 5 V. This result indicates the presence of FN tunneling: current exponentially increases with the applied voltage. According to the Eq. 4-3, this part of curve is replotted as $\ln(I/V^2)$ *vs.* 1/V, as shown in the Fig. 4-4(b). The linear relationship confirms the FN tunneling effect for the carrier injection in this region.

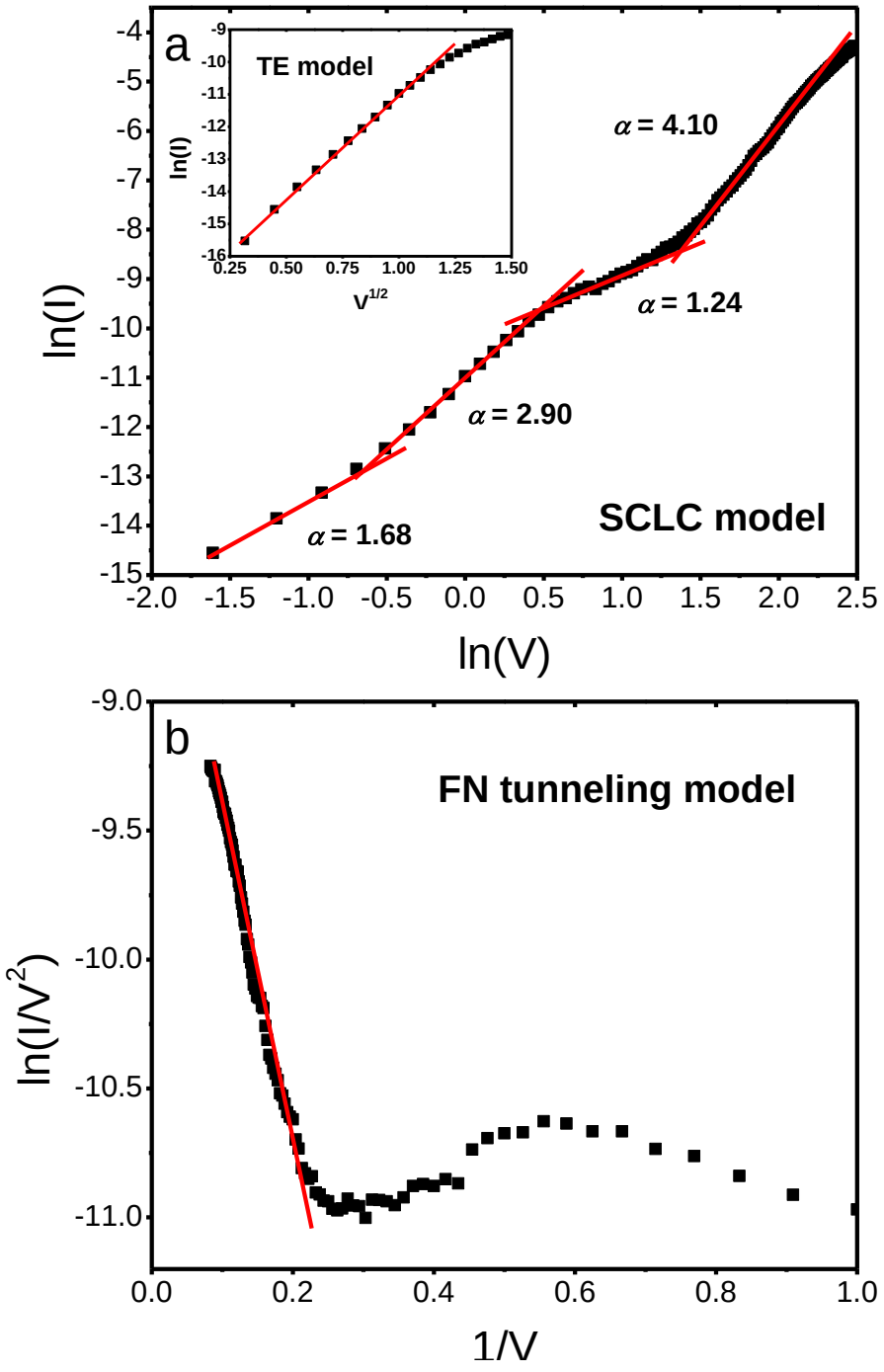

Fig. 4-4 Mechanisms for the typical I-V behavior. **a**. The ln-ln plot of current as a function of the voltage for the device B. It is fitted well with the SCLC model. The inset presents the linear relation between ln(I) and $V^{1/2}$ at low voltage, corresponding to TE conduction mechanism. **b**. Plot of $\ln(I/V^2)$ *vs.* 1/V indicates FN tunneling effect under high applied voltage.

4.3.2 Electroluminescence (EL) characteristic of PMMA/ZnO QDs nanocomposite LEDs

EL measurements of device A were performed and the emission layer, PMMA/ZnO QDs nanocomposite thin film, was deposited with spin speed of 3000 rpm. Fig. 4-5 shows the EL spectra of the LED with different forward biases, varying from 0 V to 12 V at room temperature and in ambient atmosphere. When the applied voltages were lower than the threshold voltage of the device, *e.g.*, 4V, no light from the emission area was detected and the spectra were mainly contributed from the background of measurement environment. With the applied voltage increased above the turn on voltage of the device, broad spectra covering almost the entire visible range were collected. The luminescence intensity of the LED increased with the bias voltage up to 12 V. The inset of Fig. 4-5 shows a photograph of one LED based on PMMA/ZnO QDs nanocomposite operating at 12 V under dark environment; the white emission could be perceived by human naked eyes. The photograph was captured using a Canon EOS 40D Digital SLR Camera equipped with a Canon Macro Lens EF-S 60 mm and the shutter speed was fixed as 30 s. Similar EL spectra were obtained when the bias voltage was reversed due to the similarity of the work function of ITO and Al as discussed previously.

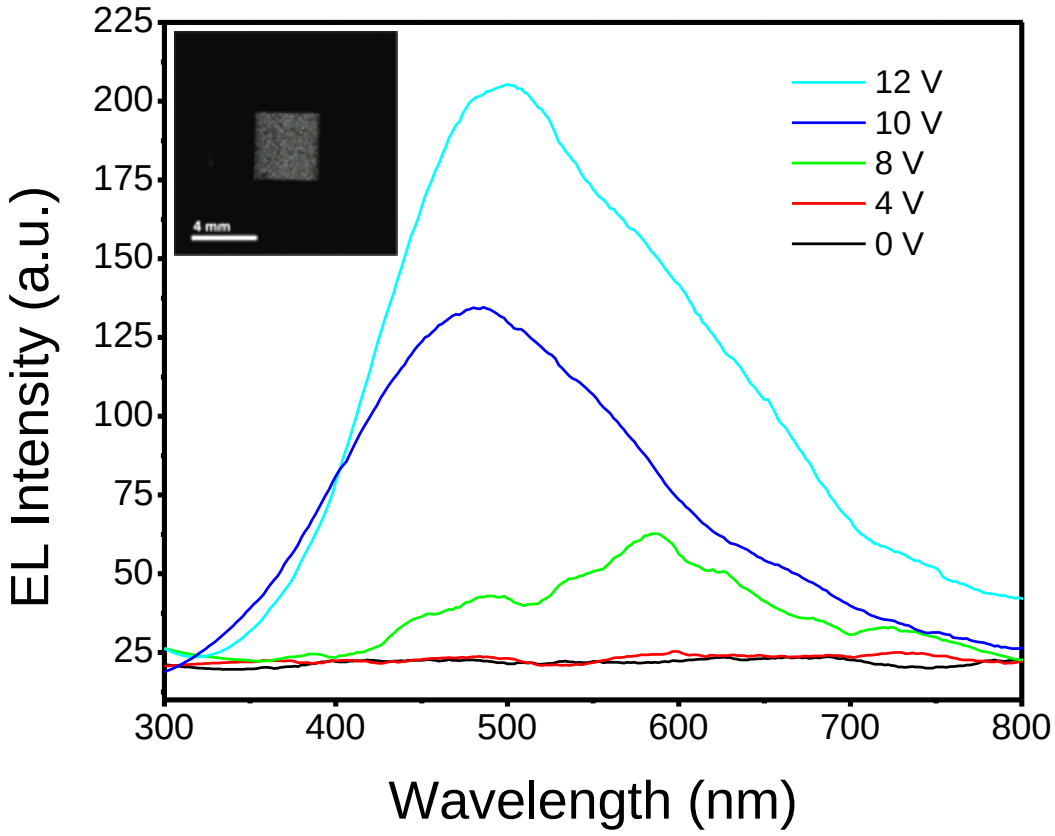

Fig. 4-5 EL spectra of device A under different applied voltage from 0 V to 12 V. The inset shows a photograph of light emission under 12 V.

In order to investigate the color change of the emission, the CIE chromaticity coordinates of the LED were calculated from the obtained EL spectra and is shown in Fig. 4-6. The chromaticity coordinates of the LED under different applied voltages are (x: 0.368, y: 0.372), (x: 0.280, y: 0.322) and (x: 0.305, y: 0.347) for 8 V, 10 V and 12 V, respectively. (Appendix - III) The red point in Fig. 4-6 presents the chromaticity coordinates for standard white color at (x: 0.333, y: 0.333). Therefore, the results clearly indicates that the EL emission from the device is very close to white color.

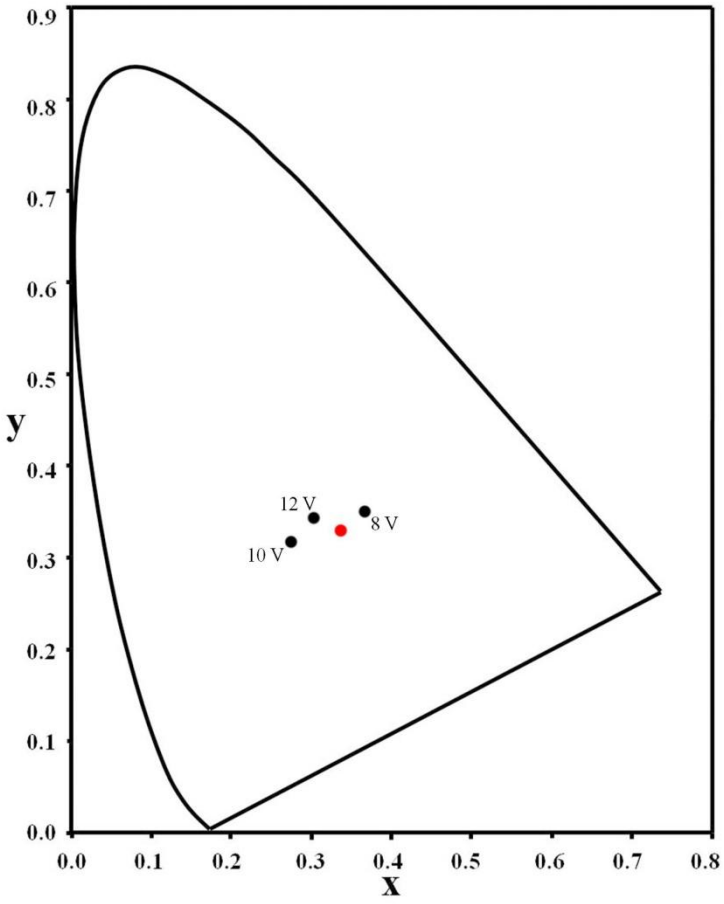

Fig. 4-6 CIE chromaticity coordinates of device A under different applied voltage of 8 V, 10 V, and 12 V. The red dot shown in the center presented white color in the chromaticity coordinates.

The simpler structure of device A consisting of a single layer of PMMA/ZnO QDs nanocomposite (thickness < 30 nm) shows the ability of emitting white color under bias, regardless of the direction of the applied voltage. However, the device performance was limited by inefficient carrier injection and poor confinement of the carriers. Sun *et al.* reported that using PEDOT:PSS as the hole injection layer helped to improve the device performance.[21] Fig. 4-7 showed the EL spectra of device B under different applied voltages. The thickness of PEDOT:PSS on top of ITO was about 50 nm and that of PMMA/ZnO QDs nanocomposite thin film was about 20 nm. Similar to device A, visible EL emission was observed when forward bias was applied on the ITO electrode; and the EL intensity increased by increasing the applied voltages.

However, unlike device A, there was no light emission under a reverse applied voltage due to insufficient electron injection from the ITO electrode. Similar conclusion could also be reached based on the current-voltage characteristics. The inset of Fig. 4-7 shows a photograph of the LED under forward bias of 12 V in the dark environment. Compared to device A, the EL emission intensity of device B was stronger. As could be seen in the spectra, despite the variation of the EL intensity, no significant changes in the spectral shape was observed under different applied bias. The CIE chromaticity coordinators of device B were (x: 0.343, y: 0.385), (x: 0.321, y: 0.364) and (x: 0.300, y: 0.341) under different applied voltage of 8 V, 10 V and 12 V, respectively. The chromaticity coordinators are shown in Fig. 4-8.

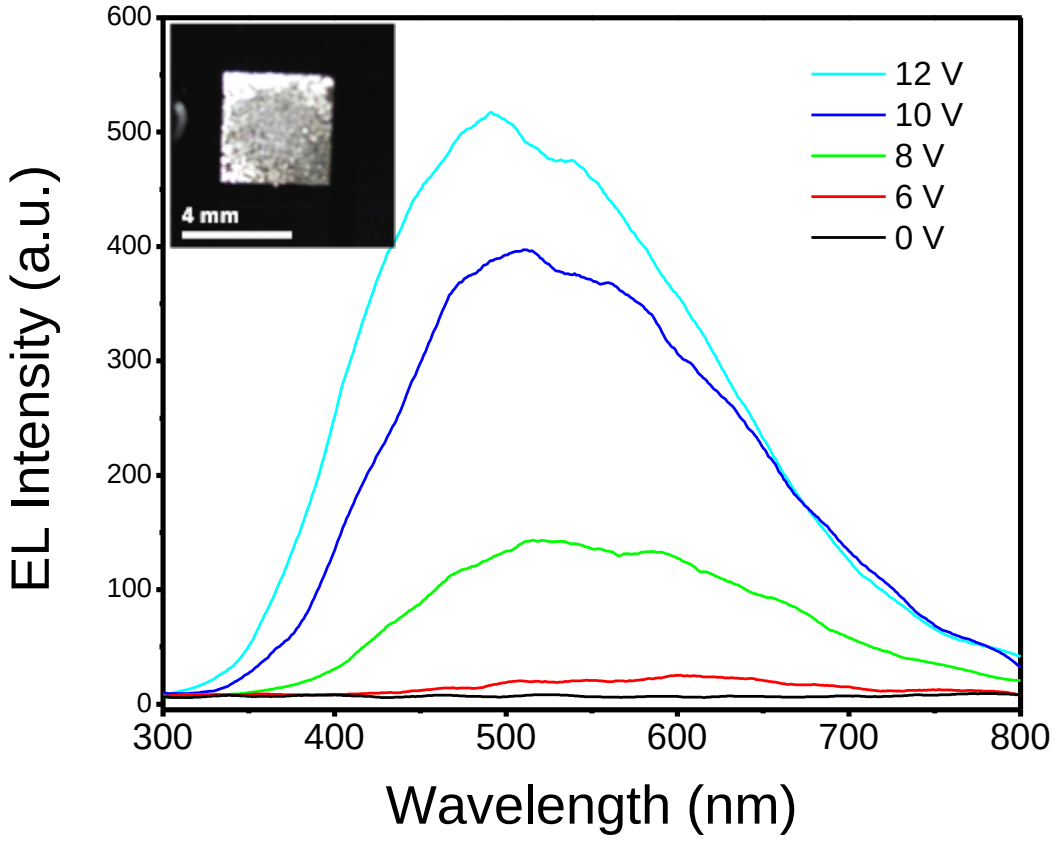

Fig. 4-7 EL spectra of device B under different applied voltage from 0 V to 12 V. The inset shows a photograph of light emission under 12 V.

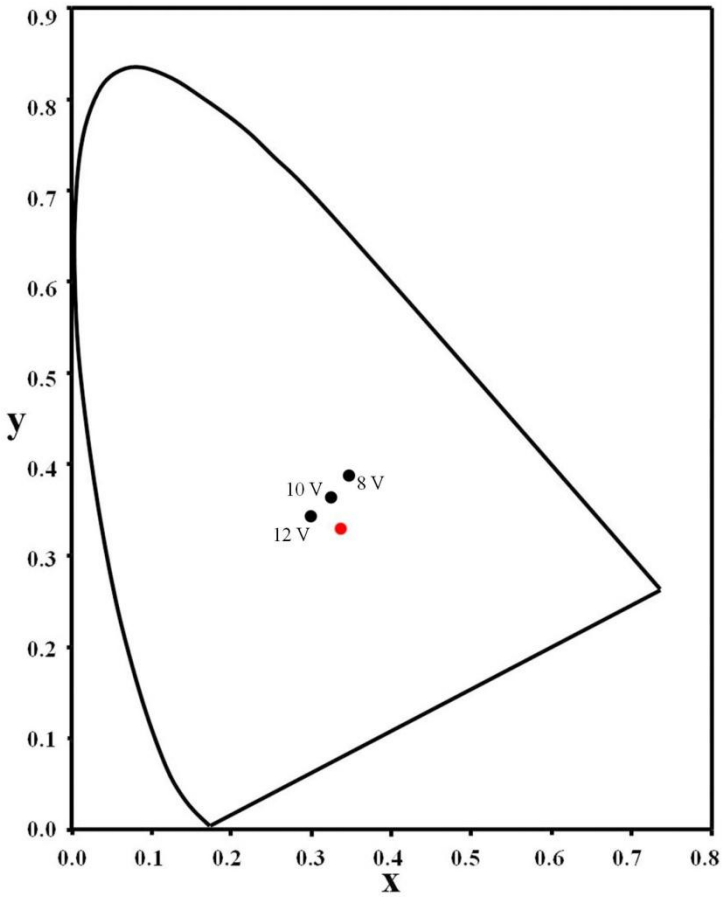

Fig. 4-8 CIE chromaticity coordinates of device B under different applied voltage of 8 V, 10 V, and 12 V. The red dot shown in the center represents white color in the chromaticity coordinates.

4.3.3 Mechanisms of electroluminescence from LEDs based on PMMA/ZnO QDs nanocomposite

For EL spectra of both device A and device B shown previously in Fig. 4-5 and Fig. 4-7, the shapes of all the spectra are similar because the emission layers in both devices are the same, although the EL intensity of device B is much higher than that of device A under the same forward bias. For our curiosity, it is more interesting to discuss about the mechanism of device B which is higher in both current density and EL intensity under the same applied bias. To further analyze the emission components, the

EL spectra can be deconvoluted into several primary Gaussian-shaped EL bands; similar to the analysis methodology used for the PL spectrum in Chapter 3.

Fig. 4-9 shows the EL spectra of device B replotted as EL intensity *vs.* photon energy. All the EL spectra of device B under different applied voltages of 8 V, 10 V and 12 V were fitted with several deconvoluted Gaussian bands as depicted in Fig. 4-9(a-c). The R^2 for all the curve fitting were 0.998, 0.999 and 0.999, respectively. It was found that two primary EL bands located at ~ 587 nm (2.11 eV, yellow-orange band) and ~ 485 nm (2.56 eV, blue band) were present in all the three EL spectra. When the magnitude of the applied voltage was higher than 10 V, two more bands with peak position at ~ 423 nm (2.93 eV, Violet band) and ~ 376 nm (3.30 eV, Near UV band or NUV band) emerged in the EL spectra. The EL intensities of all the bands increased with the applied voltages.

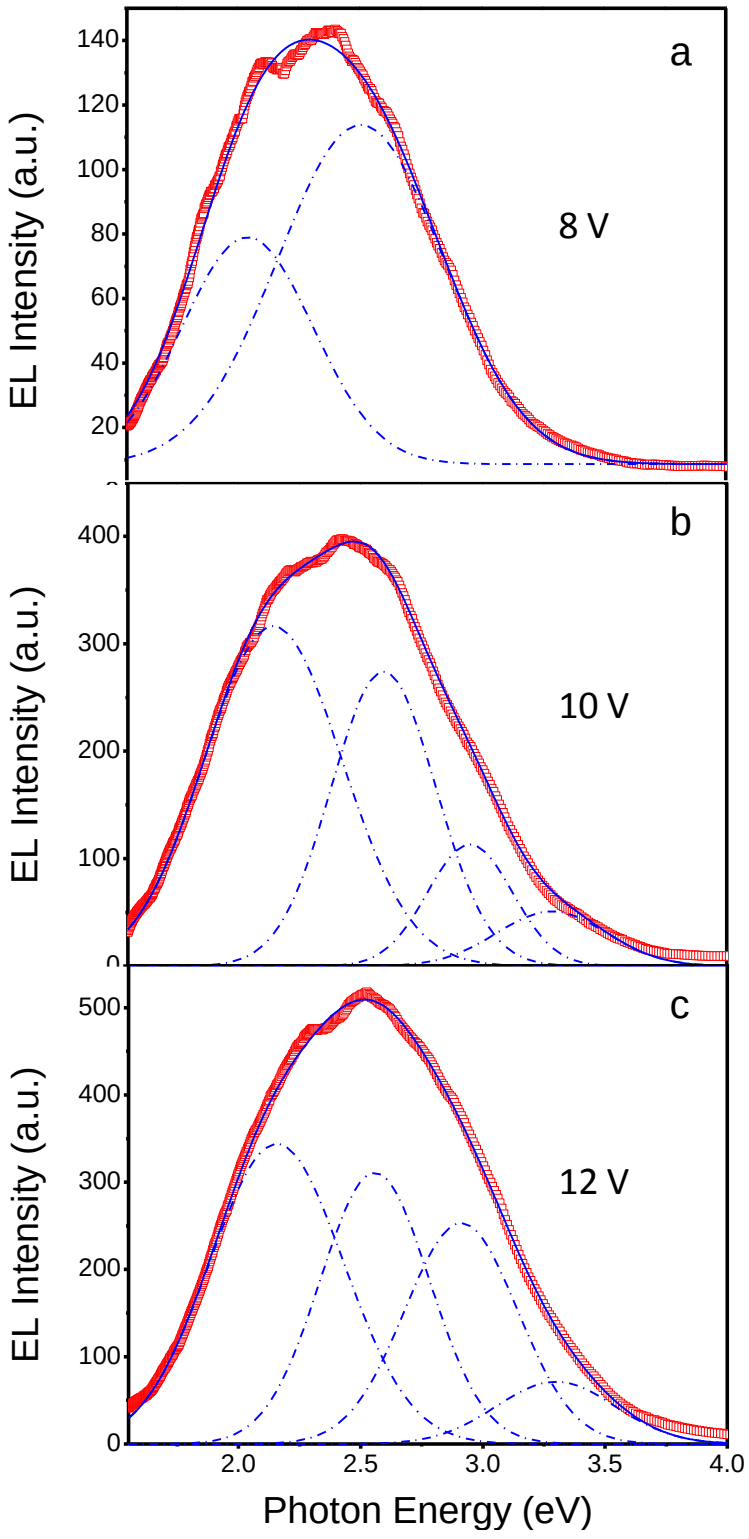

Fig. 4-9 Deconvolution of EL spectra measured at 8 V (**a**), 10 V (**b**), and 12 V (**c**).

Fig. 4-10(a) plotted the integrated intensity of each EL band as the function of applied voltages at 8 V, 10 V and 12 V. The peak positions for all the EL bands with the

voltages were shown in Fig. 4-10(b), and the corresponding full width half maximum (FWHM) of each band was shown in Fig. 4-10(c).

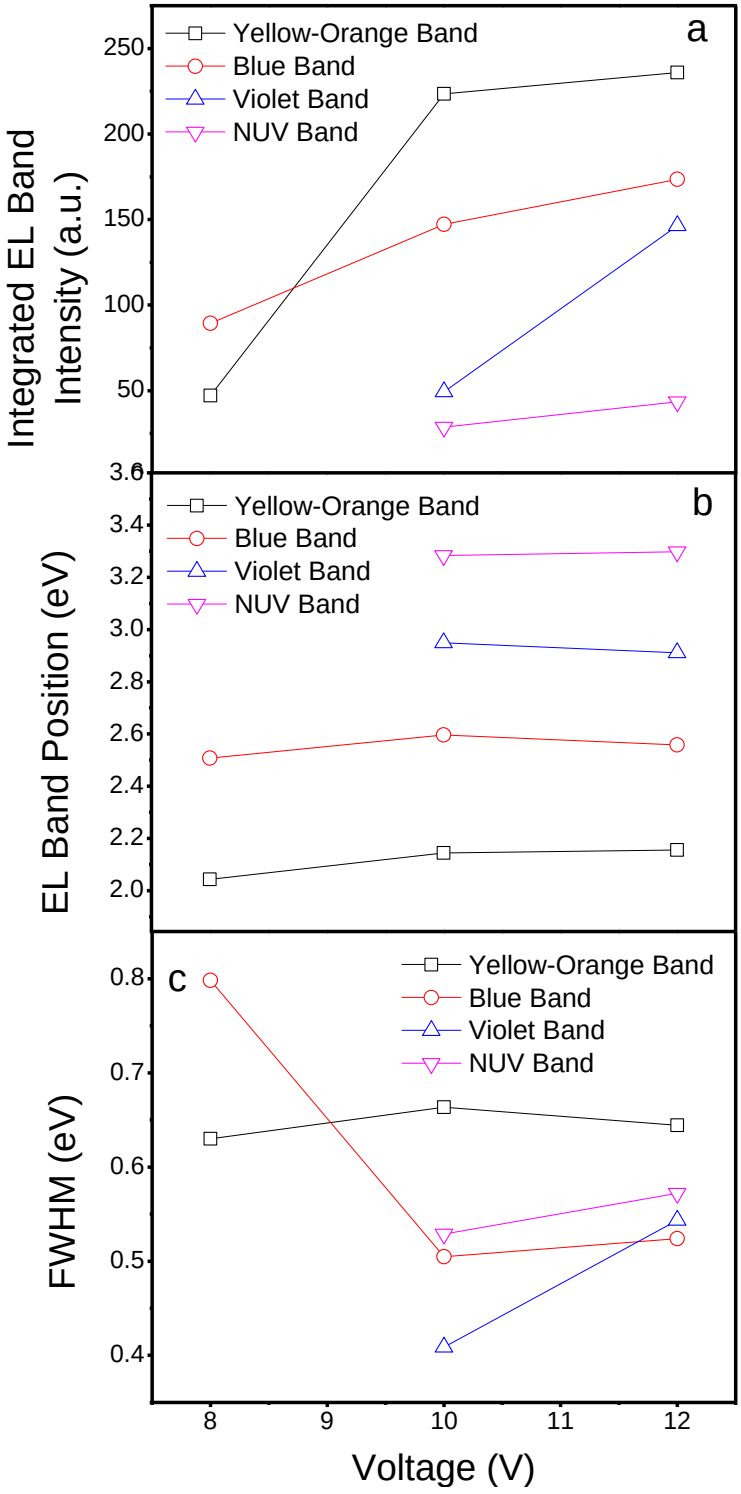

Fig. 4-10 Evolution of each deconvoluted EL band with the applied voltage; **a**. integrated intensity, **b**. peak position, and **c**. FWHM.

As could be seen in the Fig. 4-10(a), the yellow-orange and blue bands together contributed up to nearly 80 % of the total EL intensity (83 % at 10 V and 77 % at 12 V). When the voltage was increased from 10 V to 12 V, the intensity of violet band also increased significantly while that of NUV band was not that obvious. It was also found in other studies that by increasing the applied bias, light emission with shorter wavelength could be seen in the EL spectra.[116] As shown in Fig. 4-10(b), the peak positions of all the four EL bands were almost unchanged despite the changes of applied voltages. Therefore, it may be concluded that all the four EL bands originated from recombination between certain bands: either band edge of ZnO QDs or defect energy levels, but not from random recombination. Taking the PL spectrum into consideration, it is interesting to find that all the three bands shown in PL were also presented in the EL spectra, although the peak positions shifted slightly. This further confirms that the emission centers in both PL and EL were the same. A summary of all the Gaussian bands of PL and EL spectra is presented in Tab. 4-1. In the table, all the peak positions, as well as their contributions for the each spectrum, are listed. However, the spectral shape of EL significantly differs from that of PL. For example, the NUV and violet bands dominated the whole PL intensity only contributed less than 32 % of the total EL intensity. The blue band, one of the two primary bands in EL, only contributed a small portion in the PL. Furthermore, the yellow-orange band which was also one of the two primary bands in EL was not even observable in PL spectrum.

Tab. 4-1 Summary of each Gaussian band of PL and EL spectra.

	Yellow-Orange Band		Blue Band		Violet Band		NUV Band	
	Position	Intensity[a]	Position	Intensity[a]	Position	Intensity[a]	Position	Intensity[a]
PL	-[b]	-[b]	2.58 eV 481 nm	8.8%	3.08 eV 403 nm	50.3 %	3.30 eV 376 nm	40.9 %
8 V	2.04 eV 608 nm	34.6 %	2.51 eV 494 nm	65.4 %	-[b]	-[b]	-[b]	-[b]
10 V	2.14 eV 579 nm	49.8 %	2.60 eV 477 nm	32.8 %	2.95 eV 420 nm	11.0 %	3.28 eV 378 nm	6.4 %
12 V	2.16 eV 574 nm	39.4 %	2.56 eV 484 nm	28.9 %	2.91 eV 426 nm	24.4 %	3.30 eV 376 nm	7.3 %

[a]: percentage of integrated intensity for each EL band.

[b]: Peaks cannot be deconvoluted from the spectra.

The great difference in PL and EL should be assigned to the different mechanisms for EL and PL emission. The PL studies were discussed previously based on possible mechanisms responsible for the three PL bands, as depicted in Fig. 3-6. The NUV band originated from the radiative transition between electrons from CB of ZnO with holes from VB. The violet band was assigned to the recombination of electrons trapped at the shallow donor level below CB (Zn_i) and holes from VB of ZnO.[108, 163, 193, 218, 219] For the blue band, photogenerated electrons located at CB recombined with deep trapped holes at defect level which related to oxygen vacancies (V_O^{++}).[132, 133, 151, 219, 220] However, carriers transport pathways in EL were much more complicated because the electrons and holes were not photogenerated inside of ZnO QDs. Instead, the electrons were injected from the Al electrode and tunneled through the PMMA layer, followed by occupying the CB of ZnO. At the same time, the holes were injected from the ITO electrode and overcame the energy interval of the work function of ITO and the hole transport layer, PEDOT:PSS. The holes further tunneled through the PMMA layer and occupied the deep defect energy

levels and VB of ZnO. The energy band diagram of device B without any applied bias is shown in the Fig. 4-11(a); all the energy levels for ITO, PEDOT:PSS, ZnO QDs and Al were also indicated in this figure. The work function of Al, ~ 4.3 eV under vacuum level, was 0.1 eV higher than the CB of ZnO QDs (~ 4.4 eV). Therefore, the electron injection from Al electrode to CB of ZnO QDs as well as the shallow donor level was relatively easy. However, the hole injection was much more complicated and difficult. With a forward bias applied on the device, the holes firstly overcame the potential energy barrier between ITO and HOMO of PEDOT:PSS, which was 0.5 eV. With further increasing applied voltage, the holes were able to accumulate at the edge of PEDOT:PSS and PMMA/ZnO QDs nanocomposite. Following accumulation, the holes tunneled through the dielectric PMMA layer under the strong electric field, and occupied the deep defect energy levels located near the center of ZnO band gap. The recombination between electrons from CB or Zn_i and holes trapped at deep energy levels occurred and light with long wavelength (*e.g.*, red, yellow-orange, and blue bands) were emitted. With increasing applied voltage, the holes could further occupy lower energy levels, such as VB of ZnO. As a result, emission with short wavelength was given out, *i.e.*, violet and NUV bands. As a result, the total EL emission combined all the different bands from red to NUV and exhibited white color. Fig. 4-11(b) shows the energy band diagram of PMMA/ZnO QDs nanocomposite based white color LEDs under high applied voltage. The possible transport pathways of electrons and holes were also indicated in this figure. If our proposed hypothesis is correct, the two defect energy levels shown in the Fig. 4-11 corresponded to Zn_i and V_O^{++}.[108, 163, 220, 221] Furthermore, based on the above discussion, it leads us to conclude that the carrier injections of the devices were nonequilibrium, therefore, quantum efficiency of the light-emitting devices was very low.[21, 86] In the present study, the maximum

quantum efficiency of the LEDs was 0.0001 % and is much lower than that of Cd-based QD-LEDs and OLEDs. Additionally, the EL property critically relies on the carrier confinement within uniform ZnO QDs embedded in the nanocomposites. The large surface area of ZnO QDs is also required to provide carrier recombination centers of higher concentration. Both conditions cannot be achieved in a simple ZnO thin film device.[222]

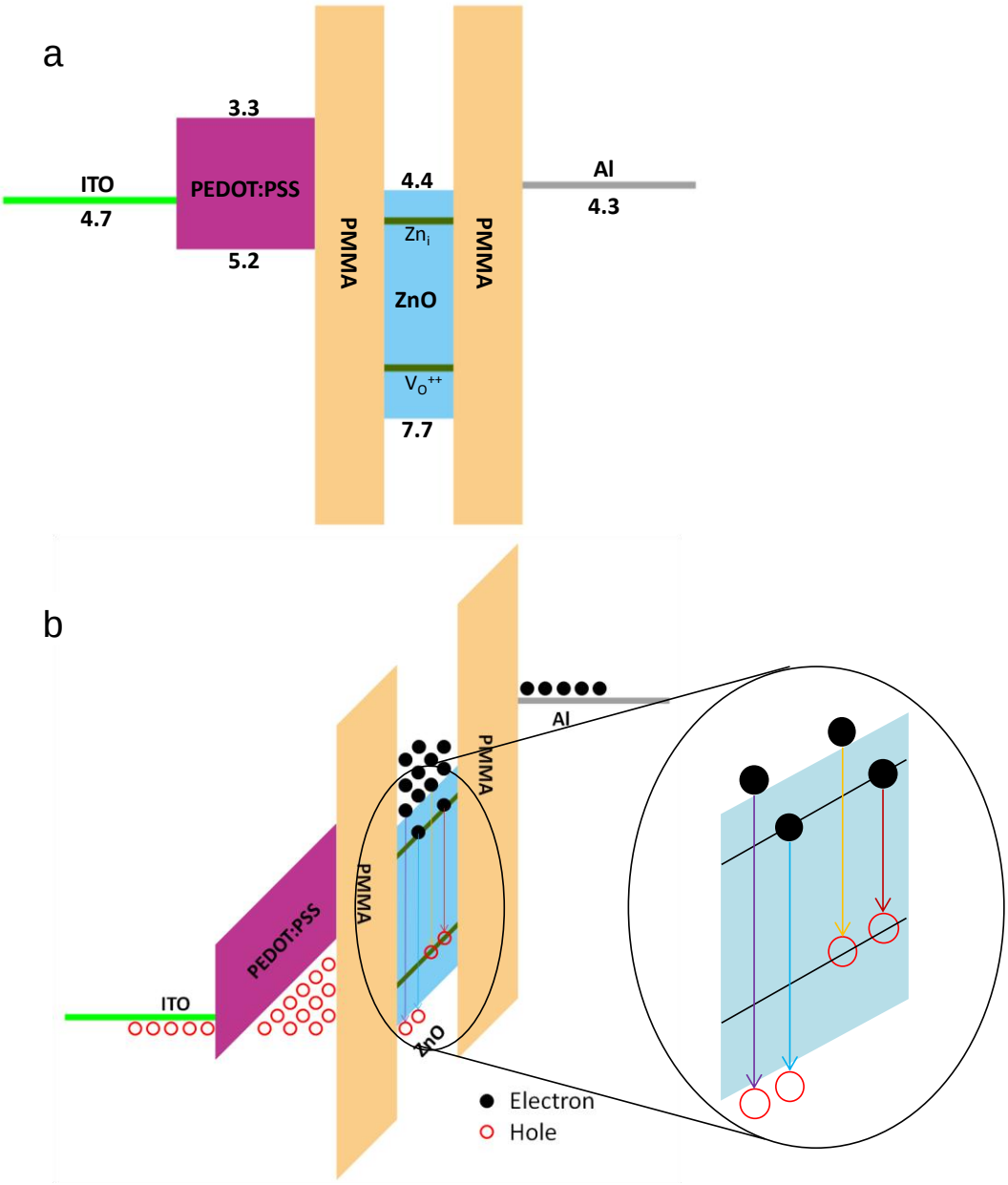

Fig. 4-11 Energy band diagram of device B. **a**. All the energy levels were indicated in the diagram of PMMA/ZnO QDs nanocomposite LEDs. **b**. Under a forward bias, the carrier transport pathways were indicated and the possible recombination was also presented.

From the FWHM of each peak shown in Fig. 4-10(c), it is easily observed that the FWHM of blue band changed from 0.80 eV to 0.50 eV when the applied voltage increased from 8 V to 10 V. At the same time, the contribution percentage of blue band decreased from 65.4 % to 32.8 %. It should be attributed to the appearance of violet and NUV bands that are originated from recombination between electrons and

holes from VB of ZnO; thus narrowing the blue band and reduced the contribution percentage in the total EL intensity. Moreover, the FWHM of violet band also changed significantly from 0.41 eV to 0.54 eV when the applied voltage increased from 10 V to 12 V. The contribution percentage of violet band also increased; thus, the emission of white color LEDs was observed to be slightly bluish. It was also observed that there was only slight change in the FWHM of yellow-orange band ($\pm$ 0.02 eV) as well as the NUV band ($\pm$ 0.02 eV). The contribution percentage of NUV band was much lower because the hole injection from ITO to VB of ZnO needed more energy and higher voltages. Based on our experiments, the LEDs based on PMMA/ZnO QDs nanocomposite easily broke down as the strong electric field across the nanocomposite thin film generated lots of heat and causing the polymer unstable.

Similar to device B, device A without hole transport layer, PEDOT:PSS, showed broad EL spectra from 350 nm to 800 nm, but the EL intensity was much lower. Fig. 4-12 showed the deconvolution of the EL spectrum of device A measured at the applied voltage of 12 V. The four Gaussian bands were depicted as blue dash curves and the blue solid curve was the sum of the four bands. The peak positions of the four Gaussian bands were 2.75 eV (451 nm, blue band), 2.45 eV (506 nm, blue-green band), 1.97 eV (629 nm, red band) and 1.56 eV (796 nm, near infrared band or NIR band); from short to long wavelength. The total EL intensity was mainly contributed from the blue (33 %) and blue-green (52 %) bands. It was also found that the NIR band together with red band contributed less than 15 % of the total EL intensity. Considering the background of measurement environment, the peak intensity of NIR band at 796 nm were only 2 times higher than the intensity of noise; which was really weak compared to the two dominant peaks. Moreover, the NIR and red bands were not even

observable in the PL spectrum of this nanocomposite. This could be attributed to the different mechanisms for EL and PL as discussed earlier.

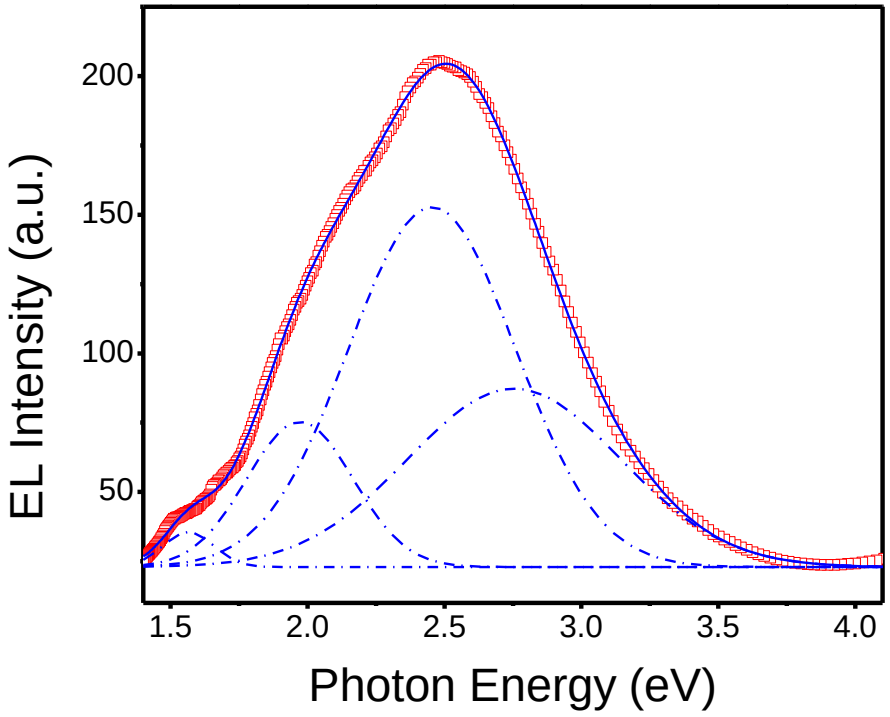

Fig. 4-12 Deconvolution of EL spectrum of device A measured at 12 V.

After carefully analyzing all the four bands, it is suggested that the blue and blue-green bands should be attributed to recombination related to double positive charged oxygen vacancies (V_O^{++}), while the red and NIR bands originated from the recombination related to deep level near the middle of ZnO band gap (V_O or V_O^{+}).[108, 199, 219, 220] The energy band diagram with all the energy levels was shown in Fig. 4-13(a). Without hole transport layer (PEDOT:PSS), higher voltage was required to reach sufficient hole injection and the hole could not accumulate at the edge of PMMA. As a result, the turn on voltage increased and the efficiency decreased. Similar conclusion was also obtained from current-voltage characteristics of device A. Fig. 4-13(b) shows the energy band diagram when the device is under forward bias and the possible recombination pathways are also indicated.

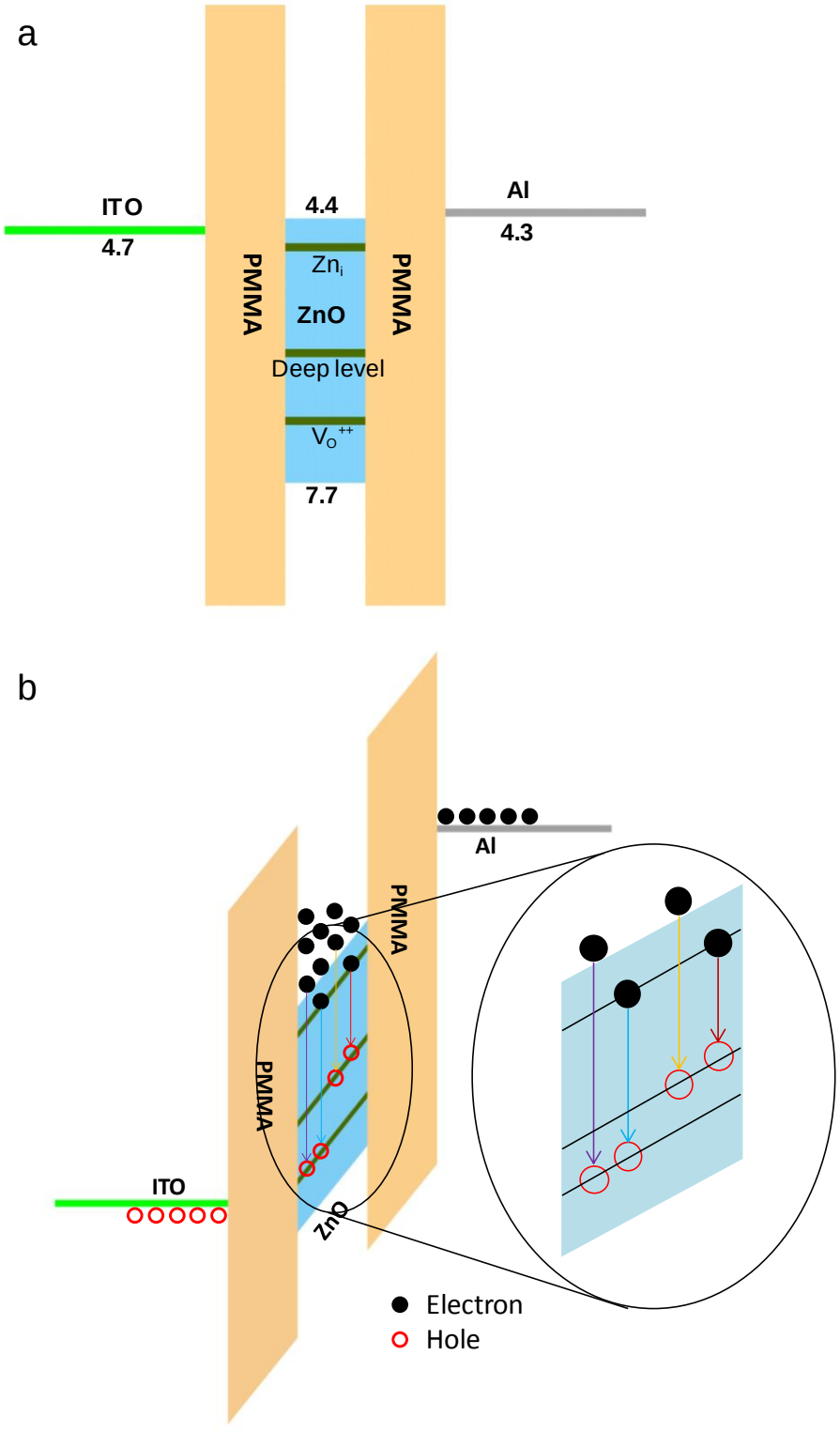

Fig. 4-13 Energy band diagram of device A. **a**. All the energy levels were indicated in the diagram of single layer PMMA/ZnO QDs nanocomposite LEDs. **b**. Under a forward bias, the carrier transport pathways were indicated and the possible recombination was also presented.

4.4 Conclusion

Light-emitting devices utilizing PMMA/ZnO QDs nanocomposite thin film as the emission layer was fabricated *via* spin coating technique. Current-voltage characteristics of LEDs with single nanocomposite layer showed diode behavior when either forward or reverse bias was applied on the device, which represented the so-called inversion symmetry. The single layer LEDs showed broad emission with relatively low EL intensity. By introducing a hole injection layer (HIL), PEDOT:PSS, between ITO and the nanocomposite emission layer, the device performance could be significantly improved. This is the first time a detailed EL study has been carried out on polymer/ZnO QDs nanocomposite. The double layer LEDs showed lower turn on voltage and higher EL intensity due to significant improvement of hole injection efficiency. In addition, LEDs with or without PEDOT:PSS layer exhibited similar EL spectra that covered the whole visible region; and the light emission from both devices was observed as white color. The deconvolution of EL spectra indicated the defect related energy levels, which correspond to visible EL emission, agreed well with the deduction made in PL study (Chapter 3). The quantum efficiency of LEDs was considered low due to nonequilibrium carrier injection; however, it can be improved through approaches such as introducing a low HOMO electron transport layer (ETL). The mechanism for the white light emission indicated that, utilizing the defect emission of ZnO QDs, it is possible to obtain emission of white color from one kind of QDs instead of mixing different color-emitted QDs. It also needs to be emphasized that the device-ready and chemically pure nanocomposite is critical for understanding the emission fundamentals; as disruptions or effects of impurities and side-products is rendered negligible.

5. Polymer/ZnO QDs Nanocomposites with Different Polymer Matrices and Their Application for Light-emitting Devices

5.1 Introduction

Surface state of ZnO QDs, including the defects or vacancies, is regarded as the main factor that determines the visible luminescence. Recently, incorporating ZnO QDs into different polymers have been proven to be an effective way to modify the surface of QDs and to impart unique properties, such as good chemical and thermal stability, good UV absorbance, high PL yield, etc.; beneficial for optical and electrical applications.[86, 223-234] The interaction between polymers and ZnO QDs are not only influenced by the nature of two components, but also by the preparation process. This type of interaction is widely reported in polymer/oxide synthesis system, not restricting to ZnO.[235-237] ZnO QDs with surface modified by double layer of MAA and PMMA showed blue emission under UV excitation.[132, 151] Tuning the size of ZnO QDs in PEGME, Xiong *et al.* synthesized nanocomposite exhibiting different colors from blue to orange.[164, 165] Incorporating ZnO QDs into light-emitting

polymers, such as PVK and PPV, the emission from polymers could be quenched by ZnO QDs due to carrier separation effect.[167, 238] Despite all these previous works, the mechanism of light emission from the ZnO QDs nanocomposites is still unclear and controversial.

In the previous chapter, we employed a new and facile method (described as polymerothermal method) to synthesize PMMA/ZnO QDs nanocomposite which exhibited strong UV emission but very weak visible emission in PL emission. Furthermore, the as-prepared nanocomposite was utilized for light-emitting application and the devices emitted white color. Extending from Chapter 3 and Chapter 4, we further apply the preparation and characterization methodologies on several polymers with representative structures. After surface modification, the nanocomposites showed interestingly different optical properties which should be attributed to different levels of surface passivation effect towards surface defect state of ZnO QDs. However, the method was not suitable for all the polymers; considerations need to be given to parameters such as polymer degradation temperature and polymer self-luminescence. Based on these considerations, light-emitting devices using several polymer/ZnO QDs nanocomposites are also demonstrated.

5.2 Experimental Details

5.2.1 Materials

Polystyrene (PS, M_w = 280,000 g·mol^{-1}), Poly(9-vinylcarbazole) (PVK, M_w = 50,000 – 100,000 g·mol^{-1}), Poly(vinyl pyrrolidone) (PVP, M_w = 10,000 g·mol^{-1}), Poly(4-vinylpyridine) (P4VP, M_w = 60,000 g·mol^{-1}), N,N-Dimethylformamide (DMF, 99.8 %), and toluene (≥ 99.7 %) were purchased from Sigma Aldrich and used without

purification. Poly(vinylidene fluoride) (PVDF) and chlorobenzene (≥ 99.5 %) were purchased from Alfa Aesar. Methanol (CH_3OH, ≥ 99.9 %) was purchased from Fisher Scientific.

5.2.2 Preparation of Polymer/ZnO QDs Nanocomposites

The preparation method for polymer/ZnO QDs nanocomposites is similar to what was described previously in Chapter 3. For a better comparison, the concentrations of different polymers in the solvents were also controlled as the same, which was 10 $mg \cdot ml^{-1}$. Due to very different natures of the polymer, their solubility in certain solvent is completely dissimilar. Therefore, in order to obtain well-soluble polymer solution, different solvents were selected for individual polymer. The solvents for different polymers were listed in Tab. 5-1. The dissolution process of all the polymers was similar to that of PMMA as described in Chapter 3. The polymer/zinc acetate hybrid precursor solutions were prepared by adding zinc acetate solution (dissolved in methanol with concentration of 10 mg/ml) into different polymer solutions at volume ratio of 1: 10, which was the same ratio to PMMA solution. The polymer/ZnO QDs nanocomposites were obtained by spin coating or drop casting the as-prepared precursor solutions onto different substrates, followed by heat treatment at 200^oC for 1 hr.

Tab. 5-1 List of the studied polymers and each solvent for individual polymer.

Polymer	Solvent
Polystyrene (PS, $[CH_2CH(C_6H_5)]_n$) 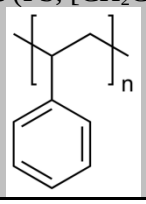	Toluene ($C_6H_5CH_3$) 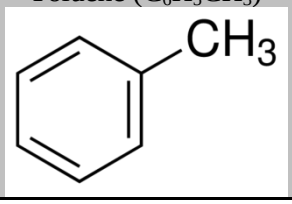
Poly(vinylidene fluoride) (PVDF, $[CH_2CF_2]_n$) 	*N*,*N*-Dimethylformamide (DMF, $HCON(CH_3)_2$) 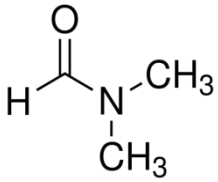
Poly(9-vinylcarbazole) (PVK, $[C_{14}H_{11}N]_n$) 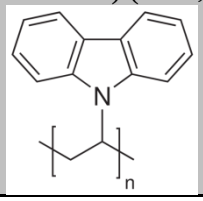	Chlorobenzene (C_6H_5Cl) 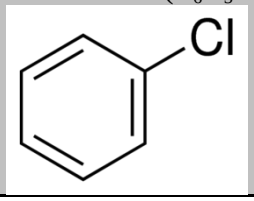
Poly(vinyl pyrrolidone) (PVP, $[C_6H_9NO]_n$) 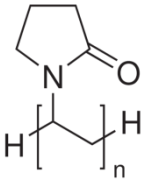	Methanol (CH_3OH) 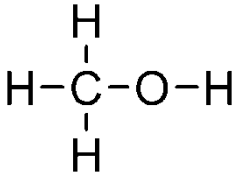
Poly(4-vinylpyridine) (P4VP, $[C_7H_7N]_n$) 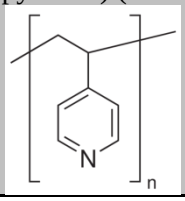	Methanol (CH_3OH) 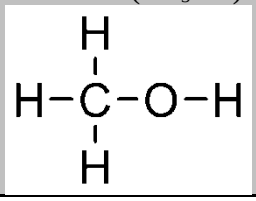

5.2.3 Fabrication of Light-emitting Devices (LEDs) based on Polymer/ZnO QDs Nanocomposites

The LEDs based on polymer/ZnO QDs nanocomposites were fabricated *via* solution process and spin coating technique. The detailed procedures were the same as that of the devices fabricated based on PMMA/ZnO QDs nanocomposite; which was described in the experimental part of Chapter 4. As discussed in Chapter 4, the device

performance of LEDs with hole transport layer, *i.e.*, PEDOT:PSS, was better than that of the devices with only nanocomposite emission layer. Therefore, in this section, only devices with PEDOT:PSS layer were fabricated. However, spin coating technique was not able to give a continuous thin film from PVDF solution. Finally, only PS, PVK and P4VP based polymer/ZnO QDs nanocomposites were successfully utilized for the light-emitting application.

5.2.4 Characterization of Nanocomposites and the LEDs

The polymer/ZnO QDs nanocomposites were characterized *via* TEM, UV-VIS, PL, and AFM. The I-V characteristic and EL of the LEDs based on the nanocomposites were studied as well. All the characterization methods and equipments were the same as those described in Chapter 3 and Chapter 4.

5.3 Results and Discussion

The properties of different polymers vary due to different polymer architectures, molecular structures, and functional groups. Therefore, the properties of nanocomposites are expected to differ from each other. In this section, the characterization results are presented and discussed.

5.3.1 TEM Characterization of Polymer/ZnO QDs Nanocomposites

The nanocomposites consisting of ZnO QDs embedded in the different polymer matrices were characterized *via* TEM and the images are shown in Fig. 5-1. ZnO QDs with average size of 4 ~ 5 nm are observed in PS (a-i, ii), PVK (b-i, ii), PVP (c-i, ii) and P4VP (d-i, ii) based nanocomposites. The series of x-i on the left show the low magnification TEM images, while the higher magnification TEM images are shown as

the series of x-ii on the right. It is necessary to point out that TEM characterization done on the ZnO QDs in PVDF matrix was unsuccessful due to the immediate crimping of polymer film when exposed under high energy electron beam. It is because PVDF is a piezoelectric material that caused this phenomenon. Therefore, other techniques, such UV-VIS and PL, were used to confirm the formation of nano-sized ZnO in PVDF matrix and the results are shown in the later part.

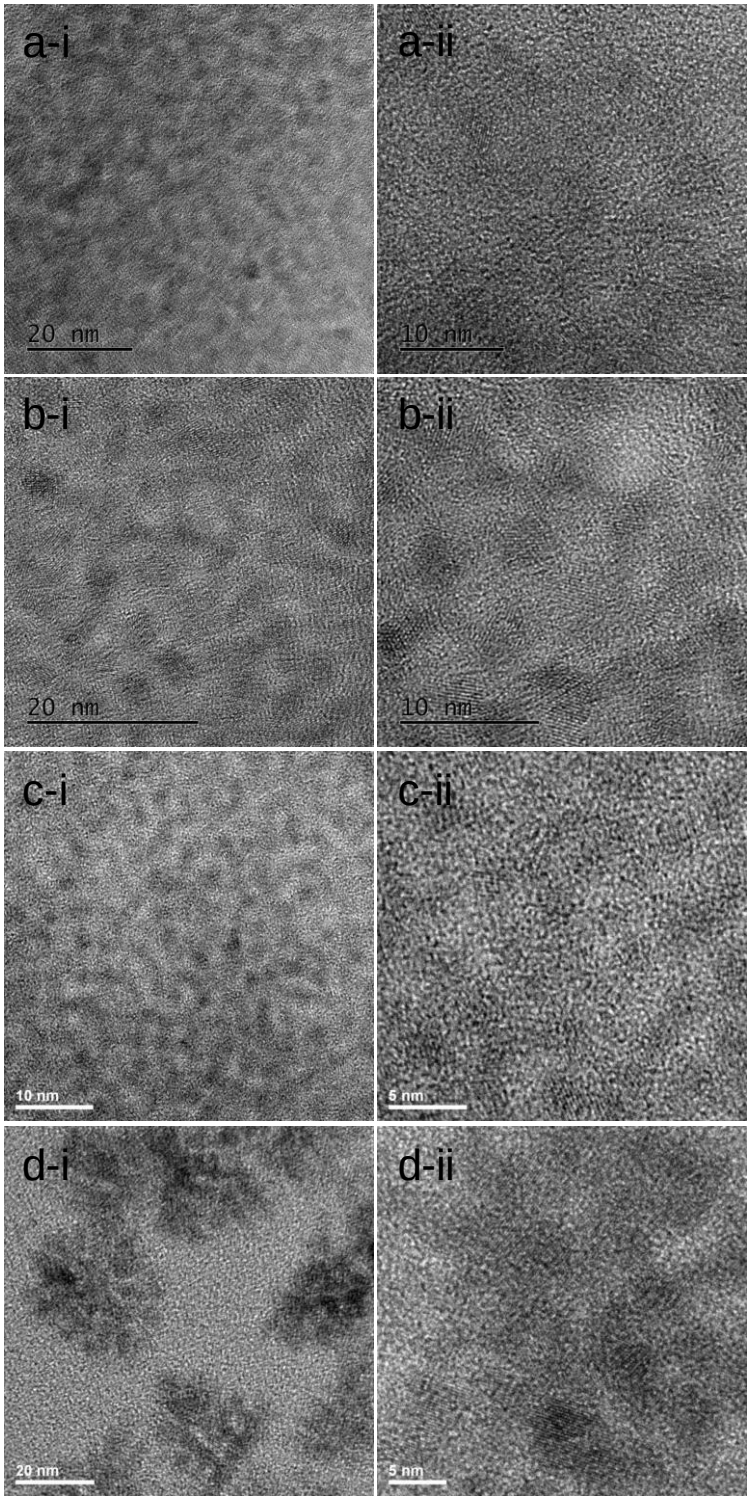

Fig. 5-1 TEM images of ZnO QDs in different nanocomposites based on PS (**a**-i, ii), PVK (**b**-i, ii), PVP (**c**-i, ii), and P4VP (**d**-i, ii). Series x-i: low magnification; series x-ii, high magnification.

As can be seen in the Fig. 5-1, the ZnO QDs are uniform in size and with the spherical shape in the PS, PVK and PVP based nanocomposites. Moreover, the lattice spacing

of ZnO could be clearly seen in the higher magnification images. However, the same situation cannot be found in the P4VP based nanocomposite. Instead, ZnO QDs in P4VP matrix easily aggregate into clusters with size about 20 ~ 30 nm. The magnified image presented in Fig. 5-1(d-ii) shows the clusters consist of several nano-sized ZnO with size comparable to those synthesized in other polymers. The formation of ZnO clusters is mainly due to the film morphologies of P4VP. Fig. 5-2 shows the AFM image of pure P4VP thin film spin coated on silicon wafer at 3000 rpm for 60 s. The average thickness of film is about 70 nm, as measured *via* AFM. It clearly shows that the surface morphology of P4VP is not uniform, while domains with different sizes are formed. During heat treatment, zinc acetate coordinated with pyridine unit is thermally decomposed in the domains with P4VP surrounded. Therefore, ZnO clusters consisted of several ZnO QDs formed in the P4VP matrix.

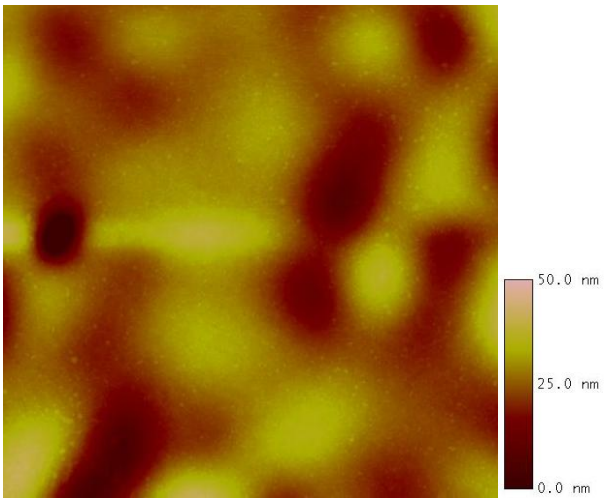

Fig. 5-2 AFM image of pure P4VP spin coated on silicon wafer. The dimension of image is 1 μm by 1 μm.

Despite certain aggregation observed in the TEM images, it is consistent with the fact that nano-sized ZnO could be synthesized from zinc acetate precursor *via* polymerothermal method in different polymer matrices. It is also indicated polymer

surface modification is an effective way to control the size of ZnO QDs and prevent them from growing into large particles.

5.3.2 UV-VIS Absorption Study of Polymer/ZnO QDs Nanocomposite

UV-VIS absorption spectroscopy is a good approach to diagnose the existence of semiconductor nanocrystal in a transparent polymer matrix. Not only the band gap, the size of the nanocrystal could also be determined through this method. In Fig. 5-3, the UV-VIS absorption spectra of different polymers/ZnO QDs nanocomposites are presented. The black curves in each figure show the absorption spectra of each pure polymer before (dash dot) and after (solid) heat treatment. The red ones represent the absorption spectra of nanocomposites based on different polymers. To further analyze the UV-VIS results, all the related spectra are replotted as $(\alpha h\nu)^2$ *vs.* $h\nu$ and shown as inset figures.

Similar to absorption spectrum of PMMA/ZnO QDs nanocomposite, the one based on PS also shows a strong absorption at the range of 350 nm ~ 380 nm (Fig. 5-3(a)), indicating the conversion of ZnO from zinc acetate. The band gap of ZnO QDs is about 3.33 eV as deduced from the inset figure. The average size of the QDs is calculated to be 6.0 nm and 5.6 nm according to Eq. 3-1 and Eq. 3-3, respectively. Similar deduction could also be obtained from P4VP based nanocomposite. Although the TEM images show clusters of nano-sized ZnO in P4VP matrix, the UV-VIS absorption shown in Fig. 5-3(d) suggested that the ZnO nanoparticles in the clusters remains in quantum confinement regime. The band gap of ZnO QDs in P4VP matrix is about 3.35 eV and the corresponding diameter of QDs is 5.7 nm and 7.4 nm, as obtained from those two models, respectively.

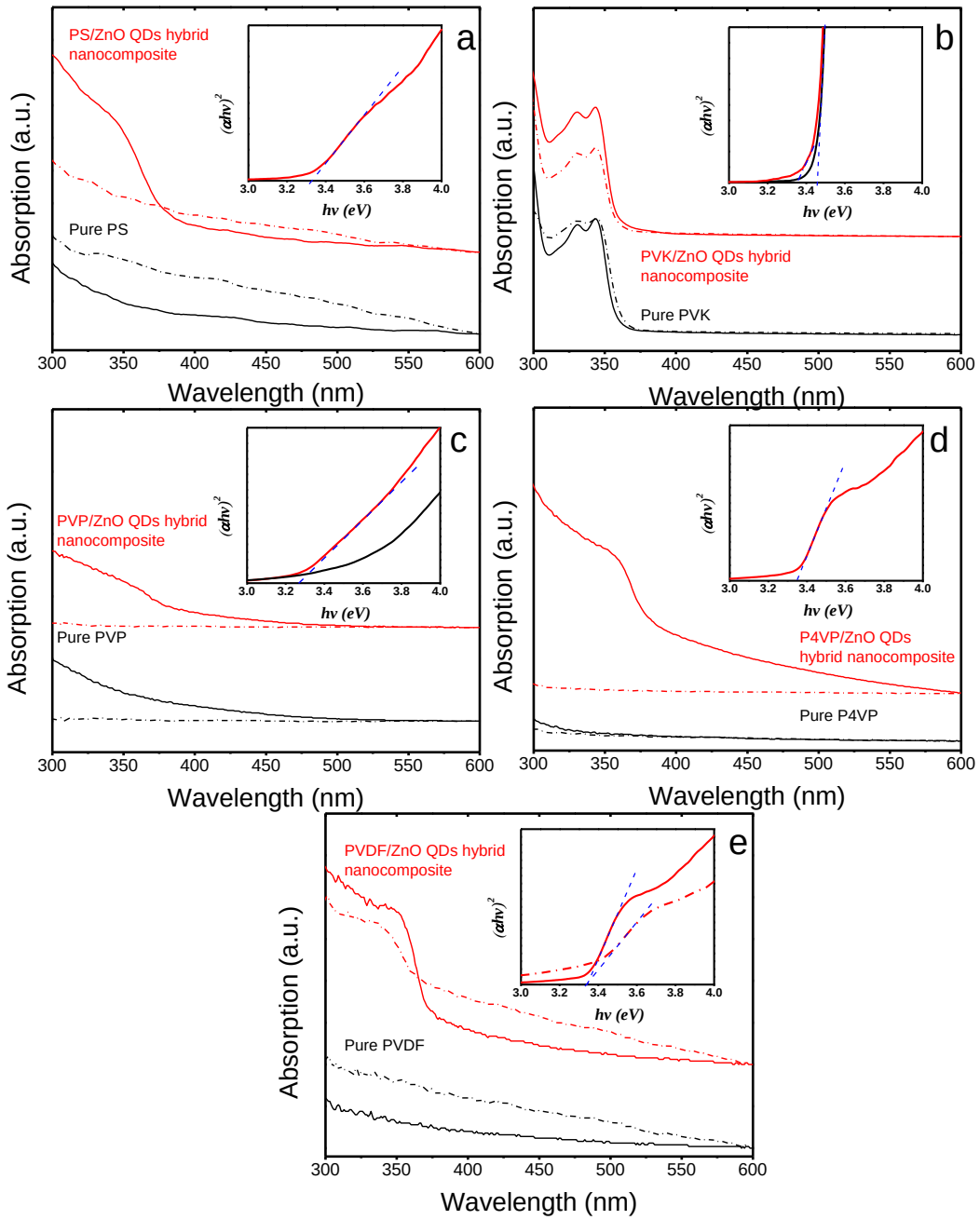

Fig. 5-3 UV-VIS absorption spectra of different polymers (black curves) and their nanocomposites (red curves). The dash dot curves represent samples before heat treatment, while the solid curves indicate samples with heat treatment. Figure **a**–**e** represent different polymers of PS (**a**), PVK (**b**), PVP (**c**), P4VP (**d**), and PVDF (**e**), respectively. The inset figures show the replotted spectra as $(\alpha h\nu)^2$ *vs. hν* for related absorption spectra.

PVK is the only polymer which is conductive among all the polymers studied in this work. In the past decades, PVK was widely used in the optoelectronic devices, for instance, OLEDs.[239, 240] The band gap of PVK is 3.5 eV, with LUMO and HOMO

at 2.3 eV and 5.8 eV under vacuum level, respectively. Therefore, the UV-VIS absorption spectrum of PVK/ZnO QDs nanocomposite included in Fig. 5-3(b) shows that the absorption of ZnO QDs is completely overlapped by the strong absorption of PVK. From the replotted $(\alpha hv)^2$ *vs. hv* curves of pure PVK and PVK/ZnO QDs nanocomposite, the slight difference at the edge might be caused by the embedded ZnO QDs. The band gaps of ZnO QDs and PVK are found to be 3.35 eV and 3.46 eV, respectively.

Fig. 5-3(c) shows the UV-VIS absorption spectra obtained from pure PVP and PVP/ZnO QDs nanocomposite. The results clearly show that, after heat treatment, the absorption coefficient of pure PVP is comparable to that of nanocomposite. Nevertheless, there is still slight difference at the absorption onset of ZnO QDs. According to the replotted $(\alpha hv)^2$ *vs. hv* curve shown in the inset, the band gap of ZnO is estimated to be 3.27 eV, which corresponds to diameter of 7.4 nm. However, the average size of ZnO QDs as observed from TEM images is about 2.5 nm. The large error in term of calculated size might be caused by the absorption of PVP. Moreover, the transparent polymer turned yellowish after heat treatment. Such observation will be discussed in the section on PL characterization.

Although TEM characterization could not be performed on PVDF based nanocomposite, UV-VIS absorption confirms the formation of ZnO QDs. As can be seen in Fig. 5-3(e), pure PVDF shows optical transparency at the range of 300 nm ~ 600 nm either before or after heat treatment. However, it is interesting to find an absorption peak at the region of 340 ~ 380 nm even when the sample with zinc precursor was prepared without heat treatment. This absorption peak should be attributed to the formation of ZnO QDs. During mixing process, ZnO QDs probably formed due to chemical reaction between zinc acetate with either solvent or polymer.

The band gap of ZnO QDs can be deduced from the replotted $(\alpha hv)^2$ *vs.* hv curves shown as the inset of Fig. 5-3(e). For the two samples with and without heat treatment, their ZnO band gaps are almost the same, *i.e.*, ~ 3.34 eV. For the sample without heat treatment, the diameters of ZnO QDs are calculated to be 5.9 nm and 3.9 nm from the two equations (Eq. 3-1 and Eq. 3-3). The sizes of ZnO QDs for the annealed sample are calculated to be 5.9 nm and 5.7 nm, respectively.

All the size of ZnO QDs in different polymers based nanocomposites are summarized in Tab 5-2. Due to the coupling effect between nearby QDs in the nanocomposites, the calculated size is always larger than that obtained from TEM results. However, the slight blueshift of absorption band edge and the corresponding size of ZnO confirm the formation of QDs in the nanocomposites.

Tab. 5-2 Summary of the size of ZnO QDs in different polymer matrices.

	Effective mass model	**Meulenkamp**	**TEM**
PS	6.0 nm	5.6 nm	4.0 nm±1.0 nm
PVDF	5.9 nm 5.9 nm (before)	5.7 nm 3.9 nm(before)	-[a]
PVK	5.7 nm	-[b]	4.0 nm±0.5 nm
PVP	7.4 nm	-[b]	2.5 nm±0.5 nm
P4VP	5.7 nm	7.4 nm	5.5 nm±1.0 nm
PMMA	5.7 nm	5.7 nm	4.0 nm±1.0 nm

[a]: TEM characterization cannot perform on PVDF/ZnO QDs nanocomposite.

[b]: It is impossible to determine the value of $\lambda_{1/2}$ due to complete overlap of absorption spectra of pure polymers with that of ZnO QDs.

5.3.3 Photoluminescence (PL) Study of Polymer/ZnO QDs Nanocomposite

As discussed in previous chapter on PMMA/ZnO QDs nanocomposite, the PL emission of ZnO QDs was significantly affected by the polymer surface modification. The interaction between polymer functional groups and ZnO QDs plays an important role. Furthermore, certain polymers could also give strong PL emission under UV excitation. This phenomenon adds up to the complexity of studying the PL emission from the nanocomposites. Nonetheless, PL spectra of ZnO QDs nanocomposites as well as the corresponding pure polymers were measured and are shown in Fig. 5-4. Similar to previous UV-VIS study, the black curves in each figure show the PL spectra of each pure polymer before (dash dot) and after (solid) heat treatment; while the red curves represent the PL spectra of nanocomposites based on different polymers.

Fig. 5-4(a) shows the PL spectra of PS based nanocomposite with ZnO QDs embedded and the pure PS. After heat treatment, a PL peak with low intensity appeared at around 367 nm, which is not found in that of sample without heat treatment. It is probably caused by polymer degradation at high temperature annealing. This peak was also found in the PL emission spectrum of PS/ZnO QDs nanocomposite shown as red solid curve in Fig. 5-4(a). Apart from this peak, it shows strong NUV emission at 387 nm which corresponds to PL emission from ZnO band edge. Defect emission originated from oxygen vacancies is fully quenched due to the surface passivation effect. Due to the delocalized electron configuration on the pendant phenyl group, there should be very weak interaction between PS and ZnO, but the pendant phenyl group could fill up the surface oxygen vacancies which reduced the defect related PL emission of ZnO. Similar deduction could be drawn on the PMMA based nanocomposite. However, the

carbonyl group in PMMA chains could somehow coordinate with Zn^{2+} on the surface and stabilizing oxygen vacancies of higher concentration than that in PS based nanocomposite. The dominant peak at 387 nm (3.21 eV) is close to PL emission from the bulk ZnO, indicating that ZnO QDs could easily agglomerate in the PS matrix. The coupling effect between nearby ZnO QDs caused redshift of the PL peak position.

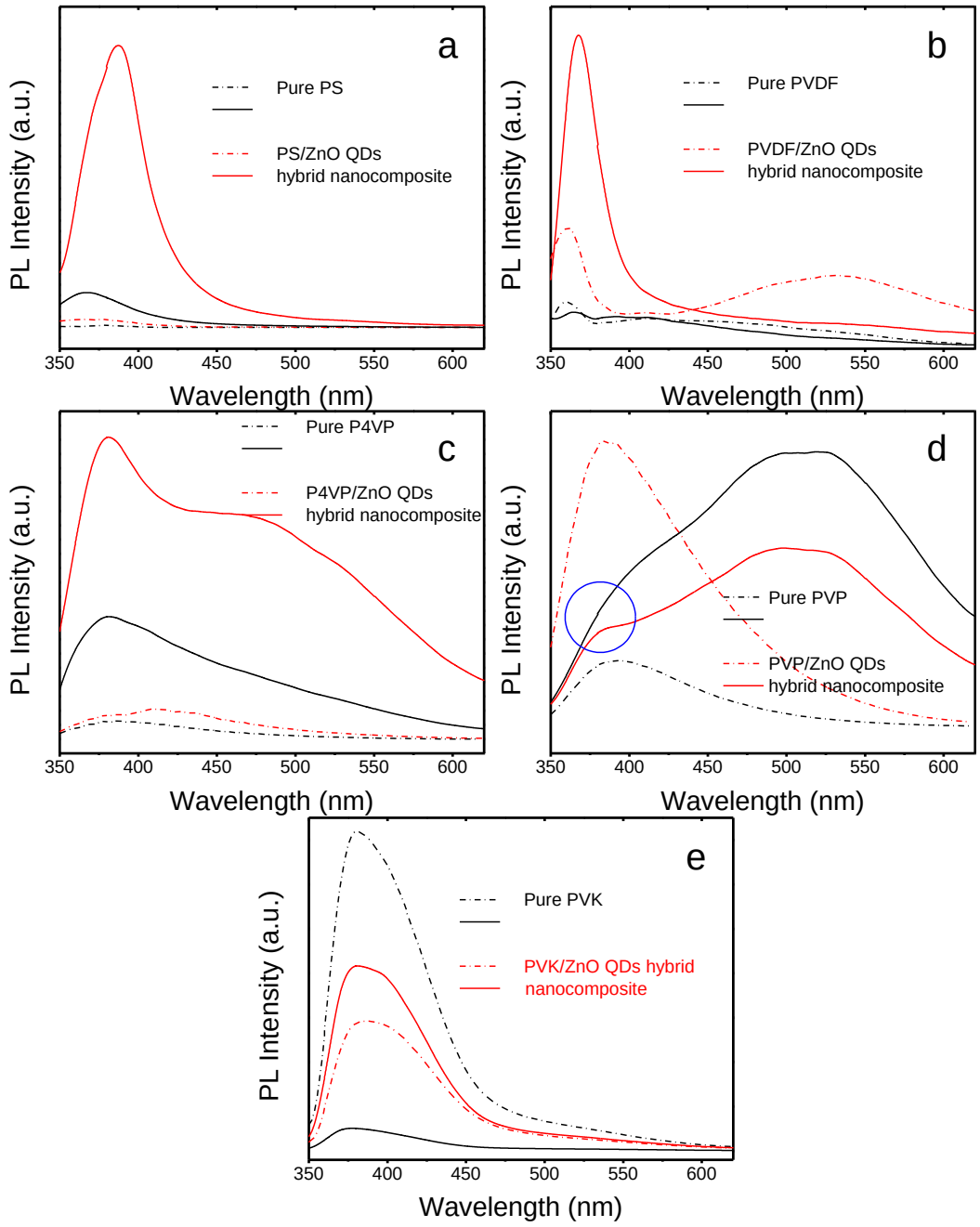

Fig. 5-4 PL spectra of different polymers (black curves) and their nanocomposites (red curves). The dash dot curves represent samples before heat treatment, while the solid curves indicate samples with heat treatment. Figure **a**–**e** represent different polymers of PS (**a**), PVDF (**b**), P4VP (**c**), PVP (**d**), and PVK (**e**), respectively.

PL spectra of pure PVDF and PVDF/ZnO QDs nanocomposite are shown in Fig. 5-5. According to the absorption study, the nanocomposite shows an absorption peak at NUV region in both samples with and without heat treatment (see Fig. 5-3(e)). For the

sample without heat treatment, its PL emission (red dash dot curve in Fig. 5-4(b)) is mainly contributed from two parts: the NUV region and the visible region. The NUV band is partially influenced by the native emission from pure PVDF as could be seen from the black dash dot curve; while the visible emission are related to the defect emission from ZnO. It is interesting to find that, after heat treatment, the PL emission at the NUV region significantly increases while the defect emission at the blue-green region is completely quenched. This phenomenon is similar to the deduction that obtained from PS based nanocomposite. However, it should be mentioned that the PL peak in the emission of PVDF/ZnO QDs nanocomposite is significantly blue-shifted which indicates better quantum confinement of ZnO QDs in the PVDF matrix. It might be attributed to the strong interaction between Zn^{2+} on the QDs surface with carbon-fluorine bond which has strong polarity that totally passivated the surface of ZnO QDs and thus, preventing them from growing into larger particles.

Fig. 5-4(c) shows the PL spectra of P4VP and P4VP based nanocomposite. TEM images show clusters consisting of several ZnO QDs formed within the nanocomposite. . The PL spectrum shows that the defect emission is comparable to the NUV emission; which is not observed in other nanocomposites. It is believed that in the cluster, oxygen vacancy related defect can easily form at the interface of connected ZnO QDs; which is similar to bare QDs without polymer surface passivation. Moreover, it has been known that the pyridine group could coordinate with Zn^{2+} located on the surface of ZnO QDs.[241-244] Therefore, the strong defect emission might originate from the well protected oxygen vacancies related defect. Additionally, it should be mentioned that P4VP itself became a light emitting material after heat treatment and the emission spectra overlapped with ZnO emission in the nanocomposite.

Fig. 5-4(d) shows the PL spectra of PVP and PVP/ZnO QDs nanocomposite. PVP is a light emitting material and itself presents a broad emission spectrum with the excitation wavelength of 325 nm from He-Cd laser. However, the luminescent property of PVP changed after heat treatment. According to the black solid curve shown in Fig. 5-4(d), PL spectrum of heat treated PVP presents a strong and broad visible emission. As mentioned earlier, the transparent polymer became yellowish color after heat treatment, which is probably attributed to polymer degradation. The nanocomposite shows similar spectrum as that of pure PVP except in the NUV region indicated within the blue circle, which is believed to be contributed from ZnO QDs. However, the defect emission of ZnO totally overlaps with the strong emission from PVP and it is not reasonable to make further quantitative interpretation from the spectra.

As shown in Fig. 5-4(d), the PL spectra of pure PVK and PVK/ZnO QDs nanocomposite before and after heat treatment exhibit similar spectral shape but different intensities. The emission range of PVK overlaps with the excitonic emission of ZnO at the UV region. Due to the low concentration of ZnO QDs in the nanocomposite, the emission from PVK dominates the whole PL intensity. Different from other polymers, the PL emission intensity of pure PVK is significantly quenched after heat treatment, shown as the black solid curve. It is probably due to the destruction of recombination centers at high temperature. However, it is interesting to find an opposite trend from observation on the nanocomposite, *i.e.*, the PL intensity of nanocomposite is higher than that before heat treatment. It suggested that ZnO QDs increases the thermal stabilities of polymer and prevents it from extensive degradation at high temperature. Another explanation is that the emission of ZnO QDs became comparable with the heat treated PVK in the nanocomposite; thus, the whole PL

emission intensity is higher because of the contribution from ZnO QDs. Energy transfer between PVK and ZnO QDs that occurred in the hybrid system will also make the interpretation of PL emission more complicated.

In summary, the PL characterization confirmed the conversion of ZnO from zinc acetate in the different polymers based nanocomposites. Moreover, the PL emission of ZnO QDs could be easily influenced by the polymer matrices either from the polymer itself or from the interaction between polymer and ZnO QDs. Normalized PL spectra of all the polymer/ZnO QDs nanocomposites are summarized in Fig. 5-5. Except P4VP and PVP based nanocomposites, the rest of the four samples show strong UV emission but very weak visible emission due to polymer surface passivation effect that reduce the defect concentration on the surface of ZnO QDs. Moreover, interaction between functional groups, such as carbonyl (C=O) in PMMA and pyridine group in P4VP, with Zn^{2+} located on the surface of ZnO QDs might help to stabilize oxygen vacancies. Therefore, the visible emission from PMMA and P4VP based nanocomposites is higher than that of nanocomposite based on PS. Besides oxygen vacancies related visible emission, zinc interstitial (Zn_i), a shallow donor below CB of ZnO, related defect emission could also be observed in the PL emission of nanocomposites. However, the corresponded emission normally showed violet or violet-blue that overlapped with the strong NUV emission from free exciton emission of ZnO. Nevertheless, the mechanism of PL emission from the polymer/ZnO QDs nanocomposites is still unclear. Currently, more studies are required to investigate the interaction effect as well as the size effect. It should emphasize that the preparation method proposed in this study is free of impurity. The obtained nanocomposites with uniform size distribution are suitable for the fundamental study of interaction between polymers and ZnO.

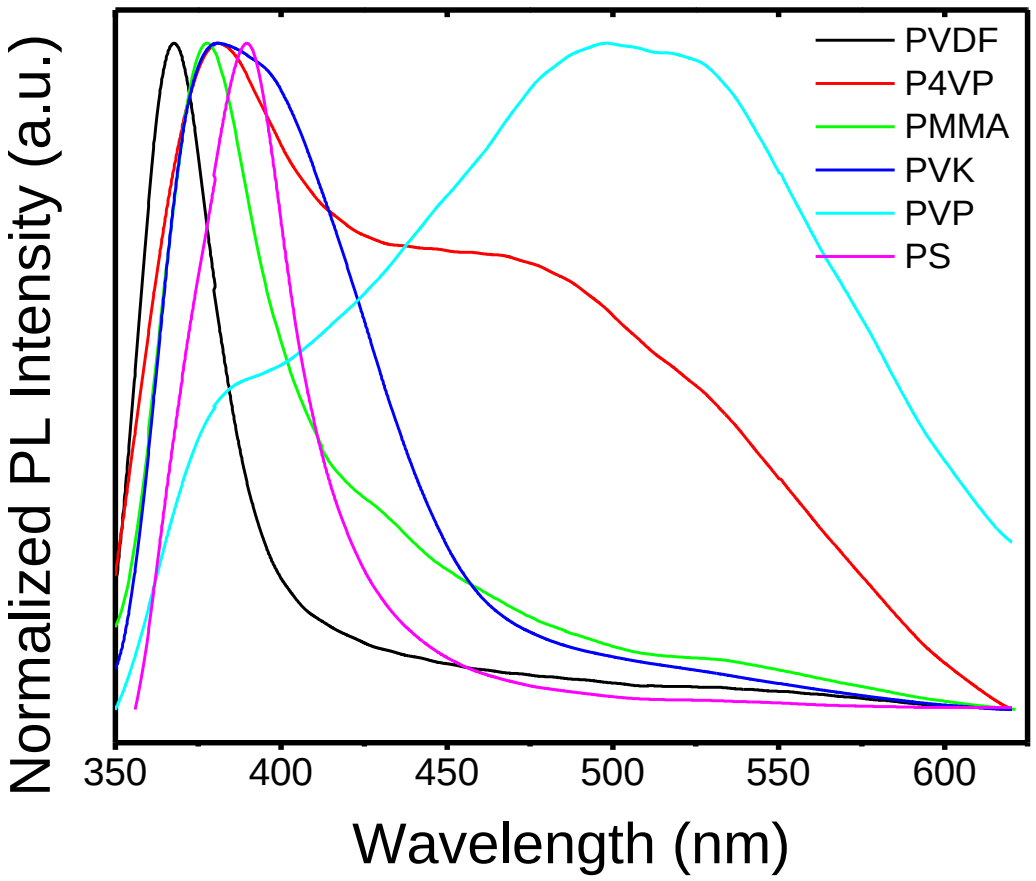

Fig. 5-5 Normalized PL spectra of polymer/ZnO QDs nanocomposites.

5.3.4 Characterization of Polymer/ZnO QDs Nanocomposites Light-emitting Devices

All the LED devices were fabricated *via* spin coating technique as described previously. However, this technique could not be performed on PVDF based nanocomposite due to its poor film forming capability. For PVP, the strong PL emission originated from the polymer overlapped with the emission of ZnO QDs. Such phenomenon would have confused the interpretation of results in present studies. Therefore, only PS, PVK and P4VP based nanocomposites were utilized for light-emitting devices.

EL spectra of the light-emitting device based on PS/ZnO QDs nanocomposite is shown in Fig. 5-6, while the current-voltage characteristic of the device is shown in the top inset. The thickness of PS/ZnO QDs nanocomposite thin film that used in the device is about 50 nm. The turn on voltage is about 13.8 V, which is larger than the PMMA based LEDs. Moreover, because of the thicker emission layer used in this device, the LEDs could be operated under voltage as high as 20 V without break down. Apart from this observation, the I-V characteristic shows similar diode behavior which has been discussed previously about the PMMA based LEDs. As can seen in Fig. 5-6, the EL spectra shows strong violet-blue emission while the emission from longer wavelength region, *i.e.*, orange and red, is much weaker. Compared to the EL spectra of LEDs based on PMMA/ZnO QDs nanocomposite, the one with PS as the matrix shows stronger blue shift. It agreed well with the deduction obtained from PL emission that the deep defect levels (mainly related to oxygen vacancies) are not apparent due to strong surface passivation effect. The strong violet-blue emission should be contributed from the recombination between electrons near CB and holes from VB of ZnO. A photograph of device emitting blue light is shown in the bottom inset of Fig. 5-6.

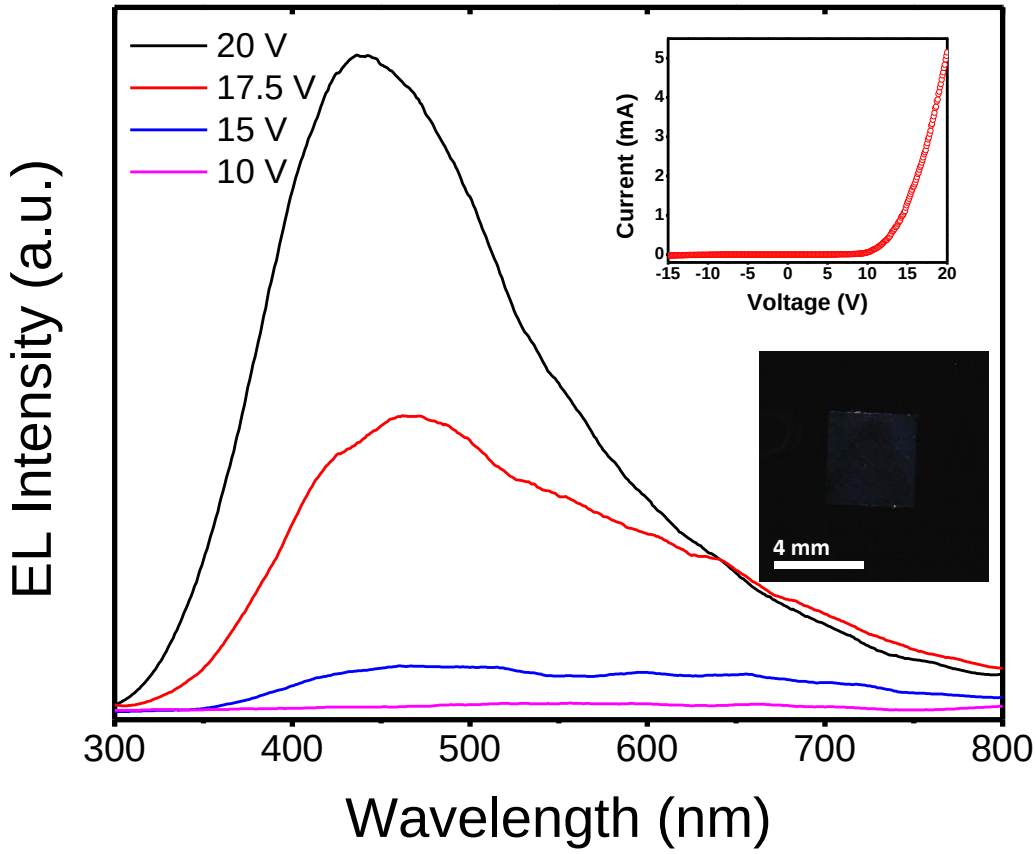

Fig. 5-6 EL spectra of PS/ZnO QDs nanocomposite based LEDs with different applied bias. The top inset shows the current-voltage characteristic and the bottom inset presents the photograph of blue light emitting from the device under operation of 20 V.

Fig. 5-7 depicts EL spectra of LEDs utilized P4VP/ZnO QDs nanocomposite (emission layer with thickness about 70 nm). Current-voltage characteristic of the LEDs shown in the top right inset of Fig. 5-7 presented similar diode behavior but much lower current, when comparing to the previously discussed polymers (PS and PMMA) based nanocomposite LEDs. EL spectra exhibited a broad emission with peak position within green region. Similar to PMMA based nanocomposite LEDs, oxygen vacancies related defect emission dominates the whole EL spectra. It is consistent with the deduction obtained from PL study which also indicated the visible emission is comparable with NUV emission. Top left inset of Fig. 5-7 presents the photograph of P4VP/ZnO QDs nanocomposites based LEDs with applied bias of 20 V. The light

emission area is not continuous, which indicates the non-uniform dispersion of ZnO QDs as previously observed in TEM images.

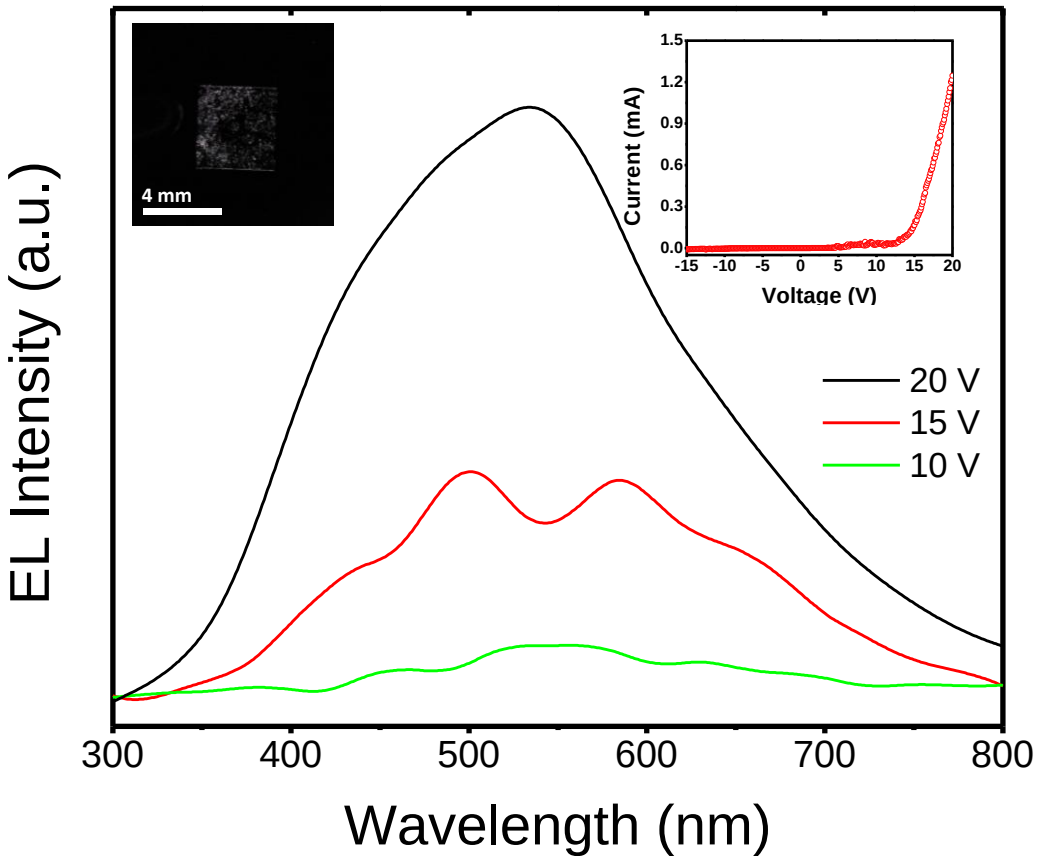

Fig. 5-7 EL spectra of P4VP/ZnO QDs nanocomposite based LEDs with different applied bias. The top right inset shows the current-voltage characteristic and the top left inset presents the photograph of blue light emitting from the device under operation of 20 V.

Fig. 5-8 shows the EL spectra of devices based on pure PVK with heat treatment and PVK/ZnO QDs nanocomposite operating under forward bias of 15 V. The PL study of PVK and the nanocomposite already showed the emission of polymer could overlap with emission from ZnO QDs. Due to low concentration of ZnO QDs in the nanocomposite, the emission of ZnO QDs could only be observed after the emission of PVK was significantly quenched because of thermal degradation. The EL intensity of nanocomposite is much higher than that of pure PVK which agreed well with the observation from PL study. For nanocomposite LEDs, emission from ZnO QDs is

indicated in the blue dash dot region. Current-voltage characteristic of corresponding devices is shown in top right inset. The left top and bottom insets show the photographs of PVK/ZnO QDs nanocomposite LED and pure PVK device, respectively. Both of the photographs were captured in the dark environment with operated voltage of 15 V; and the emission was perceived as white color.

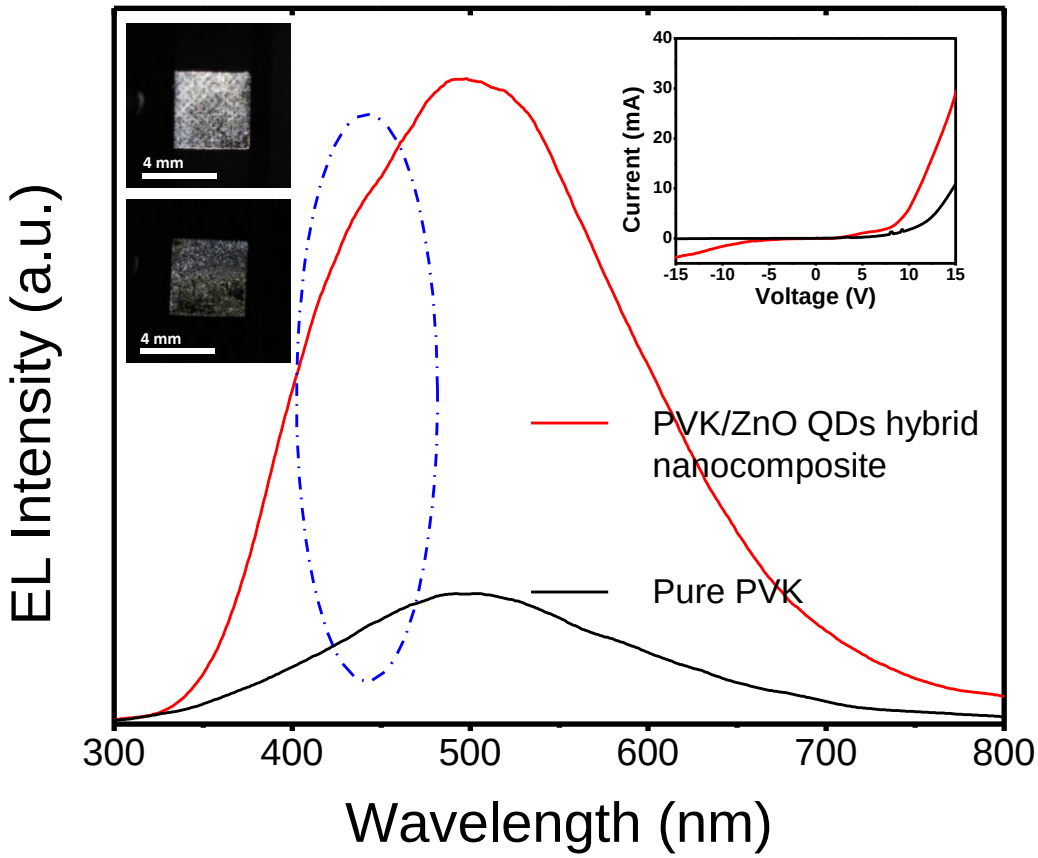

Fig. 5-8 EL spectra of pure PVK and PVK/ZnO QDs nanocomposite based LEDs under applied voltage of 15 V. The top right inset shows the current-voltage characteristic of pure PVK (black) and nanocomposite device (red). The left top and bottom insets show the photographs of PVK/ZnO QDs nanocomposite LED and pure PVK device, respectively.

The primary study of electroluminescence for the PS, P4VP and PVK based nanocomposite LEDs agreed well with the corresponding PL study. However, much more effort are required to further investigate the surface modification effect on the device performance. Nevertheless, this part of EL study highlighted the potential of

EL wavelength tuning with selection of different polymer matrices based on their structures and functional groups.

5.4 Conclusion

Polymers, which are polystyrene (PS), poly(vinylidene fluoride) (PVDF), poly(9-vinylcarbazole) (PVK), poly(vinyl pyrrolidone) (PVP), and poly(4-vinylpyridine) (P4VP), with different structures were utilized to modify the surface of ZnO QDs to control the surface defect states *via* 'polymerothermal' method. The as-prepared nanocomposites exhibited different optical properties due to different surface passivation effect on the ZnO QDs as well as the emissions originated from polymers themselves. For PS and PVDF based nanocomposites, UV emission from ZnO QDs was relatively enhanced and their visible emission was nearly disappeared. Free exciton emission with comparable defect emission was observed from P4VP/ZnO QDs nanocomposite. PL emission from PVK and PVP totally overlapped with that of ZnO; and added complexity for result interpretation. Light-emitting devices utilizing nanocomposites based on PS, P4VP and PVK were fabricated and their EL emission agreed well with the PL study. The preliminary study shows the EL emission can be slightly tuned by the selected polymers. More works are required to investigate the interaction mechanism involved between ZnO QDs and polymers inside the hybrid system.

6. Conclusions and Future Recommendations

6.1 Conclusions

Replacing toxic materials (Cd, Pb) based QDs in light-emitting devices by cheap and non-toxic oxide, such as ZnO, is very important for the further development of QD-LEDs. Incorporating ZnO QDs into polymer matrices to modify the surface of QDs has attracted considerable interest, because not only the properties of polymers, but also that of the ZnO QDs can be improved, such as chemical and thermal stability, photoluminescence efficiency, etc. In the present work, ZnO QDs were incorporated into different polymers by a facile and chemically clean method. Characterizations of the as-prepared polymer/ZnO QDs nanocomposites were performed using different techniques to study the nanocomposite properties, especially optical properties. Light-emitting application utilizing the nanocomposites was carried. The results presented in this work as well as the main contribution are summarized as follows:

1. PMMA/ZnO QDs nanocomposite was synthesized *via* a new and facile method that thermal decomposing zinc precursor into ZnO QDs in the presence of polymer. The low cost and one-step synthetic method could produce ZnO QDs with average size of 4 nm that are homogenously dispersed in PMMA matrix. PL of as-prepared nanocomposite exhibited strong NUV emission but very weak visible emission. The deconvolution of PL spectrum indicated three

emission bands: NUV, violet, and blue bands.. The violet emission was assigned to radiative transition between electrons from Zn_i with holes at VB of ZnO, while the blue emission was related to deep defect levels (V_O^{++}). It should be emphasized that the impurity free method, described as 'polymerothermal' method, avoided the effect of Li^+ and the side-products on the properties of ZnO QDs and the nanocomposites; which is very suitable for fundamental studies.

2. Light-emitting devices (LEDs) with PMMA/ZnO QDs nanocomposite as the emission layer was realized *via* low-cost spin coating technique and, to the best of our knowledge, such kind of devices was never reported. LEDs with single nanocomposite layer exhibited inversion symmetric behavior on current-voltage characteristics. This means that the LEDs showed diode characteristic when a bias voltage was applied to the devices, regardless of its direction. EL characterization of the devices showed broad emission but very low intensity. By introducing a conductive polymer, PEDOT:PSS, as the hole injection layer (HIL) between ITO and the luminescent nanocomposite layer, the device performance could be improved significantly as lower turn on voltage, but higher EL intensity was achieved in the double layer LEDs. In addition, both LEDs exhibited similar EL spectra that covered the whole visible region and the light emission from both devices was observed as white color. Analysis of the deconvoluted EL bands revealed that the visible emission related defect energy levels matched well with the deduction obtained from PL study.
3. Extending from the nanocomposites with PMMA, other representative polymers, including PS, PVDF, PVK, PVP, and P4VP, were utilized to modify the surface of ZnO QDs and control the surface defect states. Due to different

surface passivation effect on the ZnO QDs as well as the intrinsic properties of polymers, the as-prepared nanocomposites exhibited different optical properties. For nanocomposites based on PS and PVDF, NUV emission combining band edge and near band edge emission of ZnO was relatively enhanced but their visible emission was completely quenched. However, for P4VP/ZnO QDs nanocomposite, the visible emission found in PL spectrum was comparable to the NUV emission. In the case of PVK and PVP, PL emission from the polymers totally overlapped with ZnO emission and thus, it was not reasonable to further quantitatively interpret the spectra. Nevertheless, PS, P4VP and PVK based nanocomposites were further utilized for light-emitting devices and their EL emission suggested potentially tunable defect emission wavelength.

6.2 Future Recommendations

The proposed future works here is meant to be concise and could not be exhaustive. The work presented in this thesis involves a facile polymerothermal method towards the synthesis of polymer/ZnO QDs nanocomposites. Moreover, enriched understanding of the optical properties of polymer/QDs nanocomposites have been gained. However, the research of nanocomposites should not be restricted to ZnO. Meanwhile, there is still plenty of room for improvement of the light-emitting device performance.

1. To better understand the interaction between polymers and oxides

   Luminescent properties of nanocomposites utilizing ZnO QDs embedded in different polymer matrices have been discussed in the present work. However,

the size of QDs is also a key factor that influences the luminescent properties. More details are still required for understanding the effect of interaction between polymers and oxides on the size of ZnO QDs formed *via* polymerothermal method. Experimental study concerning the quantum dots size effect should be carried out using methodologies similar ours; however, additional data on FTIR and XPS should be collected. Besides ZnO QDs, other oxides, such as Al_2O_3, SnO_2 and TiO_2, can also be studied for further understanding the passivation effect on the surface of nanoparticles.

2. To improve performance of LED devices

   As mentioned in the main text, the external quantum efficiency of studied LEDs is relatively low due to nonequilibrium carrier injection. The main issues are the low efficiency of hole injection from anode and leakage of holes from emission layer to cathode. It can be improved by introducing hole block layer (HBL) with lower HOMO, such as SnO_2. The band gap of SnO_2 is about 3.6 eV with LUMO of 4.7 eV and HOMO of 8.3 eV. The HOMO of SnO_2 is 0.6 eV lower than that of ZnO, which can effectively confine the holes in ZnO emission layer. At the same time, SnO_2 is a naturally n-type semiconductor which will not affect the electron injection. Alternatively, the efficiency can also be improved by introducing polymer matrices with lower HOMO. By doing so, not only the efficiency can be improved, but also the turn-on voltage of the devices can be reduced.

3. To explore other applications

   Charge trapping effect in the polymer/ZnO QDs nanocomposite LEDs can be further studied through analyzing the I-V characteristics . Such kind of nanocomposite layer can potentially be used in the memory devices. In fact,

similar bistable devices have been studied using thick PMMA/ZnO QDs nanocomposite.[233, 234] Moreover, the trapping effect can be realized not only electrically but also *via* optical pumping. It should be very interesting to investigate such kind of optical programmable memory applications.

References

1. Colvin, V.L., Schlamp, M.C., and Alivisatos, A.P., *Light-emitting diodes made from cadmium selenide nanocrystals and a semiconducting polymer.* Nature, 1994. **370**(6488): p. 354-357.
2. Dabbousi, B.O., Bawendi, M.G., Onitsuka, O., and Rubner, M.F., *Electroluminescence from CdSe quantum-dot/polymer composites.* Applied Physics Letters, 1995. **66**(11): p. 1316-1318.
3. Greenham, N.C., Peng, X., and Alivisatos, A.P., *Charge separation and transport in conjugated-polymer/semiconductor-nanocrystal composites studied by photoluminescence quenching and photoconductivity.* Physical Review B, 1996. **54**(24): p. 17628-17637.
4. Kagan, C.R., Mitzi, D.B., and Dimitrakopoulos, C.D., *Organic-Inorganic Hybrid Materials as Semiconducting Channels in Thin-Film Field-Effect Transistors.* Science, 1999. **286**(5441): p. 945-947.
5. Zhao, Z., Arrandale, M., Vassiltsova, O.V., Petrukhina, M.A., and Carpenter, M.A., *Sensing mechanism investigation on semiconductor quantum dot/polymer thin film based hydrocarbon sensor.* Sensors and Actuators B: Chemical, 2009. **141**(1): p. 26-33.
6. Pearsall, T.P., Miller, B.I., Capik, R.J., and Bachmann, K.J., *Efficient lattice-matched double-heterostructure LED's at 1.1 mu m from Ga[sub x]In[sub 1 - x]As[sub y]P[sub 1 - y]*. Applied Physics Letters, 1976. **28**(9): p. 499-501.
7. Dadgar, A., Poschenrieder, M., Blasing, J., Fehse, K., Diez, A., and Krost, A., *Thick, crack-free blue light-emitting diodes on Si(111) using low-temperature AlN interlayers and in situ Si[sub x]N[sub y] masking.* Applied Physics Letters, 2002. **80**(20): p. 3670-3672.
8. Steigerwald, D.A., Bhat, J.C., Collins, D., Fletcher, R.M., Holcomb, M.O., Ludowise, M.J., Martin, P.S., and Rudaz, S.L., *Illumination with solid state lighting technology.* Selected Topics in Quantum Electronics, IEEE Journal of, 2002. **8**(2): p. 310-320.
9. Narendran, N. and Gu, Y., *Life of LED-based white light sources.* Display Technology, Journal of, 2005. **1**(1): p. 167-171.
10. Krames, M.R., Shchekin, O.B., Mueller-Mach, R., Mueller, G.O., Ling, Z., Harbers, G., and Craford, M.G., *Status and Future of High-Power Light-Emitting Diodes for Solid-State Lighting.* Display Technology, Journal of, 2007. **3**(2): p. 160-175.
11. Hu, B., Yang, Z., and Karasz, F.E., *Electroluminescence of pure poly(N-vinylcarbazole) and its blends with a multiblock copolymer.* Journal of Applied Physics, 1994. **76**(4): p. 2419-2422.
12. Baldo, M.A., Lamansky, S., Burrows, P.E., Thompson, M.E., and Forrest, S.R., *Very high-efficiency green organic light-emitting devices based on electrophosphorescence.* Applied Physics Letters, 1999. **75**(1): p. 4-6.
13. Muller, C.D., Falcou, A., Reckefuss, N., Rojahn, M., Wiederhirn, V., Rudati, P., Frohne, H., Nuyken, O., Becker, H., and Meerholz, K., *Multi-colour*

organic light-emitting displays by solution processing. Nature, 2003. **421**(6925): p. 829-833.
14. D'Andrade, B.W. and Forrest, S.R., *White Organic Light-Emitting Devices for Solid-State Lighting.* Advanced Materials, 2004. **16**(18): p. 1585-1595.
15. Thejo Kalyani, N. and Dhoble, S.J., *Organic light emitting diodes: Energy saving lighting technology—A review.* Renewable and Sustainable Energy Reviews, 2012. **16**(5): p. 2696-2723.
16. Coe, S., Woo, W.-K., Bawendi, M., and Bulovic, V., *Electroluminescence from single monolayers of nanocrystals in molecular organic devices.* Nature, 2002. **420**(6917): p. 800-803.
17. Coe-Sullivan, S., Woo, W.-K., Steckel, J.S., Bawendi, M., and Bulovic, V., *Tuning the performance of hybrid organic/inorganic quantum dot light-emitting devices.* Organic Electronics, 2003. **4**(2-3): p. 123-130.
18. Mueller, A.H., Petruska, M.A., Achermann, M., Werder, D.J., Akhadov, E.A., Koleske, D.D., Hoffbauer, M.A., and Klimov, V.I., *Multicolor Light-Emitting Diodes Based on Semiconductor Nanocrystals Encapsulated in GaN Charge Injection Layers.* Nano Letters, 2005. **5**(6): p. 1039-1044.
19. Caruge, J.-M., Halpert, J.E., Bulović, V., and Bawendi, M.G., *NiO as an Inorganic Hole-Transporting Layer in Quantum-Dot Light-Emitting Devices.* Nano Letters, 2006. **6**(12): p. 2991-2994.
20. Zhao, J., Bardecker, J.A., Munro, A.M., Liu, M.S., Niu, Y., Ding, I.K., Luo, J., Chen, B., Jen, A.K.Y., and Ginger, D.S., *Efficient CdSe/CdS Quantum Dot Light-Emitting Diodes Using a Thermally Polymerized Hole Transport Layer.* Nano Letters, 2006. **6**(3): p. 463-467.
21. Sun, Q., Wang, Y.A., Li, L.S., Wang, D., Zhu, T., Xu, J., Yang, C., and Li, Y., *Bright, multicoloured light-emitting diodes based on quantum dots.* Nat Photon, 2007. **1**(12): p. 717-722.
22. Bourget, C.M., *An Introduction to Light-emitting Diodes.* HortScience, 2008. **43**(7): p. 1944-1946.
23. Downing, E., Hesselink, L., Ralston, J., and Macfarlane, R., *A Three-Color, Solid-State, Three-Dimensional Display.* Science, 1996. **273**(5279): p. 1185-1189.
24. Steranka, F.M., Bhat, J., Collins, D., Cook, L., Craford, M.G., Fletcher, R., Gardner, N., Grillot, P., Goetz, W., Keuper, M., Khare, R., Kim, A., Krames, M., Harbers, G., Ludowise, M., Martin, P.S., Misra, M., Mueller, G., Mueller-Mach, R., Rudaz, S., Shen, Y.C., Steigerwald, D., Stockman, S., Subramanya, S., Trottier, T., and Wierer, J.J., *High Power LEDs – Technology Status and Market Applications.* physica status solidi (a), 2002. **194**(2): p. 380-388.
25. Narendran, N., Gu, Y., Freyssinier, J.P., Yu, H., and Deng, L., *Solid-state lighting: failure analysis of white LEDs.* Journal of Crystal Growth, 2004. **268**(3–4): p. 449-456.
26. Schubert, E.F. and Kim, J.K., *Solid-State Light Sources Getting Smart.* Science, 2005. **308**(5726): p. 1274-1278.
27. Laboratories, S.N. *Solid-State Lighting*. December 7, 2012; Available from: http://energy.sandia.gov/?page_id=452.
28. Brite, J. *LED market grew by 93% in 2010, driven by backlights*. 2011 February 24, 2011; Available from: http://ledsmagazine.com/news/8/2/26.
29. Alivisatos, A.P., *Semiconductor Clusters, Nanocrystals, and Quantum Dots.* Science, 1996. **271**(5251): p. 933-937.

30. Dabbousi, B.O., Rodriguez-Viejo, J., Mikulec, F.V., Heine, J.R., Mattoussi, H., Ober, R., Jensen, K.F., and Bawendi, M.G., *(CdSe)ZnS Core−Shell Quantum Dots: Synthesis and Characterization of a Size Series of Highly Luminescent Nanocrystallites.* The Journal of Physical Chemistry B, 1997. **101**(46): p. 9463-9475.
31. Lee, J., Sundar, V.C., Heine, J.R., Bawendi, M.G., and Jensen, K.F., *Full Color Emission from II–VI Semiconductor Quantum Dot–Polymer Composites.* Advanced Materials, 2000. **12**(15): p. 1102-1105.
32. Mekis, I., Talapin, D.V., Kornowski, A., Haase, M., and Weller, H., *One-Pot Synthesis of Highly Luminescent CdSe/CdS Core−Shell Nanocrystals via Organometallic and "Greener" Chemical Approaches†.* The Journal of Physical Chemistry B, 2003. **107**(30): p. 7454-7462.
33. Reiss, P., Protière, M., and Li, L., *Core/Shell Semiconductor Nanocrystals.* Small, 2009. **5**(2): p. 154-168.
34. Ghosh Chaudhuri, R. and Paria, S., *Core/Shell Nanoparticles: Classes, Properties, Synthesis Mechanisms, Characterization, and Applications.* Chemical Reviews, 2011.
35. Smyder, J.A. and Krauss, T.D., *Coming attractions for semiconductor quantum dots.* Materials Today, 2011. **14**(9): p. 382-387.
36. Mingyuan, G., Lesser, C., Kirstein, S., Möhwald, E., Rogach, A.L., and Weller, H., *Electroluminescence of different colors from polycation/CdTe nanocrystal self-assembled films.* Journal of Applied Physics, 2000. **87**(5): p. 2297-2302.
37. Tekin, E., Smith, P.J., Hoeppener, S., van den Berg, A.M.J., Susha, A.S., Rogach, A.L., Feldmann, J., and Schubert, U.S., *Inkjet Printing of Luminescent CdTe Nanocrystal–Polymer Composites.* Advanced Functional Materials, 2007. **17**(1): p. 23-28.
38. Kim, L., Anikeeva, P.O., Coe-Sullivan, S.A., Steckel, J.S., Bawendi, M.G., and Bulović, V., *Contact Printing of Quantum Dot Light-Emitting Devices.* Nano Letters, 2008. **8**(12): p. 4513-4517.
39. Kim, T.-H., Cho, K.-S., Lee, E.K., Lee, S.J., Chae, J., Kim, J.W., Kim, D.H., Kwon, J.-Y., Amaratunga, G., Lee, S.Y., Choi, B.L., Kuk, Y., Kim, J.M., and Kim, K., *Full-colour quantum dot displays fabricated by transfer printing.* Nat Photon, 2011. **5**(3): p. 176-182.
40. Gao, X., Yang, L., Petros, J.A., Marshall, F.F., Simons, J.W., and Nie, S., *In vivo molecular and cellular imaging with quantum dots.* Current Opinion in Biotechnology, 2005. **16**(1): p. 63-72.
41. Gao, X., Cui, Y., Levenson, R.M., Chung, L.W.K., and Nie, S., *In vivo cancer targeting and imaging with semiconductor quantum dots.* Nature biotechnology, 2004. **22**(8): p. 969-976.
42. Ghosh Chaudhuri, R. and Paria, S., *Core/Shell Nanoparticles: Classes, Properties, Synthesis Mechanisms, Characterization, and Applications.* Chemical Reviews, 2011. **112**(4): p. 2373-2433.
43. Bakueva, L., Musikhin, S., Hines, M.A., Chang, T.W.F., Tzolov, M., Scholes, G.D., and Sargent, E.H., *Size-tunable infrared (1000-1600 nm) electroluminescence from PbS quantum-dot nanocrystals in a semiconducting polymer.* Applied Physics Letters, 2003. **82**(17): p. 2895-2897.
44. Steckel, J.S., Coe-Sullivan, S., Bulović, V., and Bawendi, M.G., *1.3 μm to 1.55 μm Tunable Electroluminescence from PbSe Quantum Dots Embedded within an Organic Device.* Advanced Materials, 2003. **15**(21): p. 1862-1866.

45. Achermann, M., Petruska, M.A., Kos, S., Smith, D.L., Koleske, D.D., and Klimov, V.I., *Energy-transfer pumping of semiconductor nanocrystals using an epitaxial quantum well.* Nature, 2004. **429**(6992): p. 642-646.
46. Lunz, M., Bradley, A.L., Chen, W.-Y., Gerard, V.A., Byrne, S.J., Gun'ko, Y.K., Lesnyak, V., and Gaponik, N., *Influence of quantum dot concentration on Förster resonant energy transfer in monodispersed nanocrystal quantum dot monolayers.* Physical Review B, 2010. **81**(20): p. 205316.
47. Schlamp, M.C., Peng, X., and Alivisatos, A.P., *Improved efficiencies in light emitting diodes made with CdSe(CdS) core/shell type nanocrystals and a semiconducting polymer.* Journal of Applied Physics, 1997. **82**(11): p. 5837-5842.
48. Mattoussi, H., Radzilowski, L.H., Dabbousi, B.O., Thomas, E.L., Bawendi, M.G., and Rubner, M.F., *Electroluminescence from heterostructures of poly(phenylene vinylene) and inorganic CdSe nanocrystals.* Journal of Applied Physics, 1998. **83**(12): p. 7965-7974.
49. Caruge, J.M., Halpert, J.E., Wood, V., Bulovic, V., and Bawendi, M.G., *Colloidal quantum-dot light-emitting diodes with metal-oxide charge transport layers.* Nat Photon, 2008. **2**(4): p. 247-250.
50. Cho, K.S., Lee, E.K., Joo, W.J., Jang, E., Kim, T.H., Lee, S.J., Kwon, S.J., Han, J.Y., Kim, B.K., Choi, B.L., and Kim, J.M., *High-performance crosslinked colloidal quantum-dot light-emitting diodes.* Nature Photonics, 2009. **3**(6): p. 341-345.
51. Gopal, A., Hoshino, K., Kim, S., and Zhang, X., *Multi-color colloidal quantum dot based light emitting diodes micropatterned on silicon hole transporting layers.* Nanotechnology, 2009. **20**(23).
52. Wood, V., Panzer, M.J., Halpert, J.E., Caruge, J.M., Bawendi, M.G., and Bulović, V., *Selection of Metal Oxide Charge Transport Layers for Colloidal Quantum Dot LEDs.* ACS Nano, 2009. **3**(11): p. 3581-3586.
53. Mashford, B.S., Nguyen, T.-L., Wilson, G.J., and Mulvaney, P., *All-inorganic quantum-dot light-emitting devices formed via low-cost, wet-chemical processing.* Journal of Materials Chemistry, 2010. **20**(1): p. 167-172.
54. Vanessa Wood, V.B., *Colloidal quantum dot light-emitting devices.* Nano Rewiews, 2010. **1**: p. 7.
55. Talapin, D.V., Lee, J.-S., Kovalenko, M.V., and Shevchenko, E.V., *Prospects of Colloidal Nanocrystals for Electronic and Optoelectronic Applications.* Chemical Reviews, 2009. **110**(1): p. 389-458.
56. Qian, L., Zheng, Y., Xue, J., and Holloway, P.H., *Stable and efficient quantum-dot light-emitting diodes based on solution-processed multilayer structures.* Nat Photon, 2011. **5**(9): p. 543-548.
57. Brovelli, S., Chiodini, N., Lorenzi, R., Lauria, A., Romagnoli, M., and Paleari, A., *Fully inorganic oxide-in-oxide ultraviolet nanocrystal light emitting devices.* Nat Commun, 2012. **3**: p. 690.
58. Kwak, J., Bae, W.K., Lee, D., Park, I., Lim, J., Park, M., Cho, H., Woo, H., Yoon, D.Y., Char, K., Lee, S., and Lee, C., *Bright and Efficient Full-Color Colloidal Quantum Dot Light-Emitting Diodes Using an Inverted Device Structure.* Nano Letters, 2012. **12**(5): p. 2362-2366.
59. Lim, J., Bae, W.K., Kwak, J., Lee, S., Lee, C., and Char, K., *Perspective on synthesis, device structures, and printing processes for quantum dot displays.* Opt. Mater. Express, 2012. **2**(5): p. 594-628.

60. Sun, L., Choi, J.J., Stachnik, D., Bartnik, A.C., Hyun, B.-R., Malliaras, G.G., Hanrath, T., and Wise, F.W., *Bright infrared quantum-dot light-emitting diodes through inter-dot spacing control.* Nat Nano, 2012. **7**(6): p. 369-373.
61. Anikeeva, P.O., Halpert, J.E., Bawendi, M.G., and Bulović, V., *Electroluminescence from a Mixed Red−Green−Blue Colloidal Quantum Dot Monolayer*. Nano Letters, 2007. **7**(8): p. 2196-2200.
62. Li, Y., Rizzo, A., Mazzeo, M., Carbone, L., Manna, L., Cingolani, R., and Gigli, G., *White organic light-emitting devices with CdSe/ZnS quantum dots as a red emitter.* Journal of Applied Physics, 2005. **97**(11): p. 113501-113504.
63. Park, J.H., Kim, J.Y., Chin, B.D., Kim, Y.C., Kim, J.K., and Park, O.O., *White emission from polymer/quantum dot ternary nanocomposites by incomplete energy transfer*. Nanotechnology, 2004. **15**(9): p. 1217.
64. Li, Y.Q., Rizzo, A., Cingolani, R., and Gigli, G., *Bright White-Light-Emitting Device from Ternary Nanocrystal Composites.* Advanced Materials, 2006. **18**(19): p. 2545-2548.
65. Sun, H., Zhang, J., Zhang, H., Xuan, Y., Wang, C., Li, M., Tian, Y., Ning, Y., Ma, D., Yang, B., and Wang, Z.Y., *Pure White-Light Emission of Nanocrystal–Polymer Composites.* ChemPhysChem, 2006. **7**(12): p. 2492-2496.
66. Xuan, Y., Pan, D., Zhao, N., Ji, X., and Ma, D., *White electroluminescence from a poly(N-vinylcarbazole) layer doped with CdSe/CdS core–shell quantum dots.* Nanotechnology, 2006. **17**(19): p. 4966.
67. Ahn, J.H., Bertoni, C., Dunn, S., Wang, C., Talapin, D.V., Gaponik, N., Eychmüller, A., Hua, Y., Bryce, M.R., and Petty, M.C., *White organic light-emitting devices incorporating nanoparticles of II–VI semiconductors.* Nanotechnology, 2007. **18**(33): p. 335202.
68. Li, Y., Rizzo, A., Cingolani, R., and Gigli, G., *White-light-emitting diodes using semiconductor nanocrystals.* Microchimica Acta, 2007. **159**(3-4): p. 207-215.
69. Cheng, G., Mazzeo, M., Rizzo, A., Li, Y., Duan, Y., and Gigli, G., *White light-emitting devices based on the combined emission from red CdSe/ZnS quantum dots, green phosphorescent, and blue fluorescent organic molecules.* Applied Physics Letters, 2009. **94**(24): p. 243506-243503.
70. Torriss, B., Hachéé, A., and Gauvin, S., *White light-emitting organic device with electroluminescent quantum dots and organic molecules.* Organic Electronics, 2009. **10**(8): p. 1454-1458.
71. Cheng, G., Mazzeo, M., D'Agostino, S., Della Sala, F., Carallo, S., and Gigli, G., *Pure white hybrid light-emitting device with color rendering index higher than 90.* Opt. Lett., 2010. **35**(5): p. 616-618.
72. Dai, Q., Duty, C.E., and Hu, M.Z., *Semiconductor-Nanocrystals-Based White Light-Emitting Diodes.* Small, 2010. **6**(15): p. 1577-1588.
73. Grover, R., Srivastava, R., Chauhan, G., Kamalasanan, M.N., and Mehta, D.S., *White electroluminescence from hybrid organic inorganic LEDs based on thermally evaporated nanocrystals.* EPL (Europhysics Letters), 2012. **99**(1): p. 17003.
74. Yang, X., Zhao, D., Leck, K.S., Tan, S.T., Tang, Y.X., Zhao, J., Demir, H.V., and Sun, X.W., *Full Visible Range Covering InP/ZnS Nanocrystals with High Photometric Performance and Their Application to White Quantum Dot Light-Emitting Diodes.* Advanced Materials, 2012. **24**(30): p. 4180-4185.

75. Li, L. and Reiss, P., *One-pot Synthesis of Highly Luminescent InP/ZnS Nanocrystals without Precursor Injection.* Journal of the American Chemical Society, 2008. **130**(35): p. 11588-11589.
76. Ziegler, J., Xu, S., Kucur, E., Meister, F., Batentschuk, M., Gindele, F., and Nann, T., *Silica-Coated InP/ZnS Nanocrystals as Converter Material in White LEDs.* Advanced Materials, 2008. **20**(21): p. 4068-4073.
77. Cheah, K.W., Xu, L., and Huang, X., *White light luminescence from nano-ZnS doped porous silicon.* Nanotechnology, 2002. **13**(2): p. 238.
78. Lu, H.Y., Chu, S.Y., and Tan, S.S., *The low-temperature synthesis and optical properties of near-white light-emission nanophosphors based on manganese-doped zinc sulfide.* Japanese Journal of Applied Physics, Part 1: Regular Papers and Short Notes and Review Papers, 2005. **44**(7 A): p. 5282-5288.
79. Sun, L., Liu, C., Liao, C., and Yan, C., *ZnS nanoparticles doped with Cu(I) by controlling coordination and precipitation in aqueous solution.* Journal of Materials Chemistry, 1999. **9**(8): p. 1655-1657.
80. Panda, S.K., Hickey, S.G., Demir, H.V., and Eychmüller, A., *Bright White-Light Emitting Manganese and Copper Co-Doped ZnSe Quantum Dots.* Angewandte Chemie International Edition, 2011. **50**(19): p. 4432-4436.
81. Zhong, H., Wang, Z., Bovero, E., Lu, Z., van Veggel, F.C.J.M., and Scholes, G.D., *Colloidal CuInSe2 Nanocrystals in the Quantum Confinement Regime: Synthesis, Optical Properties, and Electroluminescence.* The Journal of Physical Chemistry C, 2011. **115**(25): p. 12396-12402.
82. Malik, M.A., O'Brien, P., and Revaprasadu, N., *A Novel Route for the Preparation of CuSe and CuInSe2 Nanoparticles.* Advanced Materials, 1999. **11**(17): p. 1441-1444.
83. Cheng, K.-Y., Anthony, R., Kortshagen, U.R., and Holmes, R.J., *High-Efficiency Silicon Nanocrystal Light-Emitting Devices.* Nano Letters, 2011. **11**(5): p. 1952-1956.
84. Puzzo, D.P., Henderson, E.J., Helander, M.G., Wang, Z., Ozin, G.A., and Lu, Z., *Visible colloidal nanocrystal silicon light-emitting diode.* Nano Letters, 2011. **11**(4): p. 1585-1590.
85. Tu, C.-C., Tang, L., Huang, J., Voutsas, A., and Lin, L.Y., *Visible electroluminescence from hybrid colloidal silicon quantum dot-organic light-emitting diodes.* Applied Physics Letters, 2011. **98**(21): p. 213102-213103.
86. Son, D.I., You, C.H., Kim, W.T., and Kim, T.W., *White light-emitting diodes fabricated utilizing hybrid polymer-colloidal ZnO quantum dots.* Nanotechnology, 2009. **20**(36).
87. Son, D.I., Kwon, B.W., Park, D.H., Seo, W.-S., Yi, Y., Angadi, B., Lee, C.-L., and Choi, W.K., *Emissive ZnO-graphene quantum dots for white-light-emitting diodes.* Nat Nano, 2012. **7**(7): p. 465-471.
88. Özgür, Ü., Alivov, Y.I., Liu, C., Teke, A., Reshchikov, M.A., Doğan, S., Avrutin, V., Cho, S.J., and Morkoç, H., *A comprehensive review of ZnO materials and devices.* Journal of Applied Physics, 2005. **98**(4): p. 1-103.
89. Djurišić, A.B. and Leung, Y.H., *Optical properties of ZnO nanostructures.* Small, 2006. **2**(8-9): p. 944-961.
90. Schmidt-Mende, L. and MacManus-Driscoll, J.L., *ZnO – nanostructures, defects, and devices.* Materials Today, 2007. **10**(5): p. 40-48.
91. Huang, M.H., Wu, Y., Feick, H., Tran, N., Weber, E., and Yang, P., *Catalytic growth of zinc oxide nanowires by vapor transport.* Advanced Materials, 2001. **13**(2): p. 113-116.

92. Kind, H., Yan, H., Messer, B., Law, M., and Yang, P., *Nanowire ultraviolet photodetectors and optical switches.* Advanced Materials, 2002. **14**(2): p. 158-160.
93. Yang, P., Yan, H., Mao, S., Russo, R., Johnson, J., Saykally, R., Morris, N., Pham, J., He, R., and Choi, H.J., *Controlled growth of ZnO nanowires and their optical properties.* Advanced Functional Materials, 2002. **12**(5): p. 323-331.
94. Greene, L.E., Law, M., Goldberger, J., Kim, F., Johnson, J.C., Zhang, Y., Saykally, R.J., and Yang, P., *Low-temperature wafer-scale production of ZnO nanowire arrays.* Angewandte Chemie - International Edition, 2003. **42**(26): p. 3031-3034.
95. Park, W.I., Kim, D.H., Jung, S.W., and Yi, G.C., *Metalorganic vapor-phase epitaxial growth of vertically well-aligned ZnO nanorods.* Applied Physics Letters, 2002. **80**(22): p. 4232-4234.
96. Liu, B. and Zeng, H.C., *Hydrothermal synthesis of ZnO nanorods in the diameter regime of 50 nm.* Journal of the American Chemical Society, 2003. **125**(15): p. 4430-4431.
97. Vayssieres, L., *Growth of arrayed nanorods and nanowires of ZnO from aqueous solutions.* Advanced Materials, 2003. **15**(5): p. 464-466.
98. Feng, X., Feng, L., Jin, M., Zhai, J., Jiang, L., and Zhu, D., *Reversible Super-hydrophobicity to Super-hydrophilicity Transition of Aligned ZnO Nanorod Films.* Journal of the American Chemical Society, 2004. **126**(1): p. 62-63.
99. Zhang, Z., Yuan, H., Gao, Y., Wang, J., Liu, D., Shen, J., Liu, L., Zhou, W., Xie, S., Wang, X., Zhu, X., Zhao, Y., and Sun, L., *Large-scale synthesis and optical behaviors of ZnO tetrapods.* Applied Physics Letters, 2007. **90**(15).
100. Zhang, Z., Sun, L., Zhao, Y., Liu, Z., Liu, D., Cao, L., Zou, B., Zhou, W., Gu, C., and Xie, S., *ZnO tetrapods designed as multiterminal sensors to distinguish false responses and increase sensitivity.* Nano Letters, 2008. **8**(2): p. 652-655.
101. Lupan, O., Chow, L., and Chai, G., *A single ZnO tetrapod-based sensor.* Sensors and Actuators, B: Chemical, 2009. **141**(2): p. 511-517.
102. Arnold, M.S., Avouris, P., Pan, Z.W., and Wang, Z.L., *Field-effect transistors based on single semiconducting oxide nanobelts.* Journal of Physical Chemistry B, 2003. **107**(3): p. 659-663.
103. Wang, Z.L., *Functional oxide nanobelts: Materials, properties and potential applications in nanosystems and biotechnology*. 2004. p. 159-196.
104. Wang, Z.L., *ZnO nanowire and nanobelt platform for nanotechnology.* Materials Science and Engineering R: Reports, 2009. **64**(3-4): p. 33-71.
105. Vanheusden, K., Warren, W.L., Seager, C.H., Tallant, D.R., Voigt, J.A., and Gnade, B.E., *Mechanisms behind green photoluminescence in ZnO phosphor powders.* Journal of Applied Physics, 1996. **79**(10): p. 7983-7990.
106. van Dijken, A., Meulenkamp, E.A., Vanmaekelbergh, D., and Meijerink, A., *The Kinetics of the Radiative and Nonradiative Processes in Nanocrystalline ZnO Particles upon Photoexcitation.* The Journal of Physical Chemistry B, 2000. **104**(8): p. 1715-1723.
107. Pacholski, C., Kornowski, A., and Weller, H., *Self-Assembly of ZnO: From Nanodots to Nanorods.* Angewandte Chemie International Edition, 2002. **41**(7): p. 1188-1191.
108. Zeng, H., Duan, G., Li, Y., Yang, S., Xu, X., and Cai, W., *Blue Luminescence of ZnO Nanoparticles Based on Non-Equilibrium Processes: Defect Origins*

and Emission Controls. Advanced Functional Materials, 2010. **20**(4): p. 561-572.
109. Aleshin, A.N. and Shcherbakov, I.P., *A light-emitting field-effect transistor based on a polyfluorene-ZnO nanoparticles film.* Journal of Physics D: Applied Physics, 2010. **43**(31).
110. Morfa, A.J., Kirkwood, N., Karg, M., Singh, T.B., and Mulvaney, P., *Effect of defects on the behavior of ZnO nanoparticle FETs.* Journal of Physical Chemistry C, 2011. **115**(16): p. 8312-8315.
111. Baruwati, B., Kumar, D.K., and Manorama, S.V., *Hydrothermal synthesis of highly crystalline ZnO nanoparticles: A competitive sensor for LPG and EtOH.* Sensors and Actuators, B: Chemical, 2006. **119**(2): p. 676-682.
112. Tang, H., Yan, M., Ma, X., Zhang, H., Wang, M., and Yang, D., *Gas sensing behavior of polyvinylpyrrolidone-modified ZnO nanoparticles for trimethylamine.* Sensors and Actuators, B: Chemical, 2006. **113**(1): p. 324-328.
113. Tang, H., Li, Y., Zheng, C., Ye, J., Hou, X., and Lv, Y., *An ethanol sensor based on cataluminescence on ZnO nanoparticles.* Talanta, 2007. **72**(4): p. 1593-1597.
114. Jin, Y., Wang, J., Sun, B., Blakesley, J.C., and Greenham, N.C., *Solution-processed ultraviolet photodetectors based on colloidal ZnO nanoparticles.* Nano Letters, 2008. **8**(6): p. 1649-1653.
115. Jun, J.H., Seong, H., Cho, K., Moon, B.M., and Kim, S., *Ultraviolet photodetectors based on ZnO nanoparticles.* Ceramics International, 2009. **35**(7): p. 2797-2801.
116. Neshataeva, E., Kummell, T., Bacher, G., and Ebbers, A., *All-inorganic light emitting device based on ZnO nanoparticles.* Applied Physics Letters, 2009. **94**(9): p. 091115-091113.
117. Omata, T., Tani, Y., Kobayashi, S., Takahashi, K., Miyanaga, A., Maeda, Y., and Otsuka-Yao-Matsuo, S., *Ultraviolet electroluminescence from colloidal ZnO quantum dots in an all-inorganic multilayer light-emitting device.* Applied Physics Letters, 2012. **100**(6): p. 061104-061103.
118. Beek, W.J.E., Wienk, M.M., and Janssen, R.A.J., *Efficient Hybrid Solar Cells from Zinc Oxide Nanoparticles and a Conjugated Polymer.* Advanced Materials, 2004. **16**(12): p. 1009-1013.
119. Beek, W.J.E., Wienk, M.M., and Janssen, R.A.J., *Hybrid Solar Cells from Regioregular Polythiophene and ZnO Nanoparticles.* Advanced Functional Materials, 2006. **16**(8): p. 1112-1116.
120. Hau, S.K., Yip, H.-L., Baek, N.S., Zou, J., O'Malley, K., and Jen, A.K.Y., *Air-stable inverted flexible polymer solar cells using zinc oxide nanoparticles as an electron selective layer.* Applied Physics Letters, 2008. **92**(25): p. 253301-253303.
121. Spanhel, L. and Anderson, M.A., *Semiconductor clusters in the sol-gel process: Quantized aggregation, gelation, and crystal growth in concentrated ZnO colloids.* Journal of the American Chemical Society, 1991. **113**(8): p. 2826-2833.
122. Meulenkamp, E.A., *Synthesis and Growth of ZnO Nanoparticles.* The Journal of Physical Chemistry B, 1998. **102**(29): p. 5566-5572.
123. Hu, Z., Oskam, G., Penn, R.L., Pesika, N., and Searson, P.C., *The Influence of Anion on the Coarsening Kinetics of ZnO Nanoparticles.* The Journal of Physical Chemistry B, 2003. **107**(14): p. 3124-3130.

124. Li, Y.-Q., Yang, Y., Sun, C.Q., and Fu, S.-Y., *Significant Enhancements in the Fluorescence and Phosphorescence of ZnO Quantum Dots/SiO2 Nanocomposites by Calcination.* The Journal of Physical Chemistry C, 2008. **112**(44): p. 17397-17401.
125. Tang, X., Choo, E.S.G., Li, L., Ding, J., and Xue, J., *Synthesis of ZnO Nanoparticles with Tunable Emission Colors and Their Cell Labeling Applications.* Chemistry of Materials, 2010. **22**(11): p. 3383-3388.
126. Zhai, J., Tao, X., Pu, Y., Zeng, X.-F., and Chen, J.-F., *Core/shell structured ZnO/SiO2 nanoparticles: Preparation, characterization and photocatalytic property.* Applied Surface Science, 2010. **257**(2): p. 393-397.
127. Fu, Y.-S., Du, X.-W., Kulinich, S.A., Qiu, J.-S., Qin, W.-J., Li, R., Sun, J., and Liu, J., *Stable Aqueous Dispersion of ZnO Quantum Dots with Strong Blue Emission via Simple Solution Route.* Journal of the American Chemical Society, 2007. **129**(51): p. 16029-16033.
128. Liu, D.-P., Li, G.-D., Su, Y., and Chen, J.-S., *Highly Luminescent ZnO Nanocrystals Stabilized by Ionic-Liquid Components.* Angewandte Chemie International Edition, 2006. **45**(44): p. 7370-7373.
129. Guo, L., Yang, S., Yang, C., Yu, P., Wang, J., Ge, W., and Wong, G.K.L., *Highly monodisperse polymer-capped ZnO nanoparticles: Preparation and optical properties.* Applied Physics Letters, 2000. **76**(20): p. 2901-2903.
130. Du, X.W., Fu, Y.S., Sun, J., Han, X., and Liu, J., *Complete UV emission of ZnO nanoparticles in a PMMA matrix.* Semiconductor Science and Technology, 2006. **21**(8): p. 1202-1206.
131. Li, S., Toprak, M.S., Jo, Y.S., Dobson, J., Kim, D.K., and Muhammed, M., *Bulk synthesis of transparent and homogeneous polymeric hybrid materials with ZnO quantum dots and PMMA.* Advanced Materials, 2007. **19**(24): p. 4347-4352.
132. Xiong, H.-M., Xie, D.-P., Guan, X.-Y., Tan, Y.-J., and Xia, Y.-Y., *Water-stable blue-emitting ZnO@polymer core-shell microspheres.* Journal of Materials Chemistry, 2007. **17**(24): p. 2490-2496.
133. Xiong, H.M., *Photoluminescent ZnO nanoparticles modified by polymers.* Journal of Materials Chemistry, 2010. **20**(21): p. 4251-4262.
134. Guo, L., Yang, S., Yang, C., Yu, P., Wang, J., Ge, W., and Wong, G.K.L., *Synthesis and characterization of poly(vinylpyrrolidone)-modified zinc oxide nanoparticles.* Chemistry of Materials, 2000. **12**(8): p. 2268-2274.
135. Abdullah, M., Morimoto, T., and Okuyama, K., *Generating Blue and Red Luminescence from ZnO/Poly(ethylene glycol) Nanocomposites Prepared Using an In-Situ Method.* Advanced Functional Materials, 2003. **13**(10): p. 800-804.
136. Neves, A.A.R., Camposeo, A., Cingolani, R., and Pisignano, D., *Interaction Scheme and Temperature Behavior of Energy Transfer in a Light-Emitting Inorganic-Organic Composite System.* Advanced Functional Materials, 2008. **18**(5): p. 751-757.
137. Liufu, S., Xiao, H., and Li, Y., *Investigation of PEG adsorption on the surface of zinc oxide nanoparticles.* Powder Technology, 2004. **145**(1): p. 20-24.
138. Guo, Z., Wei, S., Shedd, B., Scaffaro, R., Pereira, T., and Hahn, H.T., *Particle surface engineering effect on the mechanical, optical and photoluminescent properties of ZnO/vinyl-ester resin nanocomposites.* Journal of Materials Chemistry, 2007. **17**(8): p. 806-813.

139. Gao, H., Yorifuji, D., Wakita, J., Jiang, Z.-H., and Ando, S., *In situ preparation of nano ZnO/hyperbranched polyimide hybrid film and their optical properties.* Polymer, 2010. **51**(14): p. 3173-3180.
140. Xiong, H.-M., Zhao, X., and Chen, J.-S., *New Polymer−Inorganic Nanocomposites: PEO−ZnO and PEO−ZnO−LiClO4 Films.* The Journal of Physical Chemistry B, 2001. **105**(42): p. 10169-10174.
141. Khrenov, V., Schwager, F., Klapper, M., Koch, M., and Müllen, K., *Compatibilization of inorganic particles for polymeric nanocomposites. Optimization of the size and the compatibility of ZnO particles.* Polymer Bulletin, 2007. **58**(5-6): p. 799-807.
142. Tu, Y., Zhou, L., Jin, Y.Z., Gao, C., Ye, Z.Z., Yang, Y.F., and Wang, Q.L., *Transparent and flexible thin films of ZnO-polystyrene nanocomposite for UV-shielding applications.* Journal of Materials Chemistry, 2010. **20**(8): p. 1594-1599.
143. Sajimol Augustine.M, S.J., *Solvent dependent optical properties of spin-coated transparent nanocomposite films of oleic acid capped ZnO quantum dots in PVA matrix* International Conference on Advances in Polymer Technology, Feb. 26-27, 2010, India, 2010: p. 148.
144. Devi, P.I. and Ramachandran, K., *Dielectric studies on hybridised PVDF–ZnO nanocomposites.* Journal of Experimental Nanoscience, 2011. **6**(3): p. 281-293.
145. Yang, H.Y., Son, D.I., Kim, T.W., Lee, J.M., and Park, W.I., *Enhancement of the photocurrent in ultraviolet photodetectors fabricated utilizing hybrid polymer-ZnO quantum dot nanocomposites due to an embedded graphene layer.* Organic Electronics, 2010. **11**(7): p. 1313-1317.
146. Inamdar, A.I., Mujawar, S.H., Ganesan, V., and Patil, P.S., *Surfactant-mediated growth of nanostructured zinc oxide thin films via electrodeposition and their photoelectrochemical performance.* Nanotechnology, 2008. **19**(32).
147. Sun, D. and Sue, H.J., *Tunable ultraviolet emission of ZnO quantum dots in transparent poly(methyl methacrylate).* Applied Physics Letters, 2009. **94**(25).
148. Khrenov, V., Klapper, M., Koch, M., and Müllen, K., *Surface Functionalized ZnO Particles Designed for the Use in Transparent Nanocomposites.* Macromolecular Chemistry and Physics, 2005. **206**(1): p. 95-101.
149. Chen, J.H., Cheng, C.-Y., Chiu, W.-Y., Lee, C.-F., and Liang, N.-Y., *Synthesis of ZnO/polystyrene composites particles by Pickering emulsion polymerization.* European Polymer Journal, 2008. **44**(10): p. 3271-3279.
150. Tang, E., Liu, H., Sun, L., Zheng, E., and Cheng, G., *Fabrication of zinc oxide/poly(styrene) grafted nanocomposite latex and its dispersion.* European Polymer Journal, 2007. **43**(10): p. 4210-4218.
151. Zhang, Y., Wang, X., Liu, Y., Song, S., and Liu, D., *Highly transparent bulk PMMA/ZnO nanocomposites with bright visible luminescence and efficient UV-shielding capability.* Journal of Materials Chemistry, 2012. **22**(24): p. 11971-11977.
152. Zhang, L., Li, F., Chen, Y., and Wang, X., *Synthesis of transparent ZnO/PMMA nanocomposite films through free-radical copolymerization of asymmetric zinc methacrylate acetate and in-situ thermal decomposition.* Journal of Luminescence, 2011. **131**(8): p. 1701-1706.
153. Peng, X., Chen, Y., Li, F., Zhou, W., and Hu, Y., *Preparation and optical properties of ZnO@PPEGMA nanoparticles.* Applied Surface Science, 2009. **255**(16): p. 7158-7163.

154. Xiong, H.-M., Xu, Y., Ren, Q.-G., and Xia, Y.-Y., *Stable Aqueous ZnO@Polymer Core−Shell Nanoparticles with Tunable Photoluminescence and Their Application in Cell Imaging.* Journal of the American Chemical Society, 2008. **130**(24): p. 7522-7523.
155. Zhang, J., Gao, G., Zhang, M., Zhang, D., Wang, C., Zhao, D., and Liu, F., *ZnO/PS core–shell hybrid microspheres prepared with miniemulsion polymerization.* Journal of Colloid and Interface Science, 2006. **301**(1): p. 78-84.
156. Hung, C.-H. and Whang, W.-T., *Effect of surface stabilization of nanoparticles on luminescent characteristics in ZnO/poly(hydroxyethyl methacrylate) nanohybrid films.* Journal of Materials Chemistry, 2005. **15**(2): p. 267-274.
157. Singla, M.L., Shafeeq M, M., and Kumar, M., *Optical characterization of ZnO nanoparticles capped with various surfactants.* Journal of Luminescence, 2009. **129**(5): p. 434-438.
158. Chang, M., Cao, X.L., Zeng, H., and Zhang, L., *Enhancement of the ultraviolet emission of ZnO nanostructures by polyaniline modification.* Chemical Physics Letters, 2007. **446**(4–6): p. 370-373.
159. Pauporté, T., *Highly Transparent ZnO/Polyvinyl Alcohol Hybrid Films with Controlled Crystallographic Orientation Growth.* Crystal Growth & Design, 2007. **7**(11): p. 2310-2315.
160. Dhingra, M., Shrivastava, S., Senthil Kumar, P., and Annapoorni, S., *Polyaniline mediated enhancement in band gap emission of Zinc Oxide.* Composites Part B: Engineering, 2013. **45**(1): p. 1515-1520.
161. Sun, D., Sue, H.-J., and Miyatake, N., *Optical Properties of ZnO Quantum Dots in Epoxy with Controlled Dispersion.* The Journal of Physical Chemistry C, 2008. **112**(41): p. 16002-16010.
162. Janotti, A. and Van de Walle, C.G., *Oxygen vacancies in ZnO.* Applied Physics Letters, 2005. **87**(12): p. 122102-122103.
163. Xu, X., Xu, C., Wang, X., Lin, Y., Dai, J., and Hu, J., *Control mechanism behind broad fluorescence from violet to orange in ZnO quantum dots.* CrystEngComm, 2013.
164. Xiong, H.M., Wang, Z.D., Liu, D.P., Chen, J.S., Wang, Y.G., and Xia, Y.Y., *Bonding Polyether onto ZnO Nanoparticles: An Effective Method for Preparing Polymer Nanocomposites with Tunable Luminescence and Stable Conductivity.* Advanced Functional Materials, 2005. **15**(11): p. 1751-1756.
165. Xiong, H.-M., Liu, D.-P., Xia, Y.-Y., and Chen, J.-S., *Polyether-Grafted ZnO Nanoparticles with Tunable and Stable Photoluminescence at Room Temperature.* Chemistry of Materials, 2005. **17**(12): p. 3062-3064.
166. Xiong, H.M., Wang, Z.D., and Xia, Y.Y., *Polymerization Initiated by Inherent Free Radicals on Nanoparticle Surfaces: A Simple Method of Obtaining Ultrastable (ZnO)Polymer Core–Shell Nanoparticles with Strong Blue Fluorescence.* Advanced Materials, 2006. **18**(6): p. 748-751.
167. Wang, M., Lian, Y., and Wang, X., *PPV/PVA/ZnO nanocomposite prepared by complex precursor method and its photovoltaic application.* Current Applied Physics, 2009. **9**(1): p. 189-194.
168. Ton-That, C., Phillips, M.R., and Nguyen, T.-P., *Blue shift in the luminescence spectra of MEH-PPV films containing ZnO nanoparticles.* Journal of Luminescence, 2008. **128**(12): p. 2031-2034.
169. Anžlovar, A., Crnjak Orel, Z., and Žigon, M., *Poly(methyl methacrylate) composites prepared by in situ polymerization using organophillic nano-to-*

submicrometer zinc oxide particles. European Polymer Journal, 2010. **46**(6): p. 1216-1224.

170. Schwartz, V.B., Thétiot, F., Ritz, S., Pütz, S., Choritz, L., Lappas, A., Förch, R., Landfester, K., and Jonas, U., *Antibacterial Surface Coatings from Zinc Oxide Nanoparticles Embedded in Poly(N-isopropylacrylamide) Hydrogel Surface Layers.* Advanced Functional Materials, 2012. **22**(11): p. 2376-2386.
171. Liu, P. and Su, Z., *Preparation and Characterization of PMMA/ZnO Nanocomposites via In - Situ Polymerization Method.* Journal of Macromolecular Science, Part B, 2006. **45**(1): p. 131-138.
172. Ng, H.T., Han, J., Yamada, T., Nguyen, P., Chen, Y.P., and Meyyappan, M., *Single Crystal Nanowire Vertical Surround-Gate Field-Effect Transistor.* Nano Letters, 2004. **4**(7): p. 1247-1252.
173. Park, W.I., Kim, J.S., Yi, G.-C., Bae, M.H., and Lee, H.J., *Fabrication and electrical characteristics of high-performance ZnO nanorod field-effect transistors.* Applied Physics Letters, 2004. **85**(21): p. 5052-5054.
174. Ryu, Y.R., Lee, T.S., Lubguban, J.A., White, H.W., Park, Y.S., and Youn, C.J., *ZnO devices: Photodiodes and p-type field-effect transistors.* Applied Physics Letters, 2005. **87**(15): p. 153504-153503.
175. Wei, A., Sun, X.W., Wang, J.X., Lei, Y., Cai, X.P., Li, C.M., Dong, Z.L., and Huang, W., *Enzymatic glucose biosensor based on ZnO nanorod array grown by hydrothermal decomposition.* Applied Physics Letters, 2006. **89**(12).
176. Jun, J.H., Yun, J., Cho, K., Hwang, I.-S., Lee, J.-H., and Kim, S., *Necked ZnO nanoparticle-based NO2 sensors with high and fast response.* Sensors and Actuators B: Chemical, 2009. **140**(2): p. 412-417.
177. Beek, W.J.E., Wienk, M.M., and Janssen, R.A.J., *Hybrid polymer solar cells based on zinc oxide.* Journal of Materials Chemistry, 2005. **15**(29): p. 2985-2988.
178. Tsukazaki, A., Ohtomo, A., Onuma, T., Ohtani, M., Makino, T., Sumiya, M., Ohtani, K., Chichibu, S.F., Fuke, S., Segawa, Y., Ohno, H., Koinuma, H., and Kawasaki, M., *Repeated temperature modulation epitaxy for p-type doping and light-emitting diode based on ZnO.* Nat Mater, 2005. **4**(1): p. 42-46.
179. Könenkamp, R., Word, R.C., and Godinez, M., *Ultraviolet Electroluminescence from ZnO/Polymer Heterojunction Light-Emitting Diodes.* Nano Letters, 2005. **5**(10): p. 2005-2008.
180. Sun, X.W., Ling, B., Zhao, J.L., Tan, S.T., Yang, Y., Shen, Y.Q., Dong, Z.L., and Li, X.C., *Ultraviolet emission from a ZnO rod homojunction light-emitting diode.* Applied Physics Letters, 2009. **95**(13): p. 133124-133123.
181. Liu, P., *Facile preparation of monodispersed core/shell zinc oxide@polystyrene (ZnO@PS) nanoparticles via soapless seeded microemulsion polymerization.* Colloids and Surfaces A: Physicochemical and Engineering Aspects, 2006. **291**(1–3): p. 155-161.
182. Sudha, M., Senthilkumar, S., Hariharan, R., Suganthi, A., and Rajarajan, M., *Synthesis, characterization and study of photocatalytic activity of surface modified ZnO nanoparticles by PEG capping.* Journal of Sol-Gel Science and Technology, 2012: p. 1-10.
183. Yang, C.L., Wang, J.N., Ge, W.K., Guo, L., Yang, S.H., and Shen, D.Z., *Enhanced ultraviolet emission and optical properties in polyvinyl pyrrolidone surface modified ZnO quantum dots.* Journal of Applied Physics, 2001. **90**(9): p. 4489-4493.

184. Sun, D., Miyatake, N., and Sue, H.-J., *Transparent PMMA/ZnO nanocomposite films based on colloidal ZnO quantum dots.* Nanotechnology, 2007. **18**(21): p. 215606.
185. Kulyk, B., Sahraoui, B., Krupka, O., Kapustianyk, V., Rudyk, V., Berdowska, E., Tkaczyk, S., and Kityk, I., *Linear and nonlinear optical properties of ZnO/PMMA nanocomposite films.* Journal of Applied Physics, 2009. **106**(9): p. 093102-093106.
186. Agrawal, M., Gupta, S., Zafeiropoulos, N.E., Oertel, U., Häßler, R., and Stamm, M., *Nano-level mixing of ZnO into poly(Methyl methacrylate).* Macromolecular Chemistry and Physics, 2010. **211**(17): p. 1925-1932.
187. Paramo, J.A., Strzhemechny, Y.M., Anžlovar, A., Žigon, M., and Orel, Z.C., *Enhanced room temperature excitonic luminescence in ZnO/polymethyl methacrylate nanocomposites prepared by bulk polymerization.* Journal of Applied Physics, 2010. **108**(2).
188. Chaurasia, A., Wang, L., Gan, L.H., Mei, T., Li, Y., Liang, Y.N., and Hu, X., *Functional Zinc Oxide Nanoparticles/Polymer Nanocomposite via Facile 'Polymerothermal' Synthesis.* European Polymer Journal, 2012(0).
189. Pesika, N.S., Stebe, K.J., and Searson, P.C., *Determination of the Particle Size Distribution of Quantum Nanocrystals from Absorbance Spectra.* Advanced Materials, 2003. **15**(15): p. 1289-1291.
190. Brus, L.E., *Electron--electron and electron-hole interactions in small semiconductor crystallites: The size dependence of the lowest excited electronic state.* The Journal of Chemical Physics, 1984. **80**(9): p. 4403-4409.
191. Brus, L., *Electronic wave functions in semiconductor clusters: experiment and theory.* The Journal of Physical Chemistry, 1986. **90**(12): p. 2555-2560.
192. Shionoya, S., *Phosphor Handbook.* 1998, CRC, Boca Raton, FL.
193. McCluskey, M.D. and Jokela, S.J., *Defects in ZnO.* Journal of Applied Physics, 2009. **106**(7): p. 071101-071113.
194. Borseth, T.M., Svensson, B.G., Kuznetsov, A.Y., Klason, P., Zhao, Q.X., and Willander, M., *Identification of oxygen and zinc vacancy optical signals in ZnO.* Applied Physics Letters, 2006. **89**(26): p. 262112-262113.
195. Kulyk, B., Kapustianyk, V., Tsybulskyy, V., Krupka, O., and Sahraoui, B., *Optical properties of ZnO/PMMA nanocomposite films.* Journal of Alloys and Compounds, 2010. **502**(1): p. 24-27.
196. Vollath, D., Szabó, D.V., and Schlabach, S., *Oxide/polymer nanocomposites as new luminescent materials.* Journal of Nanoparticle Research, 2004. **6**(2-3): p. 181-191.
197. Wang, Z.G., Zu, X.T., Zhu, S., Xiang, X., Fang, L.M., and Wang, L.M., *Origin of luminescence from PMMA functionalized nanoparticles.* Physics Letters A, 2006. **350**(3–4): p. 252-257.
198. Chen, Q.H., Shi, S.Y., and Zhang, W.G., *Study on luminescence characteristic of the ZnO/polymer hybrid films.* Colloid and Polymer Science, 2009. **287**(5): p. 533-540.
199. Lin, B., Fu, Z., and Jia, Y., *Green luminescent center in undoped zinc oxide films deposited on silicon substrates.* Applied Physics Letters, 2001. **79**(7): p. 943-945.
200. Look, D.C., Farlow, G.C., Reunchan, P., Limpijumnong, S., Zhang, S.B., and Nordlund, K., *Evidence for Native-Defect Donors in n-Type ZnO.* Physical Review Letters, 2005. **95**(22): p. 225502.

201. Quemener, V., Vines, L., Monakhov, E.V., and Svensson, B.G., *Evolution of deep electronic states in ZnO during heat treatment in oxygen- and zinc-rich ambients.* Applied Physics Letters, 2012. **100**(11): p. 112108-112104.
202. Zeng, H., Li, Z., Cai, W., Cao, B., Liu, P., and Yang, S., *Microstructure Control of Zn/ZnO Core/Shell Nanoparticles and Their Temperature-Dependent Blue Emissions.* The Journal of Physical Chemistry B, 2007. **111**(51): p. 14311-14317.
203. Ahn, C.H., Kim, Y.Y., Kim, D.C., Mohanta, S.K., and Cho, H.K., *A comparative analysis of deep level emission in ZnO layers deposited by various methods.* Journal of Applied Physics, 2009. **105**(1): p. 013502-013505.
204. Ge, J., Zeng, X., Tao, X., Li, X., Shen, Z., Yun, J., and Chen, J., *Preparation and characterization of PS-PMMA/ZNO nanocomposite films with novel properties of high transparency and UV-shielding capacity.* Journal of Applied Polymer Science, 2010. **118**(3): p. 1507-1512.
205. Park, J., An, K., Hwang, Y., Park, J.E.G., Noh, H.J., Kim, J.Y., Park, J.H., Hwang, N.M., and Hyeon, T., *Ultra-large-scale syntheses of monodisperse nanocrystals.* Nature Materials, 2004. **3**(12): p. 891-895.
206. Coe-Sullivan, S., Steckel, J.S., Woo, W.K., Bawendi, M.G., and Bulović, V., *Large-Area Ordered Quantum-Dot Monolayers via Phase Separation During Spin-Casting.* Advanced Functional Materials, 2005. **15**(7): p. 1117-1124.
207. Steckel, J.S., Snee, P., Coe-Sullivan, S., Zimmer, J.P., Halpert, J.E., Anikeeva, P., Kim, L.A., Bulovic, V., and Bawendi, M.G., *Color-saturated green-emitting QD-LEDs.* Angewandte Chemie - International Edition, 2006. **45**(35): p. 5796-5799.
208. Haverinen, H.M., Myllylä, R.A., and Jabbour, G.E., *Inkjet printing of light emitting quantum dots*. Vol. 94. 2009: AIP. 073108.
209. Konenkamp, R., Word, R.C., and Schlegel, C., *Vertical nanowire light-emitting diode.* Applied Physics Letters, 2004. **85**(24): p. 6004-6006.
210. Chang, C.-Y., Tsao, F.-C., Pan, C.-J., Chi, G.-C., Wang, H.-T., Chen, J.-J., Ren, F., Norton, D.P., Pearton, S.J., Chen, K.-H., and Chen, L.-C., *Electroluminescence from ZnO nanowire/polymer composite p-n junction.* Applied Physics Letters, 2006. **88**(17): p. 173503-173503.
211. Dong, J.J., Zhang, X.W., Yin, Z.G., Wang, J.X., Zhang, S.G., Si, F.T., Gao, H.L., and Liu, X., *Ultraviolet electroluminescence from ordered ZnO nanorod array/p-GaN light emitting diodes.* Applied Physics Letters, 2012. **100**(17): p. 171109-171104.
212. Li, Y.-Q., Yang, Y., Fu, S.-Y., Yi, X.-Y., Wang, L.-C., and Chen, H.-D., *Transparent and Light-Emitting Epoxy Super-Nanocomposites Containing ZnO-QDs/SiO2 Nanocomposite Particles as Encapsulating Materials for Solid-State Lighting.* The Journal of Physical Chemistry C, 2008. **112**(47): p. 18616-18622.
213. Yang, Y., Li, Y.-Q., Fu, S.-Y., and Xiao, H.-M., *Transparent and Light-Emitting Epoxy Nanocomposites Containing ZnO Quantum Dots as Encapsulating Materials for Solid State Lighting.* The Journal of Physical Chemistry C, 2008. **112**(28): p. 10553-10558.
214. Que, W., Zhou, Y., Lam, Y.L., Chan, Y.C., Kam, C.H., Liu, B., Gan, L.M., Chew, C.H., Xu, G.Q., Chua, S.J., Xu, S.J., and Mendis, F.V.C., *Photoluminescence and electroluminescence from copper doped zinc sulphide nanocrystals/polymer composite.* Applied Physics Letters, 1998. **73**(19): p. 2727-2729.

215. Lampert, M.A.a.M., P., *Current Injection in Solids*, in *Academic*. 1970: New York.
216. Kao, K.C.a.H., W., *Electrical Transport in Solids*, in *International Series in The Science of Solid State*, Pamplin, B.R., Editor. 1981, Pergamon: New York. p. 64-144.
217. Sze, S.M., *Physics of Semiconductor Devices*. 2nd ed. 1981, New York: Wiley.
218. Fan, X.M., Lian, J.S., Zhao, L., and Liu, Y.H., *Single violet luminescence emitted from ZnO films obtained by oxidation of Zn film on quartz glass.* Applied Surface Science, 2005. **252**(2): p. 420-424.
219. Kahn, M.L., Cardinal, T., Bousquet, B., Monge, M., Jubera, V., and Chaudret, B., *Optical Properties of Zinc Oxide Nanoparticles and Nanorods Synthesized Using an Organometallic Method.* ChemPhysChem, 2006. **7**(11): p. 2392-2397.
220. Rakshit, S. and Vasudevan, S., *Trap-State Dynamics in Visible-Light-Emitting ZnO:MgO Nanocrystals.* The Journal of Physical Chemistry C, 2008. **112**(12): p. 4531-4537.
221. Xu, P.S., Sun, Y.M., Shi, C.S., Xu, F.Q., and Pan, H.B., *The electronic structure and spectral properties of ZnO and its defects.* Nuclear Instruments and Methods in Physics Research Section B: Beam Interactions with Materials and Atoms, 2003. **199**(0): p. 286-290.
222. Qiao, Q., Li, B.H., Shan, C.X., Liu, J.S., Yu, J., Xie, X.H., Zhang, Z.Z., Ji, T.B., Jia, Y., and Shen, D.Z., *Light-emitting diodes fabricated from small-size ZnO quantum dots.* Materials Letters, 2012. **74**(0): p. 104-106.
223. Xiong, M., Gu, G., You, B., and Wu, L., *Preparation and characterization of poly(styrene butylacrylate) latex/nano-ZnO nanocomposites.* Journal of Applied Polymer Science, 2003. **90**(7): p. 1923-1931.
224. Anglos, D., Stassinopoulos, A., Das, R.N., Zacharakis, G., Psyllaki, M., Jakubiak, R., Vaia, R.A., Giannelis, E.P., and Anastasiadis, S.H., *Random laser action in organic?inorganic nanocomposites.* J. Opt. Soc. Am. B, 2004. **21**(1): p. 208-213.
225. Peng, Y., Xu, A.-W., Deng, B., Antonietti, M., and Cölfen, H., *Polymer-Controlled Crystallization of Zinc Oxide Hexagonal Nanorings and Disks.* The Journal of Physical Chemistry B, 2006. **110**(7): p. 2988-2993.
226. Zhang, X., Yang, H., Xiong, H.-M., Li, F.-Y., and Xia, Y.-Y., *A quasi-solid-state dye-sensitized solar cell based on the stable polymer-grafted nanoparticle composite electrolyte.* Journal of Power Sources, 2006. **160**(2): p. 1451-1455.
227. Lü, N., Lü, X., Jin, X., and Lü, C., *Preparation and characterization of UV-curable ZnO/polymer nanocomposite films.* Polymer International, 2007. **56**(1): p. 138-143.
228. Xu, Z.X., Roy, V.A.L., Stallinga, P., Muccini, M., Toffanin, S., Xiang, H.F., and Che, C.M., *Nanocomposite field effect transistors based on zinc oxide/polymer blends.* Applied Physics Letters, 2007. **90**(22).
229. Li, F., Son, D.-I., Leem, J.-H., Kim, T.W., Dong, W., and Kim, Y.-H., *Enhanced ultraviolet emission from ZnO nanocrystals embedded in a hybrid polymer composite layer.* Journal of Applied Physics, 2008. **103**(7): p. 073511-073514.
230. Lee, M., Chen, C.-Y., Wang, S., Cha, S.N., Park, Y.J., Kim, J.M., Chou, L.-J., and Wang, Z.L., *A Hybrid Piezoelectric Structure for Wearable Nanogenerators.* Advanced Materials, 2012. **24**(13): p. 1759-1764.
231. Son, D.I., Oh, D.H., Jung, J.H., and Kim, T.W., *Charging and Discharging Mechanisms of Organic Bistable Devices Based on ZnO Nanoparticles Capped*

with a Poly N-Vinylcarbazole Polymer. Journal of Nanoscience and Nanotechnology, 2011. **11**(1): p. 711-715.

232. Son, D.I., Park, D.H., Choi, W.K., Cho, S.H., Kim, W.T., and Kim, T.W., *Carrier transport in flexible organic bistable devices of ZnO nanoparticles embedded in an insulating poly(methyl methacrylate) polymer layer.* Nanotechnology, 2009. **20**(19).
233. Son, D.I., You, C.H., Jung, J.H., and Kim, T.W., *Carrier transport mechanisms of organic bistable devices fabricated utilizing colloidal ZnO quantum dot-polymethylmethacrylate polymer nanocomposites.* Applied Physics Letters, 2010. **97**(1): p. 013304-013303.
234. Son, D.I., You, C.H., Kim, W.T., Jung, J.H., and Kim, T.W., *Electrical bistabilities and memory mechanisms of organic bistable devices based on colloidal ZnO quantum dot-polymethylmethacrylate polymer nanocomposites.* Applied Physics Letters, 2009. **94**(13): p. 132103-132103.
235. Szabó, T.H.a.D.V., *Polymer-Nanoparticle Composites: From Synthesis to Modern Applications.* 2010.
236. Xiong, H.-M., Shen, W.-Z., Wang, Z.-D., Zhang, X., and Xia, Y.-Y., *Liquid Polymer Nanocomposites PEGME−SnO2 and PEGME−TiO2 Prepared through Solvothermal Methods.* Chemistry of Materials, 2006. **18**(16): p. 3850-3854.
237. Yang, M., Di, Z., and Lee, J.-K., *Facile control of surface wettability in TiO2/poly(methyl methacrylate) composite films.* Journal of Colloid and Interface Science, 2012. **368**(1): p. 603-607.
238. Li, G. and Ni, X., *A novel photoconductive ZnO/PVK nanocomposite prepared through photopolymerization induced by semiconductor nanoparticles.* Materials Letters, 2008. **62**(17–18): p. 3066-3069.
239. Kido, J., Hongawa, K., Okuyama, K., and Nagai, K., *Bright blue electroluminescence from poly(N-vinylcarbazole).* Applied Physics Letters, 1993. **63**(19): p. 2627-2629.
240. Kido, J., Shionoya, H., and Nagai, K., *Single-layer white light-emitting organic electroluminescent devices based on dye-dispersed poly(N-vinylcarbazole).* Applied Physics Letters, 1995. **67**(16): p. 2281-2283.
241. Ruokolainen, J., Tanner, J., ten Brinke, G., Ikkala, O., Torkkeli, M., and Serimaa, R., *Poly(4-vinyl pyridine)/Zinc Dodecyl Benzene Sulfonate Mesomorphic State Due to Coordination Complexation.* Macromolecules, 1995. **28**(23): p. 7779-7784.
242. Fahmi, A., Pietsch, T., Mendoza, C., and Cheval, N., *Functional hybrid materials.* Materials Today, 2009. **12**(5): p. 44-50.
243. Zu, X., Hu, X., Lyon, L.A., and Deng, Y., *In situ fabrication of ordered nanoring arrays via the reconstruction of patterned block copolymer thin films.* Chemical Communications, 2010. **46**(42): p. 7927-7929.
244. Kuo, S.-W., Wu, C.-H., and Chang, F.-C., *Thermal Properties, Interactions, Morphologies, and Conductivity Behavior in Blends of Poly(vinylpyridine)s and Zinc Perchlorate.* Macromolecules, 2003. **37**(1): p. 192-200.

List of Publications

1. Chaurasia, A., **Wang, L**., Gan, L.H., Mei, T., Li, Y., Liang, Y.N., and Hu, X., *Polymerothermal Synthesis – A Facile and Versatile Method towards Functional Nanocomposites*. European Polymer Journal, **2013**. 49(3): p. 630-636 (Equally contributed)
2. Liang YN, Lok BK, **Wang L**, Feng C, Lu ACW, Mei T, *et al*. *Effects of the morphology of inkjet printed zinc oxide (ZnO) on thin film transistor performance and seeded ZnO nanorod growth.* Thin Solid Films. **2013** 10/1/; 544(0): 509-14.
3. Zeng S, Liang Y, Lu H, **Wang L**, Dinh X-Q, Yu X, *et al*. *Synthesis of symmetrical hexagonal-shape PbO nanosheets using gold nanoparticles.* Materials Letters. **2012**; 67(1): 74-7.
4. Hu Y, Qian H, Liu Y, Du G, Zhang F, **Wang L**, *et al*. *A microwave-assisted rapid route to synthesize ZnO/ZnS core-shell nanostructures via controllable surface sulfidation of ZnO nanorods*. CrystEngComm. **2011**; 13(10): 3438-43.
5. Zhang X, Li Y, Li T, Lee SY, Feng C, **Wang L**, *et al*. *Gain-assisted propagation of surface plasmon polaritons via electrically pumped quantum wells*. Opt Lett. **2010**; 35(18): 3075-7.
6. Hu Y, Mei T, **Wang L**, Qian H. *A Facile and Generic Strategy to Synthesize Large-Scale Carbon Nanotubes*. Journal of Nanomaterials. **2010**; 2010.
7. Pan SS, Li GH, **Wang LB**, Shen YD, Wang Y, Mei T and Hu X. *Atomic nitrogen doping and p-type conduction in SnO_2*. Applied Physics Letters. **2009**; 95(22): 222112-3.
8. **LB Wang**, YD Shen, CG Feng, T Mei, and X Hu. *Light emission properties of ZnO quantum dots/PMMA nanocomposites*. OSA-IEEE-COS Topical Meeting on Advances in Optoelectronics and Micro/nano-optics (AOM), Dec 3-6, **2010**, Guangzhou, China (Conference)
9. **Wang L**, Liang Y.N., Chaurasia A., Li Y., Mei T., Hu X., *Hybrid nanocomposite with one-step synthesized ZnO quantum dots embedded in PMMA matrix for light-emitting application*. (submitted)

Appendices

Appendix – I: TGA Analysis of Zinc Acetate Dehydrate

In order to explain the reaction mechanism, TGA analysis for a sample of pure zinc acetate dehydrate was done with air flow rate of 60 sccm and heating rate of 8 ^{o}C / min. The typical weight loss *vs.* temperature curve is shown in Fig. A1.

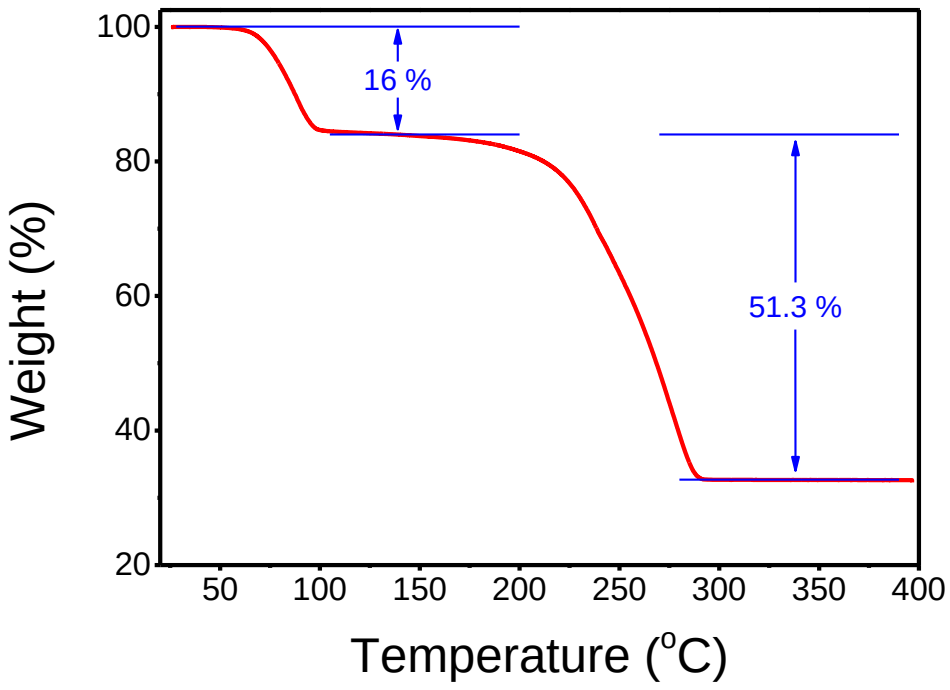

Fig. A-1 TGA analysis of pure zinc acetate dehydrate.

The process starts with the thermal dehydration process and the weight loss is approximately 16 % which corresponding to the water molecule in the precursor. The thermal decomposition process of zinc acetate causes a weight loss of 51.3 % from

150 ^{o}C to 295 ^{o}C. The calculated theoretical value for weight loss is about 46.7 %. The 4.6 wt.% difference might be caused by the sublimation of zinc compounds. As shown in Fig. A1, the thermal decomposition process starts at about 160 ^{o}C with very low processing rate. When the temperature reaches to 200 ^{o}C, the decomposition process begins to accelerate and the temperature of this value is still moderate for most of polymers.

The mechanism of thermal decomposition process for zinc acetate dehydrate is suggested by the following chemical reactions: [1, 2]

$$Zn(CH_3COO)_2 \cdot 2H_2O \xrightarrow{heat} Zn(CH_3COO)_2 + 2H_2O \uparrow$$

$$4Zn(CH_3COO)_2 + 2H_2O \xrightarrow{heat} Zn_4O(CH_3COO)_6 + 2CH_3COOH \uparrow$$

$$Zn_4O(CH_3COO)_6 + 3H_2O \xrightarrow{heat} 4ZnO + 6CH_3COOH \uparrow$$

$$Zn_4O(CH_3COO)_6 \xrightarrow{heat} 4ZnO + 3CH_3COCH_3 \uparrow + 3CO_2 \uparrow$$

When the temperature increases to approximately 200 ^{o}C, gaseous products such as acetic acid, carbon dioxide and acetone begin to form and evaporate. Khan *et al*.[3] proposed that an intermediate product, $Zn_4O(CH_3COO)_6$, was involved in the whole process. Acetic acid is formed by the reaction between the zinc compounds, $Zn_4O(CH_3COO)_6$, and water molecule from air; while the carbon dioxide and acetone was produced by the decomposition of $Zn_4O(CH_3COO)_6$.

Appendix – II: Synthesis of referential ZnO QDs

The referential ZnO QDs were synthesized *via* sol-gel method. The preparation procedure firstly reported by Spanhel and Anderson, which was also widely used by other groups, was used in our studies.[4-6] A few modifications were made in our synthesis. In the typical procedures, 1.10 g (5 mmol) $Zn(Ac)_2 \cdot 2H_2O$ was dissolved in 100 ml of methanol to form a solution with concentration of 0.05 $mol \cdot L^{-1}$, while 0.21 g (5 mmol) $LiOH \cdot H_2O$ was also dissolved in 100 ml of methanol. Both of the solutions were underwent ultra-sonication for 10 mins to 30 mins to make sure all the solutes were dissolved in the solvent and then, cooled to 0 ^oC in the ice water bath. After that, solution contains $LiOH \cdot H_2O$ was rapidly added into the solution of $Zn(Ac)_2 \cdot 2H_2O$ under vigorous stirring at room temperature. The mixture of solutions was transparent at the beginning and slowly turned to be milk-like as increasing the reaction time. After stirring for 2 h at room temperature, ZnO precipitate was obtained from the milk-like ZnO sol *via* centrifuging at 8000 RPM for 10 mins. The transparent supernatant was removed and the ZnO precipitate was redispersed in methanol. The wash procedure was repeated twice. The final precipitate was redispersed in methanol with desired concentration and stored in sealed bottle at room temperature.

Appendix – III: CIE Characteristics

The color of EL emission can be transformed into the chromaticity coordinates of x and y which are defined by the International 1931 Convention on Illumination (Commission Internationale de l'Eclairage, CIE). The transformation can be done through the following procedures:

Firstly, the tristimulus values X, Y and Z are calculated from the spectral power distribution of EL emission ($\mathrm{EL}(\lambda)$) and the standard color-matching functions $\bar{x}(\lambda), \bar{y}(\lambda)$ and $\bar{z}(\lambda)$ (Fig. A2) by

$$X = \int \mathrm{EL}(\lambda) \cdot \bar{x}(\lambda) d\lambda$$

$$Y = \int \mathrm{EL}(\lambda) \cdot \bar{y}(\lambda) d\lambda$$

$$Z = \int \mathrm{EL}(\lambda) \cdot \bar{z}(\lambda) d\lambda$$

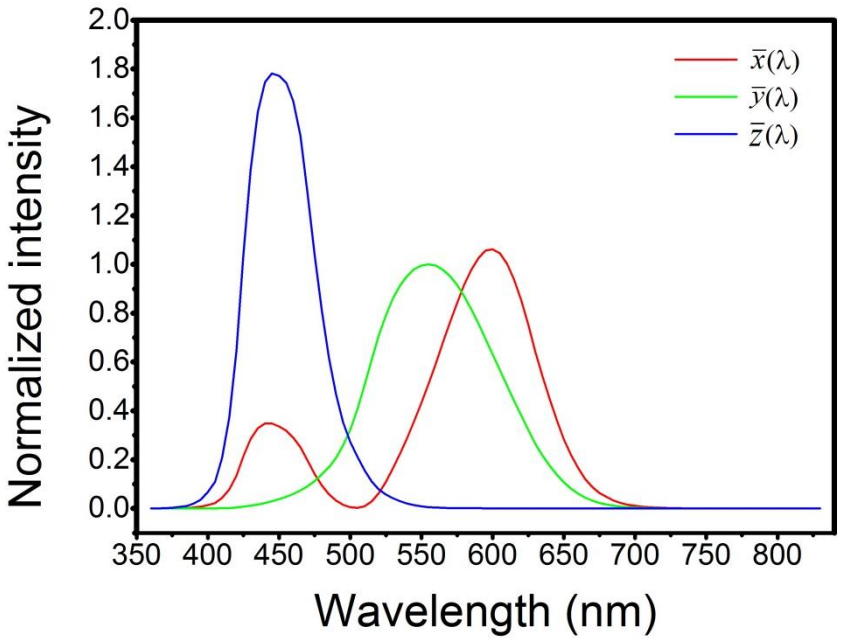

Fig. A-2 Standard observer color-matching functions.

The tristimulus values are the relative amounts of those three standard color-matching functions and the values are adopted to describe the perception of the emission color that observed by a standard human eye. By normalizing the tristimulus values, the CIE chromaticity coordinates, x and y, can be obtained as follows:

$$x = \frac{X}{X + Y + Z}$$

$$y = \frac{Y}{X + Y + Z}$$

The CIE chromaticity diagram shown in Fig. 4-6 or Fig. 4-8 can be defined by using x and y as coordinates. The outer curved boundary represents the spectral (or monochromatic) color, while the inner part of the diagram is corresponding to the mixture of different colors. Specially, the standard white color with chromaticity coordinates of x=0.333 and y=0.333 corresponds the point in the middle of the diagram (also shown in Fig. 4-6 and Fig. 4-8).

Appendix – IV: References

1. Paraguay D, F., Estrada L, W., Acosta N, D.R., Andrade, E., and Miki-Yoshida, M., *Growth, structure and optical characterization of high quality ZnO thin films obtained by spray pyrolysis.* Thin Solid Films, 1999. **350**(1–2): p. 192-202.
2. Lin, C.-C. and Li, Y.-Y., *Synthesis of ZnO nanowires by thermal decomposition of zinc acetate dihydrate.* Materials Chemistry and Physics, 2009. **113**(1): p. 334-337.
3. Khan, O.F.Z. and O'Brien, P., *On the use of zinc acetate as a novel precursor for the deposition of ZnO by low-pressure metal-organic chemical vapour deposition.* Thin Solid Films, 1989. **173**(1): p. 95-97.
4. Spanhel, L. and Anderson, M.A., *Semiconductor clusters in the sol-gel process: Quantized aggregation, gelation, and crystal growth in concentrated ZnO colloids.* Journal of the American Chemical Society, 1991. **113**(8): p. 2826-2833.
5. Meulenkamp, E.A., *Synthesis and Growth of ZnO Nanoparticles.* The Journal of Physical Chemistry B, 1998. **102**(29): p. 5566-5572.
6. van Dijken, A., Makkinje, J., and Meijerink, A., *The influence of particle size on the luminescence quantum efficiency of nanocrystalline ZnO particles.* Journal of Luminescence, 2001. **92**(4): p. 323-328.